UC San Diego

UC San Diego Electronic Theses and Dissertations

Title

Volatile Organic Compounds: The Connection Between the Ocean and Atmosphere

Permalink

https://escholarship.org/uc/item/8jn264bk

Author

Moore, Alexia Nicole

Publication Date

2024

Peer reviewed|Thesis/dissertation

eScholarship.org Powered by the California Digital Library
University of California

UNIVERSITY OF CALIFORNIA SAN DIEGO

Volatile Organic Compounds: The Connection Between the Ocean and Atmosphere

A dissertation submitted in partial satisfaction of the requirements for the degree Doctor of Philosophy

in

Chemistry

by

Alexia Nicole Moore

Committee in charge:

Professor Kimberly Prather, Chair
Professor Rommie Amaro
Professor Andrew Kummel
Professor Todd Martz
Professor Michael Tauber

2024

Copyright

Alexia Nicole Moore, 2024

All rights reserved.

The Dissertation of Alexia Nicole Moore is approved, and it is acceptable in quality and form for publication on microfilm and electronically.

University of California San Diego

2024

DEDICATION

In loving memory of my Papa for all of his love and support. I could not have done this without his belief in me.

TABLE OF CONTENTS

Dissertation Approval Page……..……....……..……..iii

Dedication.……...……...iv

Table of Contents…….……..…….....v

List of Abbreviations and Symbols.…….…….……xi

List of Figures.……..……..…….....xiv

List of Tables……..……..…….....xvii

Acknowledgements.…….…….....xviii

Vita.……...……..…….....xx

Abstract of the Dissertation.……..…….……xxiii

Chapter 1. Introduction……...……..1

1.1 Volatile Organic Compounds…….1

1.2 Biological Production of VOCs……...…….……..2

1.3 Marine Aerosols……...……..……....3

1.4 Secondary Marine Aerosols……..……..…….……...3

1.5 Mass Spectrometry…….4

1.6 Chemical Ionization Mass Spectrometer …….…….…….5

1.7 Potential Aerosol Mass Oxidative Flow Reactor……..…….…….6

1.8 Dissertation Objectives….....…….7

1.9 Dissertation Synopsis.....……..…….....8

1.10 Acknowledgements…….…..……..……..……...9

1.11 References ……..……..……10

Chapter 2. Factors Controlling Production of Dimethyl Sulfide, Methanethiol, and Dimethyl Disulfide During Controlled Phytoplankton-Bacterial Mesocosm Experiments……14

2.1 Abstract……..……...……...…….…...14

2.2 Introduction.…….……...……15

2.3 Methods...……..……...….…..….18

2.3.1 Preparation of Mesocosm Incubation Experiments.……..……...….18

2.3.2 Marine Aerosol Reference Tank Operation....……..……..…….19

2.3.3 Heterotrophic Bacterial Abundance and Community Structure…….19

2.3.4 BVOC Measurements……21

2.4. Results and Discussion …..…….……....23

2.5 Conclusion..……...……..……..…...31

2.6 Acknowledgments, Samples, and Data…….…….…...32

2.7 Figures …….…….……...34

2.8 Tables……...39

2.9 References.……..……40

2.10 Supplementary Information...…….……..……..……48

2.10.1 Supplementary Information Tables…..……..48

2.10.2 Supplementary Information Figures……...…….49

2.10.3 Supplementary Information References…….63

Chapter 3. Secondary Aerosol Formation from Mixtures of Marine Volatile Organic Compounds in a Potential Aerosol Mass Oxidative Flow Reactor ….……65

3.1 Abstract……..…...……...…….…...65

3.2 Environmental Significance…….66

3.3 Introduction.…….……...…….66

3.4 Methods…….....……..…..…...69

3.4.1 Experimental Setup……...……...….....69

3.4.2 Quantification of VOCs…….…….....…...70

3.4.3 Quantification of sulfate and methane sulfonic acid……...……...…..….....71

3.4.4 Particle size distribution measurements…..……...……...….....…72

3.4.5 Real time composition of secondary aerosols …….....72

3.5 Results and Discussion……..……...72

3.5.1 Particle size distributions for the oxidation of single VOCs……...…….…...73

3.5.2 Particle size distributions for the oxidation of mixtures …...…….74

3.5.3 Aerosol yields for the oxidation of single VOCs versus mixtures..……....76

3.5.4 MSA and sulfate ratios in bulk secondary aerosol…..……78

3.5.5 MSA and sulfate ratios in individual secondary aerosols …….. …….…….80

3.6 Conclusion……..…….……..…...81

3.7 Author contributions…….……....84

3.8 Conflicts of interest....…….…….……....84

3.9 Acknowledgments……....……..……..…..84

3.10 Figures……...……86

3.11 Tables……....……..…91

3.12 References…….…....……92

3.13 Supplemental Information…….....…….……98

3.13.1 Supplemental Information Figures……..98

3.13.2 Supplemental Information Tables…….111

Chapter 4. Secondary Marine Aerosol Formation from Volatile Organic Compounds Emitted from Phytoplankton

Blooms……...…….111

4.1 Abstract ……...……..…111

4.2 Introduction.……...111

4.3 Methods……..……..……..114

4.3.1 Experimental Setup……..……...114

4.3.2 Quantification of VOCs……...115

4.3.3 Particle Size Distribution Measurements……..……..116

4.4 Results & Discussion…….……..……...116

4.5 Conclusion……..…….……...……121

4.6 Acknowledgements……122

4.7 Figures……123

4.8 References……..……..……...…...……127

4.9 Supplemental Information……...……..…….……...…….131

Chapter 5. Conclusions …….……..…….135

5.1 Synopsis ……..……..…….135

5.2 Conclusions ……..……135

5.2.1 Factors Controlling Production of Dimethyl Sulfide, Methanethiol, and Dimethyl Disulfide During Controlled Phytoplankton-Bacterial Mesocosm Experiments…….135

5.2.2 Secondary Aerosol Formation from Mixtures of Volatile Organic Compounds in a Potential Aerosol Mass Oxidative Flow Reactor ……...136

5.2.3 Secondary Marine Aerosol Formation from Volatile Organic Compounds Emitted from Phytoplankton Blooms……...137

5.3 Ongoing and Future Directions..……..……...137

5.3.1 Factors Controlling Marine Biogenic VOCs……137

5.3.2 Secondary Aerosol Characterization Studies ……...……..138

5.3.3 Secondary Marine Aerosol Formation from Seawater ……139

5.4 References……..141

LIST OF ABBREVIATIONS AND SYMBOLS

ASV	amplicon sequence variants
ATOFMS	aerosol time-of-flight mass spectrometer
Bioaerosols	biological aerosols
BVOC	biogenic volatile organic compound
CCN	cloud condensation nuclei
Chl a	chlorophyll a
CI-TOF-MS	chemical ionization time-of-flight mass spectrometer
cMA-ATOFMS	condensation matrix-assisted aerosol time-of-flight mass spectrometer
CPC	condensation particle counter
DMA	differential mobility analyzer
DMDS	dimethyl disulfide
DMS	dimethyl sulfide
DMSO	dimethyl sulfoxide
DMSP	dimethyl sulfoniopropionate
DOM	dissolved organic matter
EC	electrostatic classifier
FEP	fluorinated ethylene propylene
HB	heterotrophic bacteria

IC	ion chromatography
IEPOX	isoprene epoxy diols
IMR	ion molecule reactor
L	liters
MALDI	matrix assisted laser desorption ionization
MART	marine aerosol reference tank
MeSH	methanethiol
MS	mass spectrometry
m/z	mass to charge ratio
ncps	normalized counts per seconds
Nd:YAG	Neodymium:YAG laser
Nss	non sea-salt
O_3	ozone
OFR	oxidative flow reactors
OH	hydroxyl radical
OSC	organic sulfur compounds
PAM-OFR	potential aerosol mass oxidative flow reactor
PCoA	principal coordinate analysis
PPTV	parts per trillion volume

PPB	parts per billion
RH	relative humidity
SCCM	standard cubic centimeter
SIO	Scripps Institution of Oceanography
SLPM	standard liters per minute
SOA	secondary organic aerosol
SMA	secondary marine aerosol
SMPS	scanning mobility particle sizer
SSA	sea spray aerosol
SSML	sea surface microlayer
TMGN	1,8-bis(tetramethylguanidino)naphthalene
UV	ultraviolet
VOC	volatile organic compound

LIST OF FIGURES

Figure 2.1: Schematic diagram of the experimental setup used to measure the organic sulfur compounds emitted from the three Marine Aerosol Reference Tanks.……...34

Figure 2.2: Mesocosm 1 (left panel), 2 (middle panel), and 3 (right panel) headspace organosulfur compounds plotted with bulk water chlorophyll. a and heterotrophic bacteria cell abundances. Error bars on organosulfur concentrations in A and B reflect ±1σ obtained from averaging three MARTs . Bloom 3 only had one replicate MART.……...…….…….35

Figure 2.3: MeSH:DMS ratio versus Chl. a and Heterotrophic Bacteria over the course of Blooms 1, 2, and 3 in panels A, B, and C, respectively……..…….…….…….36

Figure 2.4: Temporal dynamic of the microbial communities during the bloom experiments. The top fourteen families (including chloroplast) by relative abundance are shown, all other families are grouped in "Others". Replicate MARTs are aggregated in the same bar, identified by the date (mm_dd).……37

Figure 2.5: Fraction of sulfate produced from combined DMDS and MeSH compared to DMS compared between laboratory mesocosm peak chl. a and peak HB with the only known field measurement of DMDS, MeSH, and DMS.…….....…….38

Figure 2.6: Methanethiol dimerization controls: arrangement of CI-TOF-MS sampling apparatus……....49

Figure 2.7: DMDS formed on the CI-TOF-MS inlet from introduced MeSH…….....51

Figure 2.8: Conversion Ratio for DMDS formed on the CI-TOF-MS stainless steel (SS) and perfluoroalkoxy alkane (PFA) inlets from introduced MeSH ……..…..……..… 53

Figure 2.9: a) Purging of organosulfur gases from seawater directly sampled from the outdoor tank, b) MeSH:DMDS concentration ratio obtained from seawater purged with zero air……55

Figure 2.10: Time series gas concentrations of DMS, MeSH, and DMDS for mesocosms 1, 2, and 3 with the calculated conversion ratio assuming all DMDS was formed from MeSH observed…….56

Figure 2.11: Barplots which highlight the temporal dynamic of the microbial communities during the Bloom experiments. The top thirty genera (or ASV, where taxonomic assignment did not reach the genus level) by abundance are shown, all other genera are grouped in "Others". Replicate MARTs are shown aggregated in the same bar, identified by the date (mm_dd).…….57

Figure 2.12: Metadata auto-correlation (Pearson correlation coefficient; * $p < 0.05$; ** $p < 0.01$; *** $p < 0.001$)…….58

Figure 2.13: PCoA ordination based on Bray-Curtis matrix from the ASV table. Samples are colored according to the concentration of (a) DMS (b) DMDS and (c) MeSH divided into quartiles. Bloom experiments are identified by different shapes……...59

Figure 2.14: Robust Aitchison PCA. Samples are colored according to the concentration of (a) DMS, (b) DMDS and (c) MeSH. Circles, rectangles and rings identify Bloom1, Bloom2 and Bloom3, respectively…….60

Figure 2.15: Boxplots which show alpha diversity of each Bloom experiment by Shannon and Inverse Simpson indices (* $p < 0.05$; ** $p < 0.01$; *** $p < 0.001$, Kruskall-Wallis test).…….61

Figure 3.1: Schematic diagram of experimental setup used for secondary marine aerosol reaction studies.……..……..…86

Figure 3.2: Particle number (top) and volume (bottom) distributions for low, medium and high OH exposure (VOCs and mixtures combined on each panel)……...……..87

Figure 3.3: Aerosol yields for VOCs and mixtures. (A) Pure compounds. (B) Mixtures. Error bars represent the standard deviation of three trials……...…….88

Figure 3.4: MSA and sulfate molar fractions for DMS, DMDS, and mixtures with isoprene. Error bars represent the standard deviation of four trials…..……..……...89

Figure 3.5: Fraction of 60 nm particles produced by the different VOCs and mixtures that contain MSA, sulfate, and sulfuric acid. Colors represent the fraction of particles that present peak areas falling in specific ranges…….90

Figure 3.6: Calibration curve for PAM-OFR lamps…….……..……...……97

Figure 3.7: Particle number and volume distribution parameters for low, medium and high OH exposure (VOCs and mixtures).……..…..…….……..…..98

Figure 3.8: Percent non-reacted gas for DMS, DMDS and isoprene yield experiments…….....100

Figure 3.9: Non-reacted gas (in %) for mixture yield experiments (left: DMS and isoprene, right: DMDS and isoprene)…..……..…….…….……101

Figure 3.10: Aerosol yields vs. aerosol mass increase for individual VOCs and mixtures. A. Pure compounds. B. Mixtures. Dashed lines correspond to the fitting of the absorptive partitioning model from Odum et al. (1996). Error bars represent the standard deviation of three trials…..…….……..…..…….....102

Figure 3.11: MSA and sulfate aerosol concentrations molar fractions for DMS, DMDS, and mixtures with isoprene. Error bars represent the standard deviation of four trials…….…….....103

Figure 3.12: Sulfate molar fraction for DMS, DMDS, DMS/isoprene and DMDS/isoprene experiments. P-values under 0.01 and 0.05 are shown for a paired t-test (two tails). Error bars represent the standard deviation of four trials……..…….....104

Figure 3.13: MSA molar fraction for DMS, DMDS, DMS/isoprene and DMDS/isoprene experiments. P-values under 0.01 are shown for a paired t-test (two tails). Error bars represent the standard deviation of four trials……...105

Figure 3.14: Average mass spectra of 60 nm particles produced by various VOCs and mixtures after they have been coated with matrix TMGN (red lines). Black lines represent the average spectra of homogeneously nucleated TMGN particles……..……..…106

Figure 3.15: Average mass spectra of 20 nm particles produced by various VOCs and mixtures after they have been coated with matrix TMGN (red lines). Black lines represent the average spectra of homogeneously nucleated TMGN particles……...…….107

Figure 3.16: Fraction of 20 nm particles produced by the different VOCs and mixtures that contain MSA and sulfate. Colors represent the fraction of particles that present peak areas falling in specific ranges….…….108

Figure 3.17: Positive and negative mode Orbitrap spectra from the mixture of DMS, DMDS, and Isoprene. Sulfate, MSA, and dimethyl sulfoxide (DMSO) have been identified……..…109

Figure 4.1: Schematic diagram for the three experimental conditions.……..…..123

Figure 4.2: Headspace DMS, DMDS, and isoprene concentrations for bloom 1 (top), bloom 2 (middle), and bloom 3 (bottom) co-plotted with the chlorophyll a concentration. The VOC concentrations are an average of a daily 30 min sampling period…… 124

Figure 4.3: Particle number distributions over the course of bloom 1 (A), bloom 2 (B), and bloom 3 (C)…….125

Figure 4.4: Bar plot of DMS, DMDS, and isoprene concentrations co-plotted with the aerosol number concentrations over the course of each bloom.……..…….……...….....126

Figure 4.5: Calibration curve for the PAM-OFR ……..……..…….131

Figure 4.6: Correlation between DMDS concentration and methanethiol (MeSH) normalized counts per seconds…….....……...….132

Figure 4.7: Time series of MeSH and monoterpenes normalized counts per second (ncps) co-plotted with chlorophyll a (chl. a) over the course of three blooms ……..……133

Figure 4.8: Aerosol volume for each bloom co plotted with chl. a …….…….134

LIST OF TABLES

Table 2.1: Taxa identified on high concentration (4^{th} quartile) of the three gases by Indicator Species Analysis ($p < 0.001$)……..……...……...…….39

Table 2.2: Medium Nutrient Concentrations…….48

Table 3.1: Experimental conditions for aerosol yield experiments……..…….....91

Table 3.2: Experimental conditions for aerosol filter experiments ……..……110

ACKNOWLEDGEMENTS

I would like to thank my advisor and mentor, Professor Kimberly Prather, for her unwavering support and guidance throughout my time in graduate school. She has continually encouraged me to explore new ideas and think about the bigger picture. Kim has also supported my passion for education and outreach. I cannot thank her enough for all the advice and opportunities she has provided for me. I am also grateful to my committee members: Professor Rommie Amaro, Professor Andrew Kummel, Professor Todd Martz, and Professor Michael Tauber, for their guidance and feedback. All past and present Prather lab members have been a tremendous source of support both inside and outside the lab, and I will always be thankful for the guidance and friendships. A special thank you goes to Dr. Robert Pomeroy for welcoming me into his lab as an undergraduate summer student. That opportunity introduced me to the exciting field of atmospheric chemistry and the research opportunities at UCSD. He has been an exceptional mentor and has provided invaluable advice. I would also like to thank Monica Castrejon for everything she does for the lab and all our chats. This would not be possible without her. A heartfelt thank you to Brandon for his love and encouragement that helped me get to the finish line. Lastly, I would like to express my deepest gratitude to my amazing parents, Wayne and Jacqueline, and my sister, Kristen, for their endless love and support.

Chapter 2, in full, is currently being prepared for submission for publication of the material. Sauer, J. S., Moore, A. N., Malfatti, F., Ametrano, C., Minich, J. J., Dinasquet, J., Mayer, K. J., Santander, M. D., Pendergraft, M., Mitts, B., Lee, C., Wang, X., Rico, B., Knight. R., Bertram, T. B., & Prather, K. A., (2021). “Factors Controlling Production of Dimethyl Sulfide, Methanethiol, and Dimethyl Disulfide During Controlled Mesocosm Experiments” Jon Sauer is the primary

investigator and first author of the manuscript. The dissertation author is the second author of this manuscript and analyzed data, generated figures, and re-wrote and edited the manuscript.

Chapter 3, in full, is a reprint of material with permission from *Environmental Science: Atmospheres*, 2024. Moore, A. N., Cancelada, L., Kimble, K. A., & Prather, K. A. "Secondary Marine Aerosol Formation from Mixtures of Volatile Organic Compounds in a Potential Aerosol Mass Oxidative Flow Reactor" *Environmental. Sciences.: Atmospheres, 2024,**4**, 351-361*. Copyright 2024 Royal Society of Chemistry. The dissertation author and Lucia Cancelada are the primary investigators and co-first authors of this manuscript.

Chapter 4, in full, is currently being prepared for submission for publication of the material. Moore, A. N. & Prather, K. A. (2024). "Secondary Marine Aerosol Formation from Volatile Organic Compounds Emitted from Phytoplankton Blooms." The dissertation author is the primary investigator and author of this manuscript.

VITA

2018 - Bachelor of Science in Chemistry, Howard University

2020 - Master of Science in Chemistry, University of California San Diego

2024 – Doctor of Philosophy in Chemistry, University of California San Diego

Publications

- Moore, A. N., Cancelada, L, Kimble, K. A., & Prather, K. A. (2024). Secondary aerosol formation from mixtures of marine volatile organic compounds in a potential aerosol mass oxidative flow reactor. Environmental Science: Atmospheres. 4. 10.1039/d3ea00169e.

- Kilgour, D. B., Novak, G. A., Sauer, J. S., Moore, A. N., Dinasquet, J., Amiri, S., ... & Bertram, T. H. (2022). Marine gas-phase sulfur emissions during an induced phytoplankton bloom. *Atmospheric Chemistry and Physics*, *22*(2), 1601-1613.

- Sauer, J. S., Mayer, K. J., Lee, C., Alves, M. R., Amiri, S., Bahaveolos, C. J., ... & Prather, K. A. (2022). The Sea Spray Chemistry and Particle Evolution Study (SeaSCAPE): Overview and Experimental Methods. *Environmental Science: Processes & Impacts*.

- Franklin, E. B., Alves, M. R., Moore, A. N., Kilgour, D. B., Novak, G. A., Mayer, K., ... & Goldstein, A. H. (2021). Atmospheric Benzothiazoles in a Coastal Marine Environment. *Environmental science & technology*, *55*(23), 15705-15714.

- Sauer, J. S., Simkovsky, R., Moore, A. N., Camarda, L., Sherman, S. L., Prather, K. A., & Pomeroy, R. S. (2021). Continuous measurements of volatile gases as detection of algae crop health. *Proceedings of the National Academy of Sciences*, *118*(40).

- Santander, M. V., Mitts, B. A., Pendergraft, M. A., Dinasquet, J., Lee, C., Moore, A. N., ... & Prather, K. A. (2021). Tandem Fluorescence Measurements of Organic Matter and Bacteria Released in Sea Spray Aerosols. *Environmental Science & Technology*, *55*(8),

5171-5179.

- Angle, K. J., Crocker, D. R., Simpson, R. M., Mayer, K. J., Garofalo, L. A., Moore, A. N., ... & Grassian, V. H. (2021). Acidity across the interface from the ocean surface to sea spray aerosol. *Proceedings of the National Academy of Sciences*, *118*(2).

Presentations

- **Moore, A. N**., Sauer, J. S., Mayer, K. J., Amiri, S., Rico, B., & Prather, K. A. (2019, October) Quantitative Measurement of Organosulfur Compounds Over the Course of a Phytoplankton Bloom Using Cryo Purge and Trap Chemical Ionization Mass Spectrometry. NOBCChE National Meeting

- **Moore, A. N**., Sauer, J. S., Mayer, K. J., Amiri, S., Rico, B., & Prather, K. A. (2019, December). Cryo Purge and Trap Chemical Ionization Mass Spectrometry for the Quantitative Measurement of Organosulfur Compounds Over the Course of a Phytoplankton Bloom. In *AGU Fall Meeting Abstracts* (Vol. 2019, pp. A33P-2923).

- **Moore, A. N**., Cancelada, L. B., & Prather, K. A (2021, October). Analysis of Secondary Marine Aerosol Formation from a Mixture of Volatile Organic Compounds. Invited Talk, ACS Rocky Mountain Regional Meeting.

- **Moore, A. N.**, Cancelada, L. B., & Prather, K. A. (2022, September) Analysis on the Formation of Secondary Aerosols from Mixtures of VOCs. NOBCChE National Meeting

- **Moore, A. N**. & Prather, K. A. (2023, September). Chemical Composition of Secondary Marine Aerosols. NOBCChE National Meeting

- **Moore, A. N.**, Cancelada, L. B., Kimble, K. A., & Prather, K. A. (2023, August) Secondary Marine Aerosol Formation from Mixtures of VOCs in a Potential Aerosol Mass Oxidative Flow Reactor. ACS Fall Meeting

Awards

- National Science Foundation Graduate Research Fellowship Program (April 2018-Present)
- UC-HBCU Fellowship (July 2018-Present)
- UCSD Chemistry Department Miller Award (July 2018)

Volunteer Experience

- **Student and Postdoc Leadership Team,** NSF CAICE, (2020-Present)
- **Principal Member,** Black Graduate and Professional Student Association (2018-Present)
- **Member**, Society for Women in Graduate Studies (SWIGS) (2018 – Present)
- **Co-Funding Chair**, ACS Graduate Student Symposium Planning Committee (2018 – 2019)

ABSTRACT OF THE DISSERTATION

Volatile Organic Compounds: The Connection Between the Ocean and Atmosphere

by

Alexia Nicole Moore

Doctor of Philosophy in Chemistry

University of California San Diego, 2024

Professor Kimberly Prather, Chair

The oceans cover 71% of the world and are a large contributor of volatile organic compounds (VOCs) and aerosols. Marine VOCs can be produced from marine microbiology and emitted from the atmosphere to undergo oxidative processing to form secondary marine aerosols (SMA). Dimethyl sulfide (DMS) has been studied extensively because of phytoplankton and bacteria's ability to produce it in large quantities and because of its ability to form sulfate aerosol and contribute to the earths global radiative budget. However, only studying DMS has left many uncertainties on the contribution of marine VOCs on SMA formation. To better understand the

impact of marine VOCs, this dissertation utilized phytoplankton bloom experiments to quantify VOC emissions from seawater and oxidation experiments to assess the role of VOCs on the number, size, and composition of secondary marine aerosols. Throughout this dissertation, dimethyl disulfide (DMDS) was found to be produced in larger quantities than expected and play a significant role in impacting aerosol number concentrations. Overall, this dissertation highlights the importance of other VOCs, with and without sulfur, contributing to the overall composition of the atmosphere.

Chapter 1. Introduction

Oceans emit particles, known as primary marine aerosols, and gases, typically volatile organic compounds (VOCs), which contribute significantly to the dynamics of the atmosphere. (Carpenter and Nightingale, 2015) Chemical processes control the lifetime, composition, and concentrations of these marine aerosols and VOCs. Both primary aerosols and VOCs can react with oxidants, such as hydroxyl radicals and ozone, to generate secondary marine aerosols (SMA). Primary aerosols and SMA can contribute to earth's radiative budget directly by absorbing and scattering light and indirectly by acting as cloud condensation nuclei (CCN), changing the clouds' albedo and lifetime. (Carpenter et al., 2012; Twomey, 1974) The following sections will discuss VOCs and SMA more thoroughly and the tools used to analyze them throughout this dissertation.

1.1 Volatile Organic Compounds

Marine volatile organic compounds are a result of biological activity and abiotic processes such as photochemical reactions at the sea surface microlayer (SSML) (Carpenter and Nightingale, 2015). The oceans are made up of a diverse and complex mixture of VOCs, many of which have not been identified (Yu and Li, 2021a). Of that mixture, the most abundant marine compound is dimethyl sulfide (DMS), contributing 28 Tg of sulfur a year to the atmosphere. Given its abundance, DMS has been one of the most studied marine VOCs. One of the major findings of research on DMS is the CLAW hypothesis, which proposed that increased emissions of DMS from phytoplankton resulted in non-sea salt sulfate (nss-sulfate) aerosols that acted as CCN, increasing cloud albedo and thereby creating a climate feedback loop (Charlson et al., 1987). Although DMS has been the focus of marine VOC production research, other compounds such as isoprene and amines can be emitted from the ocean as well. Isoprene has been shown to be produced

biologically, as well as photochemically through the excitation of dissolved organic matter in the SSML (Ciuraru et al., 2015; Dani and Loreto, 2017).

1.2 Biological production of VOCs

Most marine VOCs are a result of interactions between marine microbes and photodegradation of organic matter. Marine organisms can utilize VOCs as a source of nutrients or produce them as a stress response, influencing the availability of VOCs to be transferred through the air-sea interface. Through various interactions, known as the microbial loop, phytoplankton will release a plethora of compounds that make up a pool of dissolved organic matter (DOM), which is then consumed by bacteria that release gases and nutrients upon consumption. One of the most abundant liable compounds found in DOM is dimethyl sulfoniopropionate (DMSP), which is an osmolyte produced by phytoplankton for regulatory and antioxidative purposes (Wolfe et al., 2002). Sulfur containing compounds such as DMS and methanethiol (MeSH) are all derived from DMSP when cleaved by heterotrophic bacteria to form either DMS or MeSH. The switch between the production of DMS and MeSH production, termed the "bacterial switch" is determined by the carbon and sulfur needs of local bacteria. Dimethyl disulfide (DMDS), is known to be produced from abiotic dimerization of MeSH and thought to have some biological production from DMSP, although the pathways are currently unknown (Cozic et al., 2008; Perraud et al., 2016). Other compounds, such as isoprene and monoterpenes, historically known as terrestrial emissions, are also found in marine systems from phytoplankton emissions (Shaw et al., 2010). In some biologically active marine regions, isoprene has been measured in the same magnitude as DMS, emphasizing the need to study the production and reaction pathways of other VOCs (Dani and Loreto, 2017). Both laboratory and field measurements have found correlations between chlorophyll a (chl. a), a proxy for measuring biological activity, and VOC emissions (Kim et al.,

2017). Furthermore, satellite measurements have found that biologically produced VOCs attributed 35-80% of CCN in the Southern Ocean (Vallina et al., 2006). While it has been shown there is a connection between biological activity and clouds, further studies are needed to determine which VOCs contribute and the processes involved in the formation of aerosols.

1.3 Marine Aerosols

With oceans covering 71% of the earth's surface, marine aerosols constitute a large source of particle mass to the atmosphere, including being the most significant contributor in remote marine regions (Mansour et al., 2020). Primary marine aerosols are emitted from wave breaking and bubble bursting and can be composed of many compounds including sea salt, organics, and biological material (Lewis and Schwartz, 2004; Facchini et al., 2008; Prather et al., 2013). Primary aerosols can undergo oxidation or experience heterogeneous reactions which alter their chemistry and ultimately their ability to form clouds or ice. Field studies have proven challenging to separate primary and secondary aerosols and assess each of their contributions to the climate. Therefore, laboratory studies have been used to isolate primary and secondary aerosols (Mayer et al., 2020).

1.4 Secondary Marine Aerosols

Secondary marine aerosols (SMA) are formed from the oxidation of VOCs by hydroxyl radical (OH) or ozone (O_3) to form low volatile products that can condense onto existing aerosols or can nucleate to form new particles (Yu and Li, 2021b). SMA are composed of sulfate, ammonia, nitrate, and organics. The oxidation of DMS occurs through two pathways, abstraction and addition, to form sulfate and methanesulfonic acid (MSA). Sulfate is known to contribute to nucleation and MSA is known to promote condensation onto existing particles thereby encouraging particle growth (Hodshire et al., 2019). While sulfate is generally the largest

contributor to SMA during periods of high biological activity, the organic fraction plays a significant role in shaping the aerosol size distributions and determining an aerosol's ability to act as a CCN. A field study in the north Atlantic detected the presence of organics in newly formed nucleation mode particles and concluded they likely derived from biological activity (Vaattovaara et al., 2006). In a laboratory experiment utilizing an oxidative flow reactor to oxidize a mixture of VOCs with isoprene, a shift in the particle size distribution to larger diameters was measured (Ahlberg et al., 2017). With secondary marine aerosols contribution to clouds strongly dependent on their number, size, and composition, it is imperative to study the impact organic compounds have on the formation of aerosols.

1.5 Mass Spectrometry

Mass spectrometry is a technique that is used to generate ions to measure the mass to charge (m/z) ratio and abundance of compounds. It is a frequently used technique that can operate on-line or off-line and measure VOCs or aerosols. In this dissertation, three mass spectrometers were used: Aerosol Time-of-Flight Mass Spectrometer (ATOFMS), High Resolution Orbitrap Mass Spectrometer, and a Chemical Ionization Time-of-Flight Mass Spectrometer (CI-TOF-MS). The ATOFMS is the first on-line single particle mass spectrometer that is used to conduct size-resolved chemical analysis. This powerful instrument works by using two continuous wave lasers to determine the size of the particle, triggering a Nd:YAG desorption ionization laser producing positive and negative ions for each particle (Gard et al., 1997). The ATOFMS is size limited below 100 nm, so a matrix assisted laser desorption ionization method was deployed to grow SMA particles 60 nm and below to 400 nm, allowing them to be detected by the ATOFMS (Li et al., 2023).

Some advantages of on-line instruments are continuous real time monitoring and lack of sample preparation, making them useful for marine and atmospheric studies. However, some limitations like lower mass resolution can make complimenting on-line techniques with off-line instruments extremely beneficial. High resolution instruments, such as the Orbitrap Mass Spectrometer, provide highly accurate and precise m/z ratios for all detected ions. These instruments use electrospray ionization, which is a soft ionization technique to reduce fragmentation, allowing for detection of the parent ion. In this dissertation, Orbitrap Mass Spectrometry was used to measure the composition of secondary marine aerosols. This has been proven to be one of the best instruments for measuring organics in aerosols because most on-line aerosol instruments fragment the organic compounds (Cui et al., 2019).

1.6 Chemical Ionization Mass Spectrometer

The CI-TOF-MS measures the m/z and abundance of gas phase compounds in both positive and negative modes (Benson et al., 2010; Brophy and Farmer, 2015; Yuan et al., 2016). CI-TOF-MS provides advantages over other mass spectrometers because it provides soft ionization leading to limited fragmentation and selective ionization. This means depending on the ionization source, a complex or simplistic spectra can be generated. Chemical ionization works by selecting a reagent gas (e.g., benzene, water clusters, acetate) to generate ions using a Po-210 source. The reagent ions then react with the analyte gas in the ion-molecule reaction (IMR) chamber (Bertram et al., 2011). Reactions will occur between the reagent ion and analyte gas, producing analyte ions, if the chemical energies of the reagent and analyte permit. The reactions will primarily occur through charge transfer, only if the ionization energy of the analyte is lower than that of the reagent ion (Kim et al., 2016). A charge transfer reaction using benzene is shown below:

$$C_6H_6^+ + M \rightarrow M^+ + C_6H_6 \qquad \text{Charge Transfer}$$

In this dissertation, the reagent ion benzene ($C_6H_6^+$) was used because it is selective to marine biogenic VOCs, due to it having an ionization energy of 9.25 EV (Allgood et al., 1990; Kim et al., 2016; Lavi et al., 2018). Specifically, it is efficient at measuring organosulfur compounds, amines, monoterpenes, and isoprene. Additionally, benzene's ionization efficiency is in the middle of the range, so it creates a more simplified spectra than something like water clusters where many compounds can be ionized with it. CI-TOF-MS has been used as an on-line instrument for many atmospheric measurements because it can be run consistently for long periods of time and the fast-sampling rate of 10 Hz has also allowed it to be effective at measuring rapid changes in gas concentrations (Kim et al., 2016) .

1.7 Potential Aerosol Mass Oxidative Flow Reactor

Oxidative flow reactors have been used for years to generate OH radicals as a means to replicate the oxidative processes occurring in the atmosphere. Oxidation with OH radicals is one of the most important and significant reactions in the atmosphere. Not only has the hydroxyl radical been termed the "detergent" of the atmosphere because of its ability to remove trace gases, it is one of the most reactive gases in the atmosphere, oxidizing a plethora of VOCs, leading to the formation of SMA (Gligorovski et al., 2015).

The Potential Aerosol Mass Oxidative Flow Reactor (PAM-OFR, Aerodyne Inc.) is a reactor that generates OH radicals from water vapor using 185 nm or 254 nm low pressure Hg lamps (E. Kang et al., 2007). In this dissertation, 185 nm lamps were used to generate OH radicals from the photolysis of H_2O through the following reactions:

$$O_2 \xrightarrow{185} O_3 \xrightarrow{254} \cdot OH$$

$$H_2O \xrightarrow{185} \cdot OH$$

The PAM-OFR was created to generate high concentrations of OH radicals with low residence times in the reactor. Using the global tropospheric concentration of hydroxyl radicals $1.5x10^6$ molecules cm^{-3}, a calculation can be used to determine the approximate days of aging in the PAM-OFR. Compared to large reaction chambers that produce low concentrations of OH radicals with residence times of hours to days and only simulate minutes to hours of aging, the PAM-OFR shortens the residence time to minutes and simulate days to weeks of aging by generating high concentrations of OH radicals. While the PAM-OFR operates best with 100 to 1,000 times higher the daily tropospheric oxidant concentrations, the ratios between OH/HO_2 and OH/O_3 are the same (E. Kang et al., 2007). The advantages of having real time oxidation measurements in a matter of minutes has made the PAM-OFR a highly utilized and well characterized flow reactor for simulating atmospheric reactions (Ahlberg et al., 2017; Lambe et al., 2015; Zhao et al., 2021). Very limited studies have used the PAM-OFR to look at marine systems and more analysis is needed to characterize the atmospheric fate of these systems in the PAM (Mayer et al., 2020; Trueblood et al., 2019).

1.8 Dissertation Objectives

This dissertation focuses on understanding the emissions of organosulfur compounds from marine biological activity and uncovering the impact different gas mixtures have on secondary marine aerosol production. Mass spectrometry techniques are used to measure VOC concentrations and to identify the composition of secondary aerosols to assess the impact marine

emissions and atmospheric oxidation has on clouds and the environment. The questions that will be addressed in this dissertation include:

1. How does biological activity impact the production of non-DMS organosulfur compounds during phytoplankton blooms?
2. How do mixtures of volatile organic compounds change the size, number concentration, and composition of secondary marine aerosols compared to single VOC studies?
3. How do changes in biological production of sulfur and non-sulfur volatile organic compounds change the production of secondary marine aerosols?

1.9 Dissertation Synopsis

Chapter 2 of this dissertation analyses the emissions of VOCs during three phytoplankton blooms to assess the connection between biological activity and organosulfur compounds. This study showed that dimethyl disulfide and methanethiol can be produced in concentrations that exceed that of dimethyl sulfide. Modeling these results uncovered that non-DMS compounds can contribute, more than expected, to the formation of sulfate aerosols.

Chapter 3 compares oxidation of single VOC and VOC mixtures to address a lack of studies observing secondary aerosol formation of complex mixtures and to understand how mixtures affect the number, size, and composition of these aerosols. This study determined that isoprene mixed with DMS and DMDS significantly impacted the aerosol yield of sulfate and methanesulfonic acid. Notably, this is the first reported aerosol yield measurement of DMS and DMDS in a PAM-OFR.

Chapter 4 describes the production of secondary marine aerosols from VOCs emitted from phytoplankton blooms to examine how realistic and complex mixtures change the aerosol formation. This study further solidifies the importance of dimethyl disulfide in enhancing the number concentration of aerosol particles as shown in Chapter 3. Additionally, changes in the size distributions determined that even at low concentrations, isoprene and monoterpenes can contribute significantly to the composition of aerosols.

1.10 Acknowledgements

Raymond Leibensperger III and Ke'La Kimble are acknowledged for their assistance in editing this chapter.

1.11 References

Ahlberg, E., Falk, J., Eriksson, A., Holst, T., Brune, W.H., Kristensson, A., Roldin, P., Svenningsson, B., 2017. Secondary organic aerosol from VOC mixtures in an oxidation flow reactor. Atmos. Environ. 161, 210–220. https://doi.org/10.1016/J.ATMOSENV.2017.05.005

Allgood, C., Lin, Y., Ma, Y. -C, Munson, B., 1990. Benzene as a selective chemical ionization reagent gas. Org. Mass Spectrom. 25, 497–502. https://doi.org/10.1002/oms.1210251003

Benson, D.R., Markovich, A., Al-Refai, M., Lee, S.H., 2010. A chemical ionization mass spectrometer for ambient measurements of ammonia. Atmospheric Meas. Tech. 3, 1075–1087. https://doi.org/10.5194/amt-3-1075-2010

Bertram, T.H., Kimmel, J.R., Crisp, T.A., Ryder, O.S., Yatavelli, R.L.N., Thornton, J.A., Cubison, M.J., Gonin, M., Worsnop, D.R., 2011. A field-deployable, chemical ionization time-of-flight mass spectrometer. Atmospheric Meas. Tech. 4, 1471–1479. https://doi.org/10.5194/amt-4-1471-2011

Brophy, P., Farmer, D.K., 2015. A switchable reagent ion high resolution time-of-flight chemical ionization mass spectrometer for real-time measurement of gas phase oxidized species: Characterization from the 2013 southern oxidant and aerosol study. Atmospheric Meas. Tech. 8, 2945–2959. https://doi.org/10.5194/amt-8-2945-2015

Carpenter, L.J., Archer, D., Beale, R., Archer, S.D., 2012. Chem Soc Rev Ocean-atmosphere trace gas exchange w 6473–6506. https://doi.org/10.1039/c2cs35121h

Carpenter, L.J., Nightingale, P.D., 2015. Chemistry and Release of Gases from the Surface Ocean. Chem. Rev. 115, 4015–4034. https://doi.org/10.1021/cr5007123

Charlson, R.J., Lovelock, J.E., Andreae, M.O., Warren, S.G., 1987. Oceanic phytoplankton, atmospheric sulphur, cloud albedo and climate. Nat. 1987 3266114 326, 655–661. https://doi.org/10.1038/326655a0

Ciuraru, R., Fine, L., Pinxteren, M.V., Anna, B.D., Herrmann, H., Lyon, U.D., Recherches, I.D., 2015. Unravelling New Processes at Interfaces: Photochemical Isoprene Production at the Sea Surface. https://doi.org/10.1021/acs.est.5b02388

Cozic, A., Viollier, E., Chiffoleau, J.-F., Knoery, J., Rozuel, E., 2008. Interactions between Volatile Reduced Sulfur Compounds and Metals in the Seine Estuary (France). Estuaries Coasts 31, 1063–1071. https://doi.org/10.1007/s12237-008-9099-7

Cui, T., Green, H.S., Selleck, P.W., Zhang, Z., O'brien, R.E., Gold, A., Keywood, M., Kroll, J.H., Surratt, J.D., 2019. Chemical Characterization of Isoprene- and Monoterpene-Derived

Secondary Organic Aerosol Tracers in Remote Marine Aerosols over a Quarter Century. ACS Earth Space Chem. 3. https://doi.org/10.1021/acsearthspacechem.9b00061

Dani, K.G.S., Loreto, F., 2017. Trade-Off Between Dimethyl Sul fi de and Isoprene Emissions from Marine Phytoplankton. Trends Plant Sci. 22, 361–372. https://doi.org/10.1016/j.tplants.2017.01.006

Facchini, M.C., Rinaldi, M., Decesari, S., Carbone, C., Finessi, E., Mircea, M., Fuzzi, S., Ceburnis, D., Flanagan, R., Nilsson, E.D., de Leeuw, G., Martino, M., Woeltjen, J., O'Dowd, C.D., 2008. Primary submicron marine aerosol dominated by insoluble organic colloids and aggregates. Geophys. Res. Lett. 35. https://doi.org/10.1029/2008GL034210

Gard, E., Mayer, J.E., Morrical, B.D., Dienes, T., Fergenson, D.P., Prather, K.A., 1997. Real-Time Analysis of Individual Atmospheric Aerosol Particles: Design and Performance of a Portable ATOFMS. Anal. Chem. 69, 4083–4091. https://doi.org/10.1021/ac970540n

Gligorovski, S., Strekowski, R., Barbati, S., Vione, D., 2015. Environmental Implications of Hydroxyl Radicals (•OH). Chem. Rev. 115, 13051–13092. https://doi.org/10.1021/cr500310b

Hodshire, A.L., Campuzano-Jost, P., Kodros, J.K., Croft, B., Nault, B.A., Schroder, J.C., Jimenez, J.L., Pierce, J.R., 2019. The potential role of methanesulfonic acid (MSA) in aerosol formation and growth and the associated radiative forcings. Atmospheric Chem. Phys. 19, 3137–3160. https://doi.org/10.5194/ACP-19-3137-2019

Kang, E., Root, M.J., Toohey, D.W., Brune, W.H., 2007. Introducing the concept of Potential Aerosol Mass (PAM). Atmospheric Chem. Phys. 7, 5727–5744. https://doi.org/10.5194/acp-7-5727-2007

Kim, M.J., Novak, G.A., Zoerb, M.C., Yang, M., Blomquist, B.W., Huebert, B.J., Cappa, C.D., Bertram, T.H., 2017. Air-Sea exchange of biogenic volatile organic compounds and the impact on aerosol particle size distributions. Geophys. Res. Lett. 44, 3887–3896. https://doi.org/10.1002/2017GL072975

Kim, M.J., Zoerb, M.C., Campbell, N.R., Zimmermann, K.J., Blomquist, B.W., Huebert, B.J., Bertram, T.H., 2016. Revisiting benzene cluster cations for the chemical ionization of dimethyl sulfide and select volatile organic compounds. Atmospheric Meas. Tech. 9, 1473–1484. https://doi.org/10.5194/amt-9-1473-2016

Lambe, A.T., Chhabra, P.S., Onasch, T.B., Brune, W.H., Hunter, J.F., Kroll, J.H., Cummings, M.J., Brogan, J.F., Parmar, Y., Worsnop, D.R., Kolb, C.E., Davidovits, P., 2015. Effect of oxidant concentration, exposure time, and seed particles on secondary organic aerosol chemical composition and yield. Atmospheric Chem. Phys. 15, 3063–3075. https://doi.org/10.5194/ACP-15-3063-2015

Lavi, A., Vermeuel, M.P., Novak, G.A., Bertram, T.H., 2018. The sensitivity of benzene cluster cation chemical ionization mass spectrometry to select biogenic terpenes. Atmospheric Meas. Tech. 11, 3251–3262. https://doi.org/10.5194/amt-11-3251-2018

Lewis, E.R., Schwartz, S.E., 2004. Sea Salt Aerosol Production: Mechanisms, Methods, Measurements and Models—A Critical Review. Geophys. Monogr. Ser. 152, 3719. https://doi.org/10.1029/GM152

Li, L., Kimble, K.A., Mitts, B.A., Heilig, M., Qiao, Y., Lee, J., Prather, K.A., Hogan, C.J., 2023. Nanoparticle growth in thermally diffusive sublimation-condensation systems with low vapor pressure solids. J. Aerosol Sci. 173. https://doi.org/10.1016/j.jaerosci.2023.106225

Mansour, K., Decesari, S., Facchini, M.C., Belosi, F., Paglione, M., Sandrini, S., Bellacicco, M., Marullo, S., Santoleri, R., Ovadnevaite, J., Ceburnis, D., O'Dowd, C., Roberts, G., Sanchez, K., Rinaldi, M., 2020. Linking Marine Biological Activity to Aerosol Chemical Composition and Cloud-Relevant Properties Over the North Atlantic Ocean. J. Geophys. Res. Atmospheres 125, e2019JD032246. https://doi.org/10.1029/2019JD032246

Mayer, K.J., Wang, X., Santander, M.V., Mitts, B.A., Sauer, J.S., Sultana, C.M., Cappa, C.D., Prather, K.A., 2020. Secondary Marine Aerosol Plays a Dominant Role over Primary Sea Spray Aerosol in Cloud Formation. https://doi.org/10.1021/acscentsci.0c00793

Perraud, V., Meinardi, S., Blake, D.R., Finlayson-Pitts, B.J., 2016. Challenges associated with the sampling and analysis of organosulfur compounds in air using real-time PTR-ToF-MS and offline GC-FID. Atmospheric Meas. Tech. 9, 1325–1340. https://doi.org/10.5194/amt-9-1325-2016

Prather, K.A., Bertram, T.H., Grassian, V.H., Deane, G.B., Stokes, M.D., DeMott, P.J., Aluwihare, L.I., Palenik, B.P., Azam, F., Seinfeld, J.H., Moffet, R.C., Molina, M.J., Cappa, C.D., Geiger, F.M., Roberts, G.C., Russell, L.M., Ault, A.P., Baltrusaitis, J., Collins, D.B., Corrigan, C.E., Cuadra-Rodriguez, L.A., Ebben, C.J., Forestieri, S.D., Guasco, T.L., Hersey, S.P., Kim, M.J., Lambert, W.F., Modini, R.L., Mui, W., Pedler, B.E., Ruppel, M.J., Ryder, O.S., Schoepp, N.G., Sullivan, R.C., Zhao, D., 2013. Bringing the ocean into the laboratory to probe the chemical complexity of sea spray aerosol. Proc. Natl. Acad. Sci. U. S. A. 110, 7550–7555. https://doi.org/10.1073/pnas.1300262110

Shaw, S.L., Gantt, B., Meskhidze, N., 2010. Production and Emissions of Marine Isoprene and Monoterpenes: A Review. Adv. Meteorol. 2010, 408696. https://doi.org/10.1155/2010/408696

Trueblood, J.V., Wang, X., Or, V.W., Alves, M.R., Santander, M.V., Prather, K.A., Grassian, V.H., 2019. The Old and the New: Aging of Sea Spray Aerosol and Formation of Secondary Marine Aerosol through OH Oxidation Reactions. ACS Earth Space Chem. 3, 2307–2314. https://doi.org/10.1021/acsearthspacechem.9b00087

Twomey, S., 1974. Pollution and the planetary albedo. Atmospheric Environ. 1967 8, 1251–1256. https://doi.org/10.1016/0004-6981(74)90004-3

Vaattovaara, P., Huttunen, P.E., Yoon, Y.J., Joutsensaari, J., Lehtinen, K.E.J., O'Dowd, C.D., Laaksonen, A., 2006. The composition of nucleation and Aitken modes particles during coastal nucleation events: evidence for marine secondary organic contribution. Atmospheric Chem. Phys. 6, 4601–4616. https://doi.org/10.5194/acp-6-4601-2006

Vallina, S.M., Simó, R., Gassó, S., 2006. What controls CCN seasonality in the Southern Ocean? A statistical analysis based on satellite-derived chlorophyll and CCN and model-estimated OH radical and rainfall. Glob. Biogeochem. Cycles 20, 2005GB002597. https://doi.org/10.1029/2005GB002597

Wolfe, G.V., Strom, S.L., Holmes, J.L., Radzio, T., BradyOlson, M., 2002. Dimethylsulfoniopropionate cleavage by marine phytoplankton in response to mechanical, chemical, or dark stress. J. Phycol. 38, 948–960. https://doi.org/10.1046/j.1529-8817.2002.t01-1-01100.x

Yu, Z., Li, Y., 2021a. Marine volatile organic compounds and their impacts on marine aerosol—A review. Sci. Total Environ. 768, 145054. https://doi.org/10.1016/j.scitotenv.2021.145054

Yu, Z., Li, Y., 2021b. Marine volatile organic compounds and their impacts on marine aerosol—A review. Sci. Total Environ. 768, 145054. https://doi.org/10.1016/j.scitotenv.2021.145054

Yuan, B., Koss, A., Warneke, C., Gilman, J.B., Lerner, B.M., Stark, H., De Gouw, J.A., 2016. A high-resolution time-of-flight chemical ionization mass spectrometer utilizing hydronium ions (H3O+ ToF-CIMS) for measurements of volatile organic compounds in the atmosphere. Atmospheric Meas. Tech. 9, 2735–2752. https://doi.org/10.5194/amt-9-2735-2016

Zhao, R., Zhang, Q., Xu, X., Zhao, W., Yu, H., Wang, W., Zhang, Y., Zhang, W., 2021. Effect of experimental conditions on secondary organic aerosol formation in an oxidation flow reactor. Atmospheric Pollut. Res. 12, 205–213. https://doi.org/10.1016/j.apr.2021.01.011

Chapter 2. Factors Controlling Production of Dimethyl Sulfide, Methanethiol, and Dimethyl Disulfide During Controlled Mesocosm Experiments

2.1 Abstract

The oceans cover 71% of the Earth's surface, yet we understand far less about biogenic volatile organic compounds (BVOCs) derived from the ocean compared to those over land. Dimethylsulfide has been the most studied oceanic BVOC due to its role in the production of sulfate aerosols which seed marine clouds and impact climate. Compared to DMS, less measurements exist of other reactive organosulfur compounds due in part to their more reactive nature and shorter atmospheric lifetimes. Here we measured the temporal evolution of DMS, methanethiol (MeSH) and dimethyl disulfide (DMDS) in isolated Marine Aerosol Reference Tanks (MARTs) over the course of three phytoplankton-bacterial blooms. Notably, the concentrations of MeSH and DMDS can rival or even exceed those of DMS. Furthermore, MeSH and DMDS display different temporal trends, peaking after DMS. These differences can be explained by the growth dynamics of phytoplankton and an increase in heterotrophic bacteria concentrations. Lastly, a model comparison using experimental (MeSH+DMDS)/DMS) production ratios with existing measurements from studies in the literature supports that under certain conditions MeSH and DMDS production can in fact dominate in marine environments, especially in coastal waters. This study highlights the necessity of considering additional reactive sulfur species in marine environments to fully account for the impact of ocean emissions on clouds and climate, as secondary aerosols produced by more than just DMS may significantly contribute to the marine atmosphere.

2.2 Introduction

Ocean emissions of organosulfur compounds (OSCs) play an important role in regulating clouds and climate. Marine dimethylsulfide (DMS), contributing 28 Tg(S) yr^{-1} to the atmosphere, has been the most studied organosulfur compound to date (Lana et al., 2011). Methanethiol (MeSH) and dimethyl disulfide (DMDS) are also emitted from the ocean but have been far less studied, leading to gaps in our understanding on the drivers of their emissions and subsequent role in atmospheric processes and climate. DMS and MeSH are produced from the multifunctional osmolyte dimethylsulfoniopropionate (DMSP) (Simó, 2001) DMSP can be degraded by heterotrophic bacteria either through enzymatic cleavage to form DMS or, preferentially, DMSP can undergo demethylation and demethiolation to form MeSH (Kiene et al., 2000). The production of DMS and MeSH from DMSP has been shown to be highly dependent on the bacterial species present, the relative expression of the two pathways, and structure of the microbial community found in the surface ocean waters (Stefels et al., 2007). Dimethyl disulfide (DMDS) in marine surface waters is thought to be from abiotic MeSH oxidation, although kinetics and details on the factors that control this process in seawater are not understood (Masdeu-Navarro et al., 2024). Even with a significant effort being placed on quantitatively constraining marine biogenic emissions of OSCs, further targeted studies are needed to elucidate the microbial connection to OSC production.

Heterotrophic bacteria play an important role in sulfur cycling in the marine environment by degrading and producing OSC compounds (Simó, 2001). As mentioned previously, bacterial enzymes can convert DMSP through two different pathways leading to DMS through cleavage and MeSH from demethylation. One of the main functions of heterotrophic bacteria is degrading and/or utilizing organic matter which include proteins, lipids, amino acids, and humic substances

(Moran and Durham, 2019). While interacting with dissolved organic matter, heterotrophic bacteria can also release sulfur-containing compounds (Sun et al., 2016). In contrast, bacteria can utilize dissolved sulfur compounds as a source of carbon and energy, creating a sink of both DMS and MeSH (Boden et al., 2010).

In the marine boundary layer, the lifetimes of DMS, MeSH, and DMDS are relatively short, 33h, 4.1h, and 0.7h respectively (Wine et al., 1981). As a result of its longer lifetime, DMS is more commonly detected and has been reported in far more studies than MeSH and DMDS. Aqueous purge and trap measurements have been able to provide more insight into these highly reactive sulfur species. In Kettle et al. (2001), field measurements transecting the Atlantic Ocean, they observed higher aqueous MeSH concentrations in coastal regions and using the aqueous concentrations, their calculated (MeSH/(MeSH+DMS)) flux ratios resulted in some periods with higher MeSH to DMS relative fluxes (Kettle et al., 2001). More recent measurements of dissolved MeSH in the North East Pacific and atmospheric MeSH in the southwest Pacific have generally agreed with these findings, with MeSH:DMS aqueous concentration ratios of 0.19-0.50 and (MeSH/(MeSH+DMS)) flux ratios of 0.14-0.24 in each of these regions of the Pacific (Lawson et al., 2020). Limited field measurements have shown DMS to be the dominant marine OSC, with MeSH occupying the remainder of the balance with trace levels of DMDS. However, in some cases, this picture changes in more productive zones with MeSH taking a greater role. To better understand the emissions of MeSH and DMDS, laboratory measurements providing better time resolution are needed.

Once in the atmosphere, DMS, MeSH, and DMDS are rapidly oxidized by OH radicals to produce lower volatility products that can partition into the aerosol phase either by condensation

onto existing aerosols, or through new particle formation. The main oxidation products of DMS and DMDS, sulfate and methanesulfonic acid, have been shown to enhance new particle formation and particle growth. DMDS is more reactive and leads to 2x more sulfate than DMS, potentially having more of an impact on cloud formation. Laboratory yield experiments have shown that DMDS can have aerosol yields that exceed those of DMS, leading to similar or even higher atmospheric concentrations (Moore et al., 2024; Van Rooy et al., 2021). While the oxidation products of MeSH are not well understood, they are expected to be similar to those of DMS (Lee and Brimblecombe, 2016). Novak et al. (2022), modeled the emissions of MeSH and showed that MeSH oxidation by OH radicals produces SO_2, a precursor to sulfate aerosols, at roughly 99% yield (Novak et al., 2022).

To address the complexity of OSC production and the impact on the composition of the marine atmosphere, we utilized controlled laboratory bloom experiments to study the underlying processes driving OSC formation. In this study, three mesocosm incubation experiments were conducted to measure the temporal evolution of the production of OSCs during a phytoplankton-bacterial bloom. Through a combination of atmospheric and seawater measurements, the evolution of the OSC concentrations were measured over the bloom lifetime. We observed DMS, MeSH, and DMDS concentration ratios similar to those measured in oceanic field studies, further substantiating the significant contribution of MeSH and DMDS to sulfate aerosol production. The findings in this study highlight the need to avoid focusing exclusively on DMS, as it may merely serve as a proxy for more reactive sulfur species that have already undergone reactions to form sulfate and other aerosols.

2.3 Methods

2.3.1 Preparation of Mesocosm Incubation Experiments

Seawater was pumped from an inlet 5 meters below the ocean surface on the Ellen Browning Scripps Pier (La Jolla, CA; 32°51´56.8"N: 117° 15´38.48"W). The seawater was filtered with a 50 µm nitex mesh to remove larger debris and zooplankton before addition to an outdoor 2400 L PTFE tank. To protect the water sample from larger falling leaves and insects, a thin polyethylene sheet was suspended ~1 m above the outdoor mesocosm tank reservoir. Natural sunlight irradiated the water surface over the course of the experiment. The seawater was periodically monitored for temperature to ensure conditions remained consistent with coastal San Diego conditions in mid-summer. The tank was aerated and mixed using bubbled air passed through HEPA-filters at ~10 LPM into Tygon tubing held ~0.5 m below the water line. For all three sequential mesocosm incubation experiments, the outdoor tank was acclimated overnight after initial filling, before nutrient addition the following morning. Seawater was supplemented with f/2 algal growth medium (Nutrient Medium Composition in Table 2.2: Proline, Aquatic Eco-Systems, Apopka, FL, Guillard and Ryther, 1962; Andersen at al., 1997), diluted 50x with added 9 µM sodium metasilicate to induce a phytoplankton diatom dominated bloom. Bloom progress was tracked using a handheld fluorometer (Aquafluor, Turner Designs, San Jose, CA) daily. For all three mesocosm experiments (Figure 2.1) water was transferred each morning from the outdoor tank reservoir to three marine aerosol reference tanks (MARTs) (Stokes et al., 2013). Subsequently, each morning after the first day, the water was transferred back from the MARTs into the outdoor tank before the MARTs were re-filled for that morning. After the phytoplankton peak in each bloom, as indicated by daily fluorescence measurements, the water was kept in all

three MART tanks with no further transfers until the end of the experiments. This methodology was implemented due to gradual shearing of phytoplankton biomass by the MART centrifugal pump which can prematurely halt phytoplankton blooms.

2.3.2 Marine Aerosol Reference Tank Operation

The Marine Aerosol Reference Tank (MART) systems were filled with ~110 L of seawater and a plunging sheet of water over a 10 cm free-falling distance. The MART systems produce atmospherically representative SSA in terms of size and composition (Stokes et al., 2013). The size distribution of the resultant bubble plume acquired by hydrophone (ITC 1089d) was referenced to pre-existing size distributions to ensure the proper physical production pathways of SSA. The waterfalls in the MARTs were plunged using a 4 second cycle with the centrifugal pump on, and 10 seconds of no pumping to permit flume degassing and foam creation. Clean air obtained continuously from a zero-air generator (Sabio 1001) was introduced into the MART headspace at a flow rate of 6.6 standard liters per minute (SLPM). The temperature of each MART was maintained at ~26 °C by circulating water through a 316 stainless steel chiller coil immersed in the tank water.

2.3.3 Heterotrophic Bacterial Abundance and Community Structure

Bulk seawater was collected in 5 ml cryovials from the MARTs via a stainless steel side port ~10 cm from the bottom (see (Stokes et al., 2013) for MART details). For bacteria abundance, samples were preserved with glutaraldehyde at 0.05% final concentration and stored at -80^{o}C after flash freezing (Noble and Fuhrman, 1998). Samples were analyzed at The Scripps Research Institute (TSRI) Flow Core Facility with a BIO-RAD, ZE5 Cell Analyzer flow cytometer. Briefly,

samples were diluted (1:10) in 1×TE buffer (pH 8), then stained with SYBR Green I at room temperature for 10 min in the dark (Gasol and Giorgio, 2000). For 16S rDNA gene amplicon sequencing, 400 µL seawater was sampled every day from the MART and immediately frozen at -80 ^{o}C to preserve microbiome integrity (Song et al., 2016). Samples were processed following the Earth Microbiome Project protocols (http://wwwearthmicrobiome.org), V4 region for primer, with modifications for low biomass input. (Caporaso et al., 2012) The DNA was extracted from samples using the KatharoSeq low biomass methodology, ((Minich et al., 2019, 2018b). Specifically, water samples were thawed on ice for 30 minutes, vortexed, and then 400 µl was transferred into individual bead beating tubes. After extraction, 50 µl of eluted DNA was transferred to 384 well plates. The miniaturized PCR protocol was used to generate libraries with a final reaction volume of 5 µl (0.2 ul gDNA, 0.2 µl barcoded primers),(Minich et al., 2018a). For sequencing, an equal volume of amplicon was pooled across all samples, followed by a cleanup using the QIAquick PCR purification kit (Qiagen, Cat# 28106). The obtained raw reads were processed performing quality control by fastQC (Andrews, 2010), they were then loaded into QIIME2 ((Bolyen et al., 2019; Gonzalez et al., 2018). to obtain the Amplicon Sequence Variants (ASV) table and the taxonomic assignment. ASV table, taxonomy and metadata (including OSCs measurement) were then analyzed by a custom R (4.2.1) script exploiting the packages microeco (Liu et al., 2021), indicspecies (De Cáceres et al., 2012), phyloseq (McMurdie and Holmes, 2013), vegan (Dixon, 2003) and mecodev. Detailed information is reported in the section “Bioinformatics and statistics” in Supplementary Information.

2.3.4 BVOC Measurements

BVOC measurements were made using a chemical ionization time-of-flight mass spectrometer (CI-TOF-MS) using benzene cluster ion chemistry, as described in (Kim et al., 2016). Benzene ion clusters were chosen as the reagent ion due to the high sensitivity towards the detection of reactive sulfur species. Briefly, ~300 ppm benzene gas is prepared via a flow of 10 standard cubic centimeters per minute (sccm) medical grade N_2 over a cylinder of liquid benzene (LCMS Grade, Sigma Aldrich). Benzene vapor was then diluted by N_2 and passed through a 20mCi Po-210 ionizer. Through N_2 collisions with alpha particles produced by Po-210, benzene cluster cations are generated and delivered into the ion-molecule region (IMR) of the CI-TOF-MS instrument via an inline critical orifice (O'Keefe) at a flow of 1.8 SLPM (Veres et al., 2008). Sample headspace was pulled into the IMR through another orifice at 1.8 SLPM. A secondary bypass pump was utilized to increase sample flow to 2.6 SLPM to reduce the gas residence time in the ~2 m (3.175mm ID) fluorinated ethylene propylene (FEP) tubing which connected the headspace of each MART to the CI-TOF-MS. A sintered glass RH probe (Vaisala) was connected in-line between a sampling tee near the CI-TOF-MS inlet and bypass pump to continuously measure the relative humidity and temperature of the MART headspace. The IMR, based on the design by Kercher et al., 2009, was maintained at empirically derived conditions, 50 °C via heat tape, a pressure of 60 Torr, and 250V DC (Kercher et al., 2009). Analyte ions produced via chemical ionization with benzene cluster cations were passed into a custom-built electrodynamic ion funnel which collects and focuses the ion beam and gently de-clusters ions that may have excess benzene or water molecules attached. A commercial RF-only quadrupole (TOFWERK) transfers the ions into an orthogonal extraction time of flight mass spectrometer. Data acquisition was performed using ToFDAQ software (TOFWERK), with co-summed spectra saved at a rate of

~1 Hz. Data analysis was performed in TOFWARE, (TOFWERK) a graphical interface plugin for IGOR (Wavemetrics), in which mass calibration and baselining procedures were applied to the raw data. Daily ion intensities from each MART tank were normalized to the summed intensity of benzene and its dimer (m/z 78, 156) and averaged for quantitation. During sampling periods in which analyte ion intensity exceeded more than 10% of reagent ion intensity, the sampled MART headspace was diluted by humidified zero air at a tee before the CI-TOF-MS inlet. On each day, at least 30 minutes of mass spectra were averaged from each MART tank. For both DMS and DMDS, external calibrations of each gas using permeation tubes (VICI Metronics) were performed across the humidity range to account for the humidity-dependent sensitivities of each compound. For MeSH, an external calibration was performed after the mesocosm experiments using a 1 ppm MeSH in N2 calibrated gas canister (Airgas) in dry and humid conditions diluted between 0.1 – 80 ppbv matching the MART experiments. The sensitivity for DMS at the water vapor mixing ratio of the MART tanks (17.0 g/kg) was found to be 9.8 normalized counts per second (ncps)/pptv, DMDS 21.2 ncps/pptv, and MeSH 0.3 ncps/pptv. DMS was measured as $[M]^+$ as m/z 62, MeSH as a benzene adduct $[M+78]^+$ at m/z 126, and DMDS as $[M]^+$ at m/z 94. Given the lower-mass resolution of the CI-TOF-MS (<1200 full width at half maximum) ion assignments were made using unit mass resolution leading tothe possibility of unknown ions contributing to ion intensity at the same unit mass. During periods of high OSC ion intensity, isotope ratios for ^{34}S were used to verify the identity of each OSC compound. All three MART tanks daily mass spectra were averaged for phytoplankton blooms 1 and 2. For mesocosm 3, only one MART was used.

2.4 Results and Discussion

Each bloom progressed through three distinct phases, exponential growth, peak bloom, and senescence as indicated by changes in the bulk fluorescence (Figure 2.2). Notably, all three blooms reached different levels of peak fluorescence, equating upon calibration to values ranging from 2.3 – 11.5 µg L^{-1}. These values fall within previous measurements of Chl. a made at the current sampling location (La Jolla, CA), ranging from 0.1 -20 µg L^{-1}, where the 95% quantile resides below 7.73 µg L^{-1} (McGowan et al., 2017). At the start of each experiment, heterotrophic bacteria (HB) counts decreased after the first day, likely in response to the water transfer and adaptation to new conditions (Figure 2.2D-F). After the initial decline, HB counts increased steadily during the bloom lifecycle reaching a max 3.3-9.4 times their minimum concentrations until decreasing during the senescence phase. Daily average measurements of headspace DMS, MeSH, and DMDS (Figure 2.2A-C) showed significant concentration variations over the bloom lifetimes. The observed peak headspace concentrations of each OSC are higher than marine field measurements, due to the lack of reactive species in the tanks, ventilation caused by the plunging waterfall of the MART, and the relatively low flow of zero air through the MART headspace (Davis et al., 1998). The Henry's Law solubility constants for DMS, DMDS, and MeSH, 5.0×10^{-3} mol m^{-3} Pa^{-1}, 7.0×10^{-3} mol m^{-3} Pa^{-1} and 3.8×10^{-3} mol m^{-3} Pa^{-1} respectively, are similar, indicating that the measured headspace ratios of DMDS and MeSH to DMS are not likely caused by disproportionate ventilation effects (Sander, 2015).

During all three blooms, DMS peak coincides with the peak in Chl. a. Furthermore, the magnitude of DMS concentration correlates with the intensity of the Chl. a concentration, with Bloom 1 exhibiting the highest concentrations of both species. Blooms 2 and 3 display lower Chl.

a intensities, resulting in smaller DMS peak concentrations. This result is consistent with global satellite and field measurements that have shown Chl. a serves a strong indicator for the concentration of DMS (Galí et al., 2018; Gros et al., 2023; Wang et al., 2020). In contrast, MeSH and DMDS both peak after Chl. a. In the case of blooms 2 and 3, the maximum concentrations of MeSH and DMDS surpass that of DMS. Notably, heterotrophic bacteria concentrations in the water track MeSH and DMDS, peaking during the death phase of each bloom. We hypothesize that in our setting the interactions among the different bacteria and the bacterial communities were responsible for the production of MeSH and subsequently DMDS.

Measured concentration ratios of MeSH:DMS for all three experiments span two orders of magnitude ranging from values of ~0.2-30 (Figure 2.3A-C). Compared to literature values, the upper end of these values is significantly higher, likely due to the combination of the rich bloom conditions in a laboratory (non-reactive) setting coupled with the coastal seawater microbial community (Leck and Rodhe, 1991). Specifically, Lawson et al. (2020), found the ratio of MeSH:DMS in the gas phase to range from 0.03 to 0.36 during high biological activity in the southwest Pacific Ocean (Lawson et al., 2020). MeSH:DMS concentration ratios were still comparatively high (~10) at the onset of each bloom before the growth phase, suggesting the concentration ratio of MeSH:DMS can reach surprisingly high levels in coastal environments, consistent with ratios observed in marine sediments (Sørensen, 1988; Visscher et al., 1991). Gros et al. (2023), found that the MeSH fraction in relation to the total concentration of DMS + MeSH in the aqueous phase reached a maximum of 50% in the north Atlantic (Gros et al., 2023). In our bloom experiments, the MeSH:DMS ratio peaked during the senescence of the algal bloom, moreover heterotrophic bacteria are known to peak at the expense of senescent phytoplankton biomass (Biddanda and Pomeroy, 1988; Seymour et al., 2017). Our data suggest similar dynamics,

more evident in Bloom 1 and 2 (Figure 2.3A-B). Abundant heterotrophic bacterial communities possibly led to a MeSH:DMS peak, with both MeSH and DMS production mediated by microbes, and DMS possibly being highly utilized by bacteria. However, in Bloom 1 the peaks of heterotrophic bacteria and MeSH:DMS were simultaneous, whereas in Bloom 2 and 3 the sulfur species peaked a few days after the bacteria (Figure 2.3B-C), possibly due to the diversity in the intensity of the phytoplankton bloom. The difference between the MeSH:DMS in bloom 1 vs blooms 2 and 3 can be a result of the changes in the bacterial community and their associated gene expression. We cannot rule out the possibility that the differences among the blooms are driven by the bacterial and phytoplankton production pathways and bacterial degradation processes.

The high levels of DMDS observed in these mesocosm experiments were unexpected given the lack of previous field study observations for DMDS (Leck and Rodhe, 1991; Tanzer and Heumann, 1992). DMDS has been shown to be produced from the conversion of MeSH on stainless steel surfaces (Perraud et al., 2016). To assess whether DMDS was artificially being produced by oxidation in the ~20 cm stainless CI-TOF-MS inlet, several control experiments were performed (Figure 2.7). These controls found as much as ~35% of MeSH could be converted to DMDS in the instrument inlet (Figure 2.8). After changing the CI-TOF-MS inlet to PFA, the conversion ratio was decreased to ~11-15% (Figure 2.8). This indicates the additional DMDS was created by upstream dimerization in the gas regulator, used in the control experiment, or by conversion on the walls of the CI-TOF-MS IMR chamber itself. To contextualize these controls within the mesocosm experiments, the control-obtained conversion ratio (35%) was utilized to calculate the expected MeSH and subsequent DMDS concentrations under the expectation that only the CI-TOF-MS inlet was responsible for MeSH dimerization. We found that on 9 of the 27 days of the mesocosm experiments, DMDS concentrations were 50% higher than those that could

be explained by MeSH dimerization on the inlet alone, indicating that DMDS was indeed being formed naturally during the experiments (Figure 2.10). The submerged stainless steel chiller coil in the MART was found to not contribute to MeSH to DMDS dimerization (Figure 2.9a,b). Our findings agree with recent investigations of OSC measurements which highlight the importance of using materials which limit MeSH conversion to DMDS on instrument and sampling vessel surfaces (Perraud et al., 2016).

The dynamics of the phytoplankton communities and correlations to OSCs were studied over the course of three blooms (Moran and Durham, 2019; Reisch et al., 2011). By gas intensity and similarity of microbial bacterial community, bloom 1 was different than bloom 2 and 3. In all three blooms (Figure 2.4, Figure 2.11 for genus level dynamics), five main families were common and shifted over time. Microbes, especially heterotrophic bacteria, were tightly linked to the source of dissolved organic matter that phytoplankton (and bacteria via microbial loop) produce over the bloom dynamic (Riemann et al., 2000; Teeling et al., 2016, 2012). Flavobacteriaceae, a family characterized by microbes that degrade complex polymers (Cottrell and Kirchman, 2000) and commonly found to be associated with phytoplankton bloom and bloom demise displaying high hydrolytic activities targeting polysaccharides and proteins (Buchan et al., 2014; Nowinski et al., 2019), increased in terms of relative abundance over time. Alteromonadaceae family dominated the community in the early phase and bloom peak. Alteromonadaceae are opportunistic bacteria that are capable of utilizing a wide range of organic species associated with phytoplankton primary production (Pontiller et al., 2022; Bergauer et al., 2017). Rhodobacteraceae are found often associated with the phytoplankton bloom dynamic with taxa that are able to take up organic matter produced by the growing phytoplankton and establishing symbiotic relationship with the microalgae ((Luo and Moran, 2014; Pontiller et al.,

2022). Saprospiraceae play a major role in organic matter degradation in the demise of the phytoplankton bloom due to their enzymatic repertoire mostly proteases (Pontiller et al., 2022; Sakami et al., 2016). Finally, Pseudohongiellaceae (Francis et al., 2021) were consistently present over the bloom dynamics and it is known that they have adaptive strategies to degrade complex to simple algal polysaccharides (Francis et al., 2021).

Based on the OSC species measured, it was possible to link the communities from high to low gas production for all gases measured. High gas production communities were rather diverse in terms of taxonomic composition, thus suggesting the redundancy of the microbial metabolic potentials in transforming the OSCs. While dissolved and particulate DMSP were not measured during these experiments, the distinct temporal shifts in measured OSCs (Figure 2.2) and prokaryotic communities (Figure 2.4 and Figure 2.11) indicate putative relationships between microbes and DMS, DMDS and MeSH. A Mantel test was performed between the distance matrix from the ASV table and distance matrix based on gas metadata for all three blooms combined. The test highlighted a moderate, highly significant, positive correlation (Spearman coefficient 0.352 $p < 0.001$) when DMS, DMDS and MeSH were included (regardless of the presence or the absence of the Chlorophyll a data). DMS and Chlorophyll a were indeed highly auto-correlated (Pearson coeff. = 0.691, $p < 0.001$) (Figure 2.12), contributing in a similar way to the overall correlation. This is consistent with the knowledge that DMSP, the precursor of DMS, is produced by phytoplankton. When considering heterotrophic bacterial and/or viral abundances (which are positively autocorrelated) the positive correlation was slightly weaker (0.261-0.273, $p < 0.001$). Among the OSCs, DMS had the highest correlation with the diversity distance matrix (Spearman coefficient of 0.304, adjusted $p < 0.001$). DMDS and MeSH did not show a highly significant correlation with the diversity distance matrix (Spearman coefficient of 0.102, $p < 0.05$ and 0.169,

$p < 0.01$, respectively). This is possibly due to the diversity being driven by the autotrophic component of the community, which contributes to DMS production in seawater (Kiene et al., 2000), at the beginning of each bloom, as shown by the relative abundance of ASVs assigned to chloroplast (Figure 2.4).

We further analyzed the microbial community data in order to determine if some ASVs were correlated with high OSCs data over the bloom dynamics. The PCoA analysis highlights the temporal dynamic of the blooms. We didn't observe a strong segregation of the bacterial communities according to the OSC concentration (Figure 2.13). Despite this, by using the Indicator Species analysis (Table 1), we found 17 taxa putatively correlated with the highest emission of the three OSCs. Two ASVs characterized the sample with the highest concentration of all three gasses (*Winogradskyella* and ASV2363 in Rhodobacteraceae); three ASVs were identified in sample with the highest concentration of two gasses (*Aestuariibacter*, ASV530 in Rhodobacteriaceae and ASV1192 in Saprospiraceae), while the rest of indicator ASVs were suitable indicators in only one OSC. Among these 5/17 ASVs belonged to Rhodobacteriaceae, 3/17 ASVs to Flavobacteriaceae, 3/17 ASVs to Alteromonadaceae, 3/17 ASVs to Cryomorphaceae, 2/17 ASVs to Saprospiraceae and finally 1/17 ASV to Pseudohogiellaceae. As expected most of the ASVs being indicators for high DMS samples were taxonomically assigned to chloroplasts (data not shown). Based on the taxon finding, we have searched within the bacterial genomes annotated in the KEGG database (Kanehisa and Goto, 2000; https://www.genome.jp/kegg/) OSCs related genes. We found a handful of genes for *Winograskiella*, *Formosa*, *Pseudohongiella*, but no complete pathways were present in the annotations. Moreover the genera *Pseudophaeobacter* and *Aestuariibacter* were not annotated in

KEGG, highlighting the need for more comprehensive marine bacteria reference genome and annotations.

It needs to be stressed that such analyses using ASVs and their taxonomic identification could miss important relationships which are linked more to the ecological role of a taxa rather than to its name, as pointed out in the context of symbiosis, with a concept which is relevant for any ecological relationship (Doolittle and Booth, 2017). Among the most abundant indicator species ASVs, Rhodobacteraceae are known to be important in sulfur cycling in the ocean (Moran and Durham, 2019). Sulfur is intertwined with the carbon biogeochemical cycle since microbes can use it for energy production and also as starting substrates for the synthesis of vitamins, cofactors, signaling compounds and antibiotics. Rhodobacteraceae possess both DMSP demethylation and cleavage pathways (Moran and Durham, 2019 and references therein). *Pseudophaeobacter* and *Alteromonas* were tested in a study for their ability to use DMSP (Liu et al., 2022) as a carbon and energy source. Furthermore, *Alteromonas* presents in its genome genes related to the DMSP demethylation and cleavage pathways (Zhang et al., 2022).

Over the course of the three blooms, the shift from DMS production to MeSH is hypothesized to primarily be the result of a change in bacterial degradation of DMSP. A phenomenon termed “bacterial switch” is theorized to be a change in the processing of DMSP that influences the production of DMS and MeSH (Simó, 2001). Bacteria will switch from the cleavage pathways to the demethylation pathways depending on their demand for carbon or sulfur from DMSP and the availability of other substrates in the water (Simó, 2001). Previous work has shown that the bacterial switch does not necessarily require a change in the bacterial communities because many heterotrophic bacteria contain both genes needed to produce DMS and MeSH. In addition,

the marine bacterium Pelagibacter has been shown to simultaneously produce DMS and MeSH (Sun et al., 2016). While we didn't detect Pelagibacter, further work looking at the dominant marine bacterium in the blooms that contain both pathways, Rhodobacteraceae, should also include testing for the simultaneous production of DMS and MeSH. With the increase of Rhodobacteraceae over the course of the blooms, its presence during high periods of MeSH concentrations, and the knowledge of it containing the demethylation gene, we hypothesize Rhodobacteraceae played an important role in the production of MeSH. Other factors may also have an impact on the production of MeSH and subsequent loss of DMS, such as the transformation of DMS and DMSO from marine bacteria (González et al., 1999).

OSCs in the atmosphere play a major role in the production of secondary marine aerosols, which can act as cloud condensation nuclei, thereby significantly impacting cloud properties and Earth's radiative budget. To assess the potential contribution of DMDS and MeSH to sulfate aerosol production, we calculated the fraction of particulate sulfate formed from DMS, MeSH, and DMDS as a function of the emission ratios of MeSH+DMDS relative to DMS. Estimates of the emission ratios of (MeSH+DMDS)/DMS for ocean conditions (< 0.1) were calculated from the simultaneous measurements of DMS, MeSH, and DMDS aqueous concentrations measured in the North Atlantic (Leck and Rodhe, 1991), using a two-film air-sea transfer model (Johnson, 2010). The (MeSH+DMDS)/DMS emission ratios for this study were reported for both peak Chl. a (0.2 – 0.8) and peak bacteria concentrations (30). By assuming that the aerosol sulfate yield for DMS and MeSH oxidation is 1 and the sulfate yield of DMDS oxidation is 2, the fraction of OSC-derived particulate sulfate is calculated that formed from MeSH + DMDS. As shown in Figure 2.5, for conditions relevant to the North Atlantic, MeSH and DMDS may account for as much as 10% of the non-sea salt sulfate produced from OSC emissions. For the conditions discussed in this study,

MeSH and DMDS emissions would account for over 40% of the non-seasalt sulfate produced from OSC emissions. This represents a potentially significant unappreciated source of OSC and by extension sulfate aerosols in marine environments. DMS to MeSH ratios have been measured to be 2:1 in a coastal environment and 10:1 in a remote environment in the Pacific Ocean (Lawson et al., 2020; Novak et al., 2022). More studies are needed to understand the factors controlling the ratios of non-DMS OSC species.

2.5 Conclusion

During three laboratory phytoplankton-bacteria blooms, MeSH and DMDS were shown to have different temporal behavior and be produced in higher amounts relative to DMS. DMS tracked phytoplankton abundance as indicated by Chl. a concentrations during each bloom. In contrast, both MeSH and DMDS peaked after phytoplankton maxima when heterotrophic bacteria began to increase. This study highlights the impact highly diverse bacterial communities can have on the production of non-DMS OSCs. Bloom 1 had a larger phytoplankton biomass (higher Chl. a concentrations), thus creating in a more intense algal senescence phase, leading to high concentrations of DMS, but low MeSH and DMDS. Whereas, during less intense blooms (blooms 2 and 3) MeSH and DMDS concentrations were higher than DMS.

During the intense senescent phase, we hypothesize that the DOM was highly enriched with sulfur species (eg., methionine, cysteine, sulfur lipids, and coenzyme A) (Pohlabeln and Dittmar, 2015), therefore bacteria did not need to produce MeSH and DMDS to fulfill their sulfur needs. Whereas we hypothesize high MeSH and DMDS concentrations during less intense bloom 2 and 3 were attributed to DMS or DMSP enzymatically modified by bacteria through lysis and demethylation pathways in order to satisfy their S quota (Zhang et al., 2019).

We also observed DMDS at unexpectedly high concentrations; no field observations of ambient DMDS exist for comparison. While we attribute some (up to 35%) of the DMDS detected in the MART experiments to dimerization of MeSH on the instrument inlet, multiple periods of high DMDS significantly exceeded values (>50%) predicted by MeSH conversion indicating production occurred through natural processes in seawater. The faster reactivity and shorter lifetime of DMDS compared to DMS could explain the lack of ambient observations. Based on the consistent observation of DMDS in these blooms, further investigations of MeSH dimerization in natural seawater should be investigated as an additional pathway.

With the production of MeSH occurring over short time periods coupled with the higher reactivity of MeSH and DMDS, few ambient measurements exist of these other important sulfur species. Through modeling, we compare these mesocosm OSC production ratios with measurements from the field. Particularly in coastal regions where heterotrophic bacteria can be highly active, non-DMS OSCs may represent a significant fraction of reactive sulfur species. These additional gas phase sulfur species could result in more secondary marine aerosols which has significant implications for air quality in coastal marine environments. These results highlight the insights that can be gained from complex laboratory experiments by being able to detect reactive compounds that are difficult to detect in the highly reactive atmosphere.

2.6 Acknowledgments, Samples, and Data

The authors gratefully acknowledge the support of the National Science Foundation through the Centers of Chemical Innovation Program via the Center for Aerosol Impacts on Chemistry of the Environment (CHE-1801971). The authors thank Meinrat Andreae for his

constructive comments on this study. The authors declare no financial interests or conflicts of interest pertaining to this work.

Chapter 2, in full, is currently being prepared for submission for publication of the material. Sauer, J. S., Moore, A. N., Malfatti, F., Ametrano, C., Minich, J. J., Dinasquet, J., Mayer, K. J., Santander, M. D., Pendergraft, M., Mitts, B., Lee, C., Wang, X., Rico, B., Knight. R., Bertram, T. B., & Prather, K. A., (2021). "Factors Controlling Production of Dimethyl Sulfide, Methanethiol, and Dimethyl Disulfide During Controlled Mesocosm Experiments" Jon Sauer is the primary investigator and first author of the manuscript. The dissertation author is the second author of this manuscript and analyzed data, generated figures, and re-wrote and edited the manuscript.

2.7 Figures

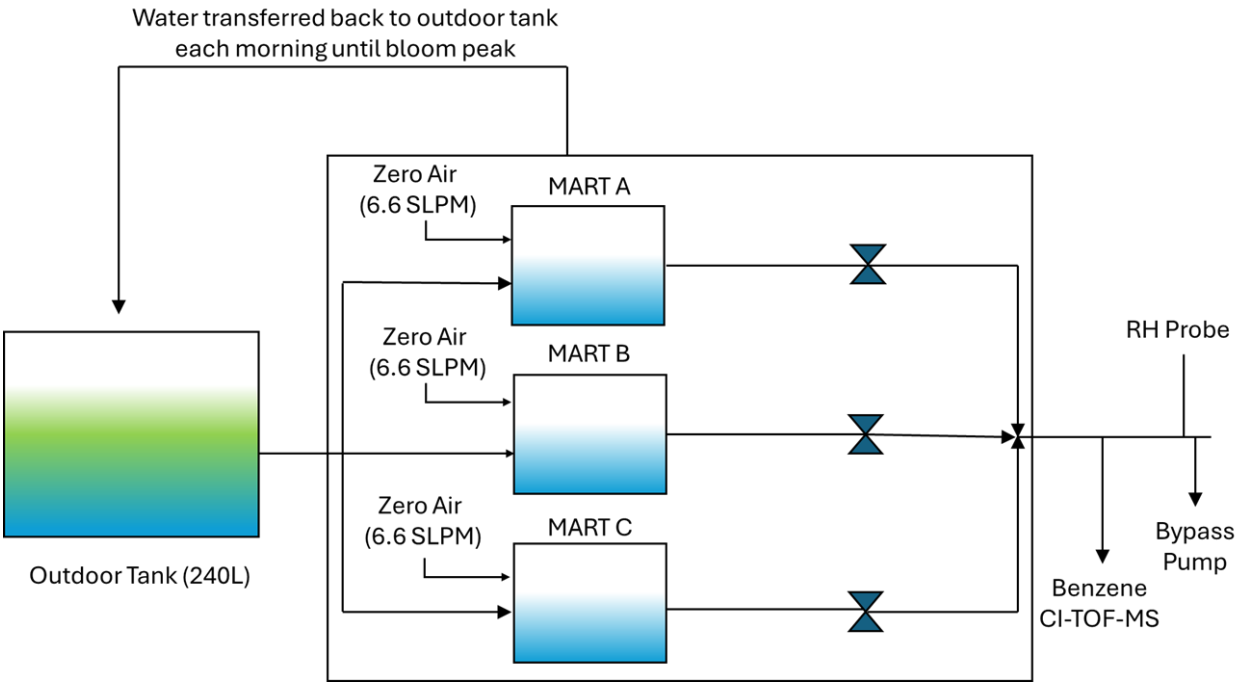


Figure 2.1: Schematic diagram of the experimental setup used to measure the organic sulfur compounds emitted from the three Marine Aerosol Reference Tanks.

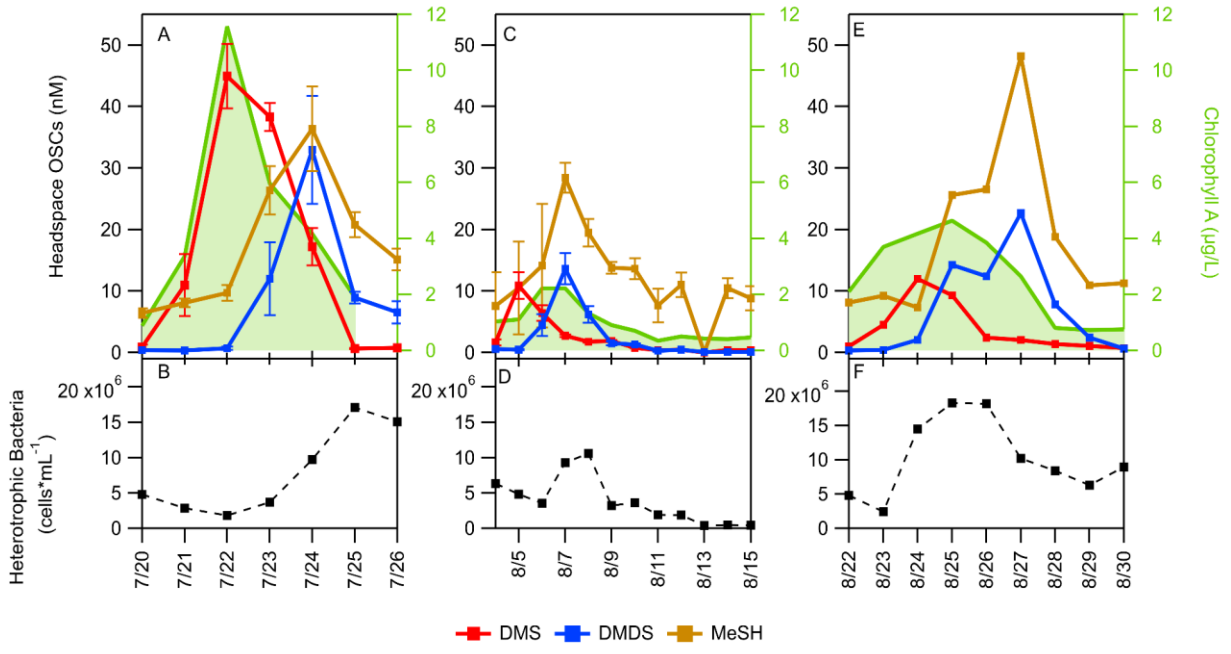


Figure 2.2: Mesocosm 1 (left panel), 2 (middle panel), and 3 (right panel) headspace organosulfur compounds plotted with bulk water chlorophyll a and heterotrophic bacteria cell abundances. Error bars on organosulfur concentrations in A and B reflect ±1σ obtained from averaging three MARTs . Bloom 3 only had one replicate MART.

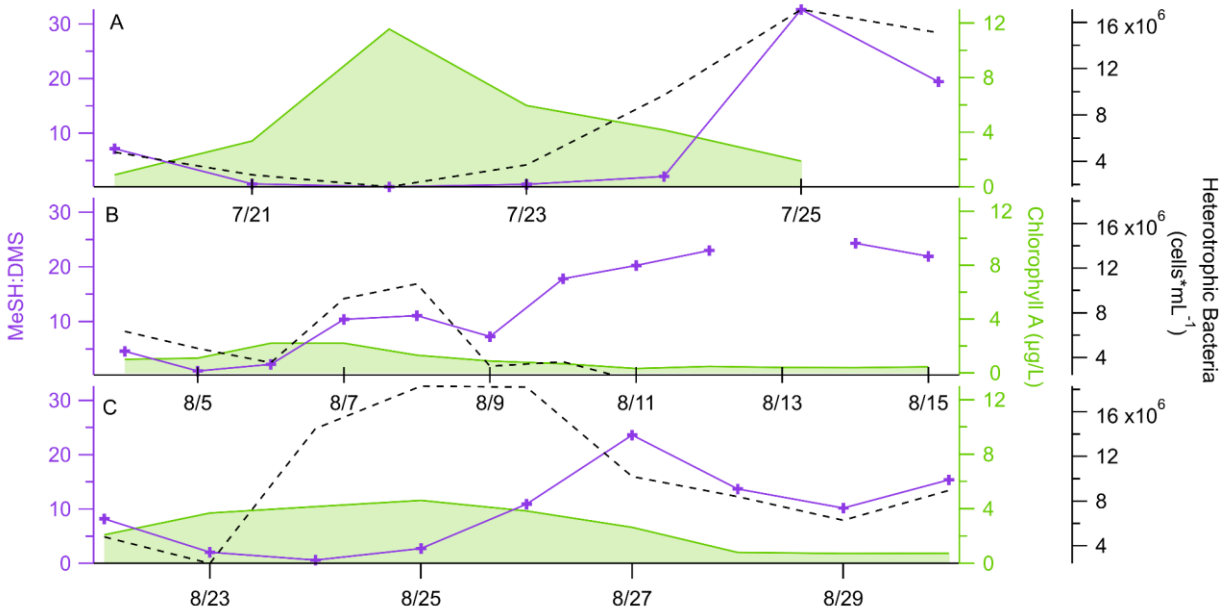


Figure 2.3: MeSH:DMS ratio versus Chl. a and Heterotrophic Bacteria over the course of Blooms 1, 2, and 3 in panels A, B, and C, respectively.

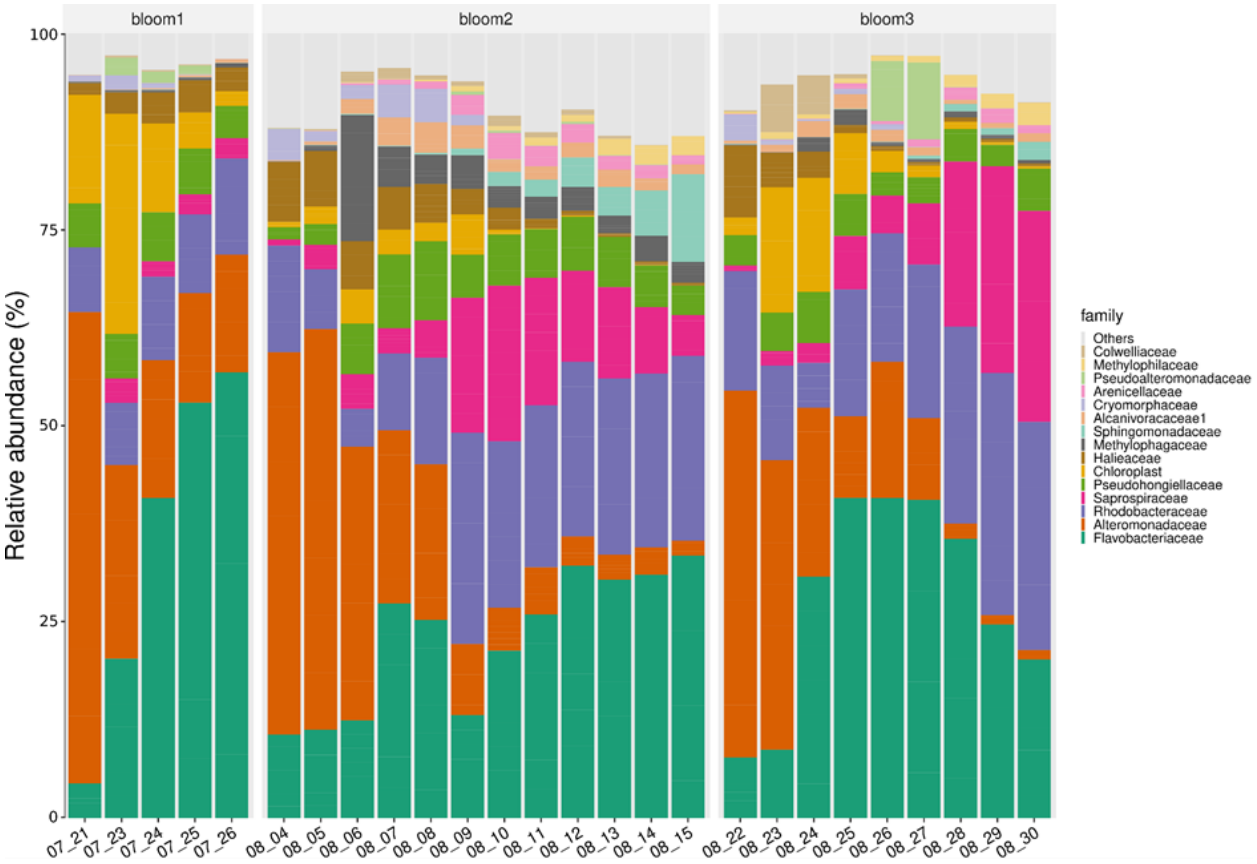


Figure 2.4. Temporal dynamic of the microbial communities during the bloom experiments. The top fourteen families (including chloroplast) by relative abundance are shown, all other families are grouped in "Others". Replicate MARTs are aggregated in the same bar, identified by the date (mm_dd).

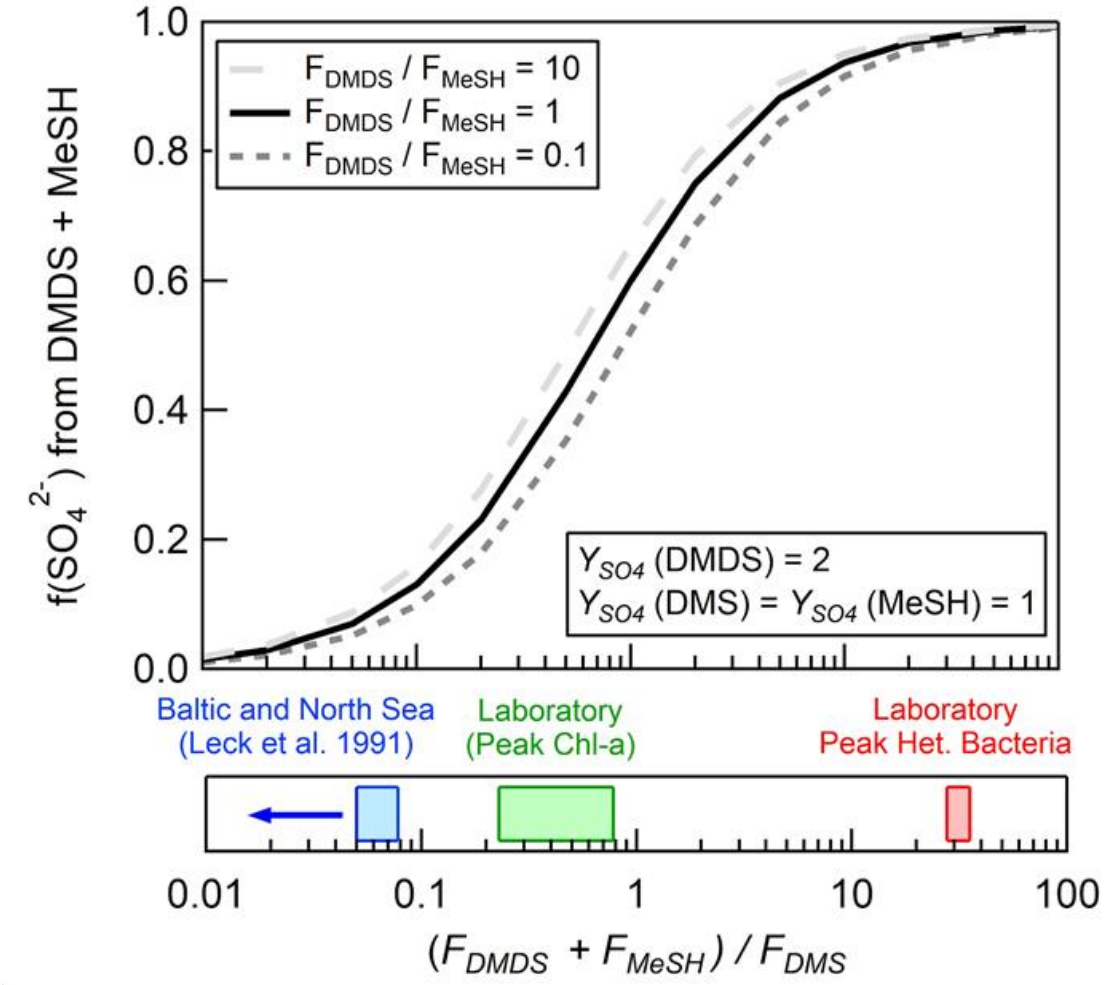


Figure 2.5. Fraction of sulfate produced from combined DMDS and MeSH compared to DMS compared between laboratory mesocosm peak chl. a and peak HB with the only known field measurement of DMDS, MeSH, and DMS.

2.8 Tables

Table 2.1: Taxa identified on high concentration (4th quartile) of the three gases by Indicator Species Analysis ($p < 0.001$)

ASV name	DMS	DMDS	MeSH	family	genus
ASV1840	x	x	x	Flavobacteriaceae	*Winogradskyella*
ASV2363	x	x	x	Rhodobacteraceae	-
ASV1316		x	x	Alteromonadaceae	*Aestuariibacter*
ASV530		x	x	Rhodobacteraceae	-
ASV1192	x		x	Saprospiraceae	-
ASV1454	x			Alteromonadaceae	*Alteromonas*
ASV722	x			Alteromonadaceae	*Alteromonas*
ASV2624		x		Cryomorphaceae	-
ASV231		x		Rhodobacteraceae	-
ASV2813		x		Saprospiraceae	-
ASV14			x	Flavobacteriaceae	*Formosa*
ASV2800			x	Flavobacteriaceae	*Tenacibaculum*
ASV2213			x	Rhodobacteraceae	-
ASV1781			x	Cryomorphaceae	-
ASV117			x	Pseudohongiellaceae	*Pseudohongiella*
ASV761			x	Rhodobacteraceae	*Pseudophaeobacter*
ASV625			x	Cryomorphaceae	-

2.9 References

Biddanda, B., Pomeroy, L., 1988. Microbial aggregation and degradation of phytoplankton-derived detritus in seawater. I. Microbial succession. Mar. Ecol. Prog. Ser. 42, 79–88. https://doi.org/10.3354/meps042079

Boden, R., Kelly, D.P., Murrell, J.C., Schäfer, H., 2010. Oxidation of dimethylsulfide to tetrathionate by Methylophaga thiooxidans sp. nov.: a new link in the sulfur cycle. Environmental Microbiology 12, 2688–2699. https://doi.org/10.1111/j.1462-2920.2010.02238.x

Bolyen, E., Rideout, J.R., Dillon, M.R., Bokulich, N.A., Abnet, C.C., Al-Ghalith, G.A., Alexander, H., Alm, E.J., Arumugam, M., Asnicar, F., Bai, Y., Bisanz, J.E., Bittinger, K., Brejnrod, A., Brislawn, C.J., Brown, C.T., Callahan, B.J., Caraballo-Rodríguez, A.M., Chase, J., Cope, E.K., Da Silva, R., Diener, C., Dorrestein, P.C., Douglas, G.M., Durall, D.M., Duvallet, C., Edwardson, C.F., Ernst, M., Estaki, M., Fouquier, J., Gauglitz, J.M., Gibbons, S.M., Gibson, D.L., Gonzalez, A., Gorlick, K., Guo, J., Hillmann, B., Holmes, S., Holste, H., Huttenhower, C., Huttley, G.A., Janssen, S., Jarmusch, A.K., Jiang, L., Kaehler, B.D., Kang, K.B., Keefe, C.R., Keim, P., Kelley, S.T., Knights, D., Koester, I., Kosciolek, T., Kreps, J., Langille, M.G.I., Lee, J., Ley, R., Liu, Y.-X., Loftfield, E., Lozupone, C., Maher, M., Marotz, C., Martin, B.D., McDonald, D., McIver, L.J., Melnik, A.V., Metcalf, J.L., Morgan, S.C., Morton, J.T., Naimey, A.T., Navas-Molina, J.A., Nothias, L.F., Orchanian, S.B., Pearson, T., Peoples, S.L., Petras, D., Preuss, M.L., Pruesse, E., Rasmussen, L.B., Rivers, A., Robeson, M.S., Rosenthal, P., Segata, N., Shaffer, M., Shiffer, A., Sinha, R., Song, S.J., Spear, J.R., Swafford, A.D., Thompson, L.R., Torres, P.J., Trinh, P., Tripathi, A., Turnbaugh, P.J., Ul-Hasan, S., van der Hooft, J.J.J., Vargas, F., Vázquez-Baeza, Y., Vogtmann, E., von Hippel, M., Walters, W., Wan, Y., Wang, M., Warren, J., Weber, K.C., Williamson, C.H.D., Willis, A.D., Xu, Z.Z., Zaneveld, J.R., Zhang, Y., Zhu, Q., Knight, R., Caporaso, J.G., 2019. Reproducible, interactive, scalable and extensible microbiome data science using QIIME 2. Nat Biotechnol 37, 852–857. https://doi.org/10.1038/s41587-019-0209-9

Buchan, A., LeCleir, G.R., Gulvik, C.A., González, J.M., 2014. Master recyclers: features and functions of bacteria associated with phytoplankton blooms. Nat Rev Microbiol 12, 686–698. https://doi.org/10.1038/nrmicro3326

Caporaso, J.G., Lauber, C.L., Walters, W.A., Berg-Lyons, D., Huntley, J., Fierer, N., Owens, S.M., Betley, J., Fraser, L., Bauer, M., Gormley, N., Gilbert, J.A., Smith, G., Knight, R., 2012. Ultra-high-throughput microbial community analysis on the Illumina HiSeq and MiSeq platforms. ISME J 6, 1621–1624. https://doi.org/10.1038/ismej.2012.8

Cottrell, M.T., Kirchman, D.L., 2000. Natural assemblages of marine proteobacteria and members of the Cytophaga-Flavobacter cluster consuming low- and high-molecular-weight

dissolved organic matter. Appl Environ Microbiol 66, 1692–1697. https://doi.org/10.1128/AEM.66.4.1692-1697.2000

Davis, D., Chen, G., Kasibhatla, P., Jefferson, A., Tanner, D., Eisele, F., Lenschow, D., Neff, W., Berresheim, H., 1998. DMS oxidation in the Antarctic marine boundary layer: Comparison of model simulations and held observations of DMS, DMSO, DMSO2, H2SO4(g), MSA(g), and MSA(p). Journal of Geophysical Research: Atmospheres 103, 1657–1678. https://doi.org/10.1029/97JD03452

De Cáceres, M., Legendre, P., Wiser, S.K., Brotons, L., 2012. Using species combinations in indicator value analyses. Methods in Ecology and Evolution 3, 973–982. https://doi.org/10.1111/j.2041-210X.2012.00246.x

Doolittle, W.F., Booth, A., 2017. It's the song, not the singer: an exploration of holobiosis and evolutionary theory. Biol Philos 32, 5–24. https://doi.org/10.1007/s10539-016-9542-2

Francis, B., Urich, T., Mikolasch, A., Teeling, H., Amann, R., 2021. North Sea spring bloom-associated Gammaproteobacteria fill diverse heterotrophic niches. Environ Microbiome 16, 15. https://doi.org/10.1186/s40793-021-00385-y

Galí, M., Levasseur, M., Devred, E., Simó, R., Babin, M., 2018. Sea-surface dimethylsulfide (DMS) concentration from satellite data at global and regional scales. Biogeosciences 15, 3497–3519. https://doi.org/10.5194/bg-15-3497-2018

Gasol, J.M., Giorgio, P.A.D., 2000. Using flow cytometry for counting natural planktonic bacteria and understanding the structure of planktonic bacterial communities. Scientia Marina 64, 197–224. https://doi.org/10.3989/scimar.2000.64n2197

Gonzalez, A., Navas-Molina, J.A., Kosciolek, T., McDonald, D., Vázquez-Baeza, Y., Ackermann, G., DeReus, J., Janssen, S., Swafford, A.D., Orchanian, S.B., Sanders, J.G., Shorenstein, J., Holste, H., Petrus, S., Robbins-Pianka, A., Brislawn, C.J., Wang, M., Rideout, J.R., Bolyen, E., Dillon, M., Caporaso, J.G., Dorrestein, P.C., Knight, R., 2018. Qiita: rapid, web-enabled microbiome meta-analysis. Nat Methods 15, 796–798. https://doi.org/10.1038/s41592-018-0141-9

González, J.M., Kiene, R.P., Moran, M.A., 1999. Transformation of Sulfur Compounds by an Abundant Lineage of Marine Bacteria in the α-Subclass of the ClassProteobacteria. Applied and Environmental Microbiology 65, 3810–3819. https://doi.org/10.1128/AEM.65.9.3810-3819.1999

Gros, V., Bonsang, B., Sarda-Estève, R., Nikolopoulos, A., Metfies, K., Wietz, M., Peeken, I., 2023. Concentrations of dissolved dimethyl sulfide (DMS), methanethiol and other trace gases in context of microbial communities from the temperate Atlantic to the Arctic Ocean. Biogeosciences 20, 851–867. https://doi.org/10.5194/bg-20-851-2023

Johnson, M.T., 2010. A numerical scheme to calculate temperature and salinity dependent air-water transfer velocities for any gas. Ocean Science 6, 913–932. https://doi.org/10.5194/os-6-913-2010

Kanehisa, M., Goto, S., 2000. KEGG: kyoto encyclopedia of genes and genomes. Nucleic Acids Res 28, 27–30. https://doi.org/10.1093/nar/28.1.27

Kercher, J.P., Riedel, T.P., Thornton, J.A., 2009. Chlorine activation by N_2O_5: simultaneous, in situ detection of $ClNO_2$ and N_2O_5 by chemical ionization mass spectrometry. Atmospheric Measurement Techniques 2, 193–204. https://doi.org/10.5194/amt-2-193-2009

Kettle, A.J., Rhee, T.S., von Hobe, M., Poulton, A., Aiken, J., Andreae, M.O., 2001. Assessing the flux of different volatile sulfur gases from the ocean to the atmosphere. Journal of Geophysical Research: Atmospheres 106, 12193–12209. https://doi.org/10.1029/2000JD900630

Kiene, R.P., Linn, L.J., Bruton, J.A., 2000. New and important roles for DMSP in marine microbial communities, in: Journal of Sea Research. pp. 209–224. https://doi.org/10.1016/S1385-1101(00)00023-X

Kim, M.J., Zoerb, M.C., Campbell, N.R., Zimmermann, K.J., Blomquist, B.W., Huebert, B.J., Bertram, T.H., 2016. Revisiting benzene cluster cations for the chemical ionization of dimethyl sulfide and select volatile organic compounds. Atmospheric Measurement Techniques 9, 1473–1484. https://doi.org/10.5194/amt-9-1473-2016

Lana, A., Bell, T.G., Simó, R., Vallina, S.M., Ballabrera-Poy, J., Kettle, A.J., Dachs, J., Bopp, L., Saltzman, E.S., Stefels, J., Johnson, J.E., Liss, P.S., 2011. An updated climatology of surface dimethlysulfide concentrations and emission fluxes in the global ocean: UPDATED DMS CLIMATOLOGY. Global Biogeochem. Cycles 25, n/a-n/a. https://doi.org/10.1029/2010GB003850

Lawson, S.J., Law, C.S., Harvey, M.J., Bell, T.G., Walker, C.F., de Bruyn, W.J., Saltzman, E.S., 2020. Methanethiol, dimethyl sulfide and acetone over biologically productive waters in the southwest Pacific Ocean. Atmospheric Chemistry and Physics 20, 3061–3078. https://doi.org/10.5194/acp-20-3061-2020

Leck, C., Rodhe, H., 1991. Emissions of marine biogenic sulfur to the atmosphere of northern Europe. J Atmos Chem 12, 63–86. https://doi.org/10.1007/BF00053934

Lee, C.L., Brimblecombe, P., 2016. Anthropogenic contributions to global carbonyl sulfide, carbon disulfide and organosulfides fluxes. Earth-Science Reviews 160, 1–18. https://doi.org/10.1016/j.earscirev.2016.06.005

Liu, C., Cui, Y., Li, X., Yao, M., 2021. microeco: an R package for data mining in microbial community ecology. FEMS Microbiol Ecol 97, fiaa255. https://doi.org/10.1093/femsec/fiaa255

Liu, Jingli, Xue, C.-X., Wang, J., Crombie, A.T., Carrión, O., Johnston, A.W.B., Murrell, J.C., Liu, Ji, Zheng, Y., Zhang, X.-H., Todd, J.D., 2022. Oceanospirillales containing the DMSP lyase DddD are key utilisers of carbon from DMSP in coastal seawater. Microbiome 10, 110. https://doi.org/10.1186/s40168-022-01304-0

Luo, H., Moran, M.A., 2014. Evolutionary Ecology of the Marine Roseobacter Clade. Microbiol Mol Biol Rev 78, 573–587. https://doi.org/10.1128/MMBR.00020-14

Masdeu-Navarro, M., Mangot, J.-F., Xue, L., Cabrera-Brufau, M., Kieber, D.J., Rodríguez-Ros, P., Gardner, S.G., Bergauer, K., Herndl, G.J., Marrasé, C., Simó, R., 2024. Diel variation of seawater volatile organic compounds, DMSP-related compounds, and microbial plankton inside and outside a tropical coral reef ecosystem. Front. Mar. Sci. 11. https://doi.org/10.3389/fmars.2024.1341619

McGowan, J.A., Deyle, E.R., Ye, H., Carter, M.L., Perretti, C.T., Seger, K.D., de Verneil, A., Sugihara, G., 2017. Predicting coastal algal blooms in southern California. Ecology 98, 1419–1433. https://doi.org/10.1002/ecy.1804

McMurdie, P.J., Holmes, S., 2013. phyloseq: an R package for reproducible interactive analysis and graphics of microbiome census data. PLoS One 8, e61217. https://doi.org/10.1371/journal.pone.0061217

Minich, J.J., Humphrey, G., Benitez, R.A.S., Sanders, J., Swafford, A., Allen, E.E., Knight, R., 2018a. High-Throughput Miniaturized 16S rRNA Amplicon Library Preparation Reduces Costs while Preserving Microbiome Integrity. mSystems 3, e00166-18. https://doi.org/10.1128/mSystems.00166-18

Minich, J.J., Sanders, J.G., Amir, A., Humphrey, G., Gilbert, J.A., Knight, R., 2019. Quantifying and Understanding Well-to-Well Contamination in Microbiome Research. mSystems 4, e00186-19. https://doi.org/10.1128/mSystems.00186-19

Minich, J.J., Zhu, Q., Janssen, S., Hendrickson, R., Amir, A., Vetter, R., Hyde, J., Doty, M.M., Stillwell, K., Benardini, J., Kim, J.H., Allen, E.E., Venkateswaran, K., Knight, R., 2018b. KatharoSeq Enables High-Throughput Microbiome Analysis from Low-Biomass Samples. mSystems 3, e00218-17. https://doi.org/10.1128/mSystems.00218-17

Moore, A.N., Cancelada, L., Kimble, K.A., Prather, K.A., 2024. Secondary aerosol formation from mixtures of marine volatile organic compounds in a potential aerosol mass oxidative flow reactor. Environ. Sci.: Atmos. 4, 351–361. https://doi.org/10.1039/D3EA00169E

Moran, M.A., Durham, B.P., 2019. Sulfur metabolites in the pelagic ocean. Nat Rev Microbiol 17, 665–678. https://doi.org/10.1038/s41579-019-0250-1

Noble, R., Fuhrman, J., 1998. Use of SYBR Green I for rapid epifluorescence counts of marine viruses and bacteria. Aquat. Microb. Ecol. 14, 113–118. https://doi.org/10.3354/ame014113

Novak, G.A., Kilgour, D.B., Jernigan, C.M., Vermeuel, M.P., Bertram, T.H., 2022. Oceanic emissions of dimethyl sulfide and methanethiol and their contribution to sulfur dioxide production in the marine atmosphere. Atmos. Chem. Phys 22, 6309–6325. https://doi.org/10.5194/acp-22-6309-2022

Nowinski, B., Motard-Côté, J., Landa, M., Preston, C.M., Scholin, C.A., Birch, J.M., Kiene, R.P., Moran, M.A., 2019. Microdiversity and temporal dynamics of marine bacterial dimethylsulfoniopropionate genes. Environmental Microbiology 21, 1687–1701. https://doi.org/10.1111/1462-2920.14560

Perraud, V., Meinardi, S., Blake, D.R., Finlayson-Pitts, B.J., 2016. Challenges associated with the sampling and analysis of organosulfur compounds in air using real-time PTR-ToF-MS and offline GC-FID. Atmospheric Measurement Techniques 9, 1325–1340. https://doi.org/10.5194/amt-9-1325-2016

Pohlabeln, A.M., Dittmar, T., 2015. Novel insights into the molecular structure of non-volatile marine dissolved organic sulfur. Marine Chemistry 168, 86–94. https://doi.org/10.1016/j.marchem.2014.10.018

Pontiller, B., Martínez-García, S., Joglar, V., Amnebrink, D., Pérez-Martínez, C., González, J.M., Lundin, D., Fernández, E., Teira, E., Pinhassi, J., 2022. Rapid bacterioplankton transcription cascades regulate organic matter utilization during phytoplankton bloom progression in a coastal upwelling system. The ISME Journal 16, 2360–2372. https://doi.org/10.1038/s41396-022-01273-0

Reisch, C.R., Moran, M.A., Whitman, W.B., 2011. Bacterial Catabolism of Dimethylsulfoniopropionate (DMSP). Front Microbiol 2, 172. https://doi.org/10.3389/fmicb.2011.00172

Riemann, L., Steward, G.F., Azam, F., 2000. Dynamics of bacterial community composition and activity during a mesocosm diatom bloom. Appl Environ Microbiol 66, 578–587. https://doi.org/10.1128/AEM.66.2.578-587.2000

Sakami, T., Watanabe, T., Kakehi, S., Taniuchi, Y., Kuwata, A., 2016. Spatial variation of bacterial community composition at the expiry of spring phytoplankton bloom in Sendai Bay, Japan. Gene 576, 610–617. https://doi.org/10.1016/j.gene.2015.10.011

Sander, R., 2015. Compilation of Henry's law constants (version 4.0) for water as solvent. Atmospheric Chemistry and Physics 15, 4399–4981. https://doi.org/10.5194/acp-15-4399-2015

Seymour, J.R., Amin, S.A., Raina, J.-B., Stocker, R., 2017. Zooming in on the phycosphere: the ecological interface for phytoplankton–bacteria relationships. Nat Microbiol 2, 1–12. https://doi.org/10.1038/nmicrobiol.2017.65

Simó, R., 2001. Production of atmospheric sulfur by oceanic plankton: biogeochemical, ecological and evolutionary links. Trends in Ecology & Evolution 16, 287–294. https://doi.org/10.1016/S0169-5347(01)02152-8

Simon, Andrews, n.d. Babraham Bioinformatics - FastQC A Quality Control tool for High Throughput Sequence Data [WWW Document]. URL https://www.bioinformatics.babraham.ac.uk/projects/fastqc/ (accessed 8.27.24).

Song, S.J., Amir, A., Metcalf, J.L., Amato, K.R., Xu, Z.Z., Humphrey, G., Knight, R., 2016. Preservation Methods Differ in Fecal Microbiome Stability, Affecting Suitability for Field Studies. mSystems 1, e00021-16. https://doi.org/10.1128/mSystems.00021-16

Sørensen, J., 1988. Dimethylsulfide and methane thiol in sediment porewater of a Danish estuary. Biogeochemistry 6, 201–210. https://doi.org/10.1007/BF02182996

Stefels, J., Steinke, M., Turner, S., Malin, G., Belviso, S., 2007. Environmental constraints on the production and removal of the climatically active gas dimethylsulphide (DMS) and implications for ecosystem modelling. Biogeochemistry 83, 245–275. https://doi.org/10.1007/s10533-007-9091-5

Stokes, M.D., Deane, G.B., Prather, K., Bertram, T.H., Ruppel, M.J., Ryder, O.S., Brady, J.M., Zhao, D., 2013. A Marine Aerosol Reference Tank system as a breaking wave analogue

for the production of foam and sea-spray aerosols. Atmospheric Measurement Techniques 6, 1085–1094. https://doi.org/10.5194/amt-6-1085-2013

Sun, J., Todd, J.D., Thrash, J.C., Qian, Y., Qian, M.C., Temperton, B., Guo, J., Fowler, E.K., Aldrich, J.T., Nicora, C.D., Lipton, M.S., Smith, R.D., De Leenheer, P., Payne, S.H., Johnston, A.W.B., Davie-Martin, C.L., Halsey, K.H., Giovannoni, S.J., 2016. The abundant marine bacterium Pelagibacter simultaneously catabolizes dimethylsulfoniopropionate to the gases dimethyl sulfide and methanethiol. Nature Microbiology 1, 16065. https://doi.org/10.1038/nmicrobiol.2016.65

Tanzer, D., Heumann, K.G., 1992. Gas Chromatographic Trace-Level Determination of Volatile Organic Sulfides and Selenides and of Methyl Iodide in Atlantic Surface Water. International Journal of Environmental Analytical Chemistry 48, 17–31. https://doi.org/10.1080/03067319208027039

Teeling, H., Fuchs, B.M., Becher, D., Klockow, C., Gardebrecht, A., Bennke, C.M., Kassabgy, M., Huang, S., Mann, A.J., Waldmann, J., Weber, M., Klindworth, A., Otto, A., Lange, J., Bernhardt, J., Reinsch, C., Hecker, M., Peplies, J., Bockelmann, F.D., Callies, U., Gerdts, G., Wichels, A., Wiltshire, K.H., Glöckner, F.O., Schweder, T., Amann, R., 2012. Substrate-Controlled Succession of Marine Bacterioplankton Populations Induced by a Phytoplankton Bloom. Science 336, 608–611. https://doi.org/10.1126/science.1218344

Teeling, H., Fuchs, B.M., Bennke, C.M., Krüger, K., Chafee, M., Kappelmann, L., Reintjes, G., Waldmann, J., Quast, C., Glöckner, F.O., Lucas, J., Wichels, A., Gerdts, G., Wiltshire, K.H., Amann, R.I., 2016. Recurring patterns in bacterioplankton dynamics during coastal spring algae blooms. eLife 5, e11888. https://doi.org/10.7554/eLife.11888

Van Rooy, P., Purvis-Roberts, K.L., Silva, P.J., Nee, M.J., Cocker, D., 2021. Characterization of secondary products formed through oxidation of reduced sulfur compounds. Atmospheric Environment 256, 118148. https://doi.org/10.1016/j.atmosenv.2020.118148

VEGAN, a package of R functions for community ecology - Dixon - 2003 - Journal of Vegetation Science - Wiley Online Library [WWW Document], n.d. URL https://onlinelibrary.wiley.com/doi/abs/10.1111/j.1654-1103.2003.tb02228.x (accessed 8.27.24).

Veres, P., Roberts, J.M., Warneke, C., Welsh-Bon, D., Zahniser, M., Herndon, S., Fall, R., de Gouw, J., 2008. Development of negative-ion proton-transfer chemical-ionization mass spectrometry (NI-PT-CIMS) for the measurement of gas-phase organic acids in the atmosphere. International Journal of Mass Spectrometry 274, 48–55. https://doi.org/10.1016/j.ijms.2008.04.032

Visscher, P.T., Quist, P., van Gemerden, H., 1991. Methylated sulfur compounds in microbial mats: in situ concentrations and metabolism by a colorless sulfur bacterium. Appl Environ Microbiol 57, 1758–1763. https://doi.org/10.1128/aem.57.6.1758-1763.1991

Wang, W.-L., Song, G., Primeau, F., Saltzman, E.S., Bell, T.G., Moore, J.K., 2020. Global ocean dimethyl sulfide climatology estimated from observations and an artificial neural network. Biogeosciences 17, 5335–5354. https://doi.org/10.5194/bg-17-5335-2020

Wine, P.H., Kreutter, N.M., Gump, C.A., Ravishankara, A.R., 1981. Kinetics of hydroxyl radical reactions with the atmospheric sulfur compounds hydrogen sulfide, methanethiol, ethanethiol, and dimethyl disulfide. J. Phys. Chem. 85, 2660–2665. https://doi.org/10.1021/j150618a019

Zhang, S., Cao, H.-Y., Zhang, N., Teng, Z.-J., Yu, Y., Wang, Z.-B., Wang, P., Fu, H.-H., Chen, X.-L., Zhang, Y.-Z., Li, C.-Y., 2022. Novel Insights into Dimethylsulfoniopropionate Catabolism by Cultivable Bacteria in the Arctic Kongsfjorden. Applied and Environmental Microbiology 88, e01806-21. https://doi.org/10.1128/AEM.01806-21

Zhang, X.-H., Liu, Ji, Liu, Jingli, Yang, G., Xue, C.-X., Curson, A.R.J., Todd, J.D., 2019. Biogenic production of DMSP and its degradation to DMS—their roles in the global sulfur cycle. Sci. China Life Sci. 62, 1296–1319. https://doi.org/10.1007/s11427-018-9524-y

2.10 Supplementary Information

2.10.1 Supplementary Information Tables

Table 2.2: Medium Nutrient Concentrations

Nutrients	Concentrations
$NaNO_3$	75 gL^{-1}
NaH_2PO_4	5 gL^{-1}
Na_2H_2EDTA	4.36 gL^{-1}
$FeCl_3*6H_2O$	3.15 gL^{-1}
$MnCl_2*4H_2O$	180 mgL^{-1}
$ZnSO_4$	22 mg

2.10.1 Supplementary Information Figures

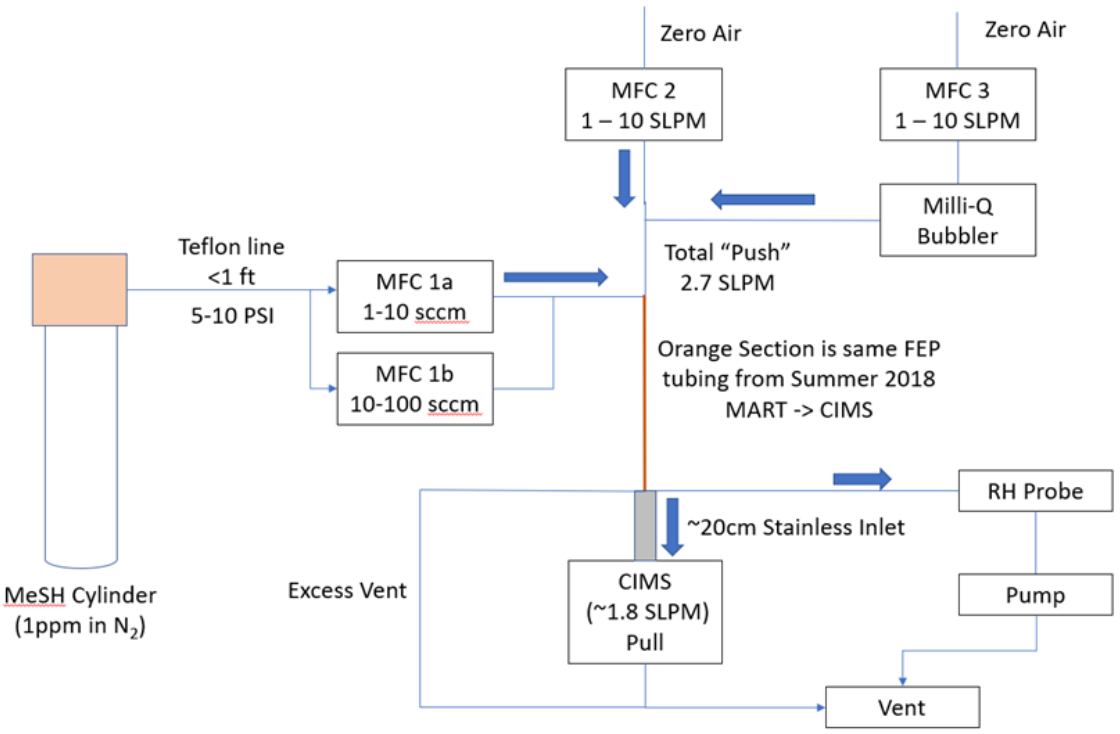


Figure 2.6: Methanethiol dimerization controls: arrangement of CI-TOF-MS sampling apparatus

Compressed MeSH at 1ppm, balanced in N_2, was obtained commercially from Airgas and dispensed using a clean 316 stainless steel diaphragm dual-stage regulator. Before analysis, MeSH was purged through the regulator manifold and calibration setup to remove residual DMDS which had accumulated on the walls. All sample tubing used was 0.25" Fluorinated Ethylene Propylene (FEP) tubing attached with FEP compression connectors (Swagelok) used where MeSH was present. Humidified air was produced through bubbling zero air into borosilicate bottles, previously combusted at 500C, filled with Milli-Q H_2O (Millipore). Humified zero air was mixed with MeSH to produce concentrations in the range measured by the CI-TOFMS. Sample flow rates were maintained at 2.7 SLPM, and passed through the same tubing used during the mesocosm

experiments. An inlet bypass pump was utilized to increase total “pull” flow and deliver sample air past a RH probe (Vaisala). Two inlets were utilized in these experiments, the 20cm SS inlet used during the bloom experiments as well as a PFA inlet that significantly reduced the amount of stainless steel encountered by the gas stream before entering the IMR of the CI-TOFMS.

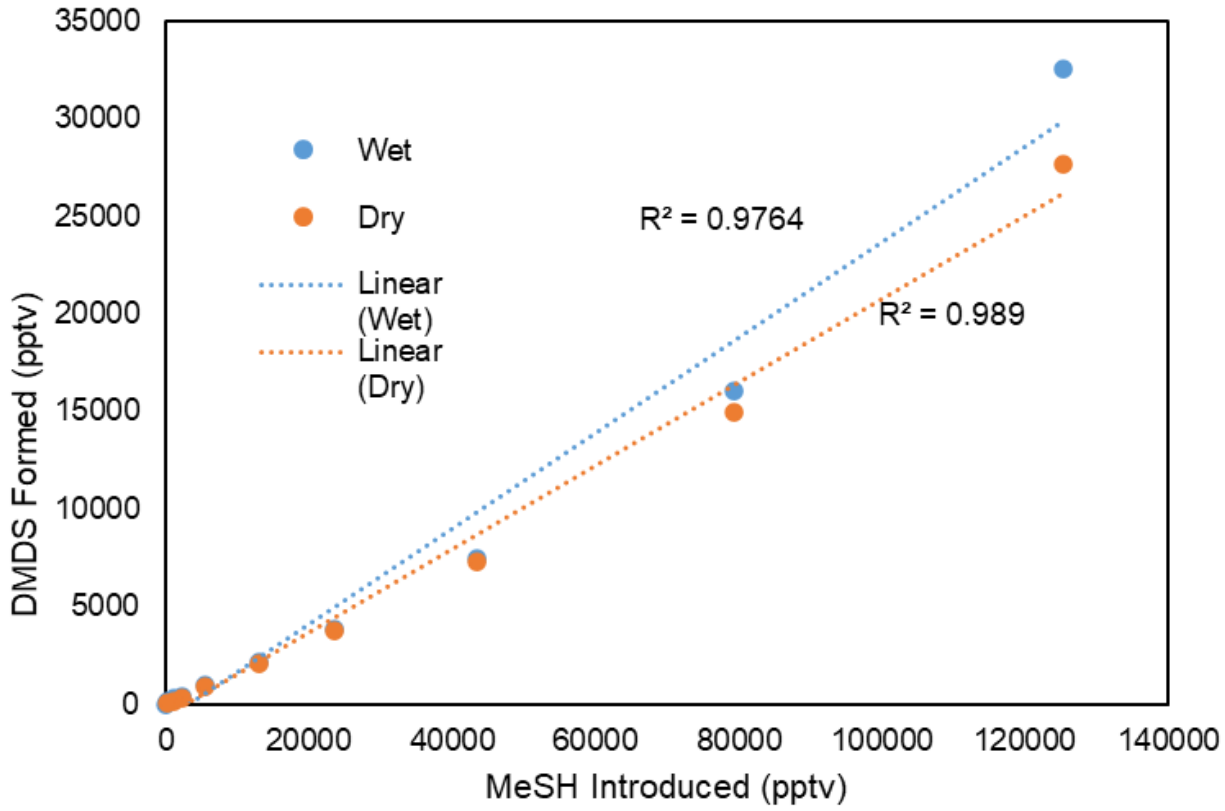


Figure 2.7: DMDS formed on the CI-TOF-MS inlet from introduced MeSH

Controls were performed to assess the quantitative conversion of MeSH to DMDS on the CI-TOF-MS inlet. 1 parts per billion mass MeSH in N_2 was diluted by zero air either at 0-5% RH or ~17.0 g*kg^{-1} water vapor mixing ratio. The resultant air flowed through the same length of tubing used for sampling during BEAST 2018 and was measured for gas composition by the CI-TOF-MS. Shown in Figure S2, the concentration of DMDS increased as more MeSH was added in a highly linear fashion until added [MeSH] > 60 ppbv.

Here we define the "actual" MeSH concentration detected by the CI-TOFMS using SI Equation 1:

1. $[MeSH_a] = [MeSH_i] - 2 * [DMDS]$

Where [$MeSH_i$]is the expected concentration introduced from the calibrated MeSH gas cylinder to the CI-TOFMS and [DMDS] is the measured DMDS concentration calculated from the ion signal and humidity-dependent calibration factors (19.2ncps/pptv @ low humidity, 21.2ncps/pptv @ high humidity). Through obtaining $MeSH_a$, calibration factors were calculated for MeSH and found to be 0.3 ncps/pptv at a mixing ratio of ~17.0 g/kg.

Lastly, in SI equation 2, the MeSH conversion ratio (CR_{MeSH}) is defined as:

2. $CR_{MeSH} = 1 - [MeSH_a]/[MeSH_i]$

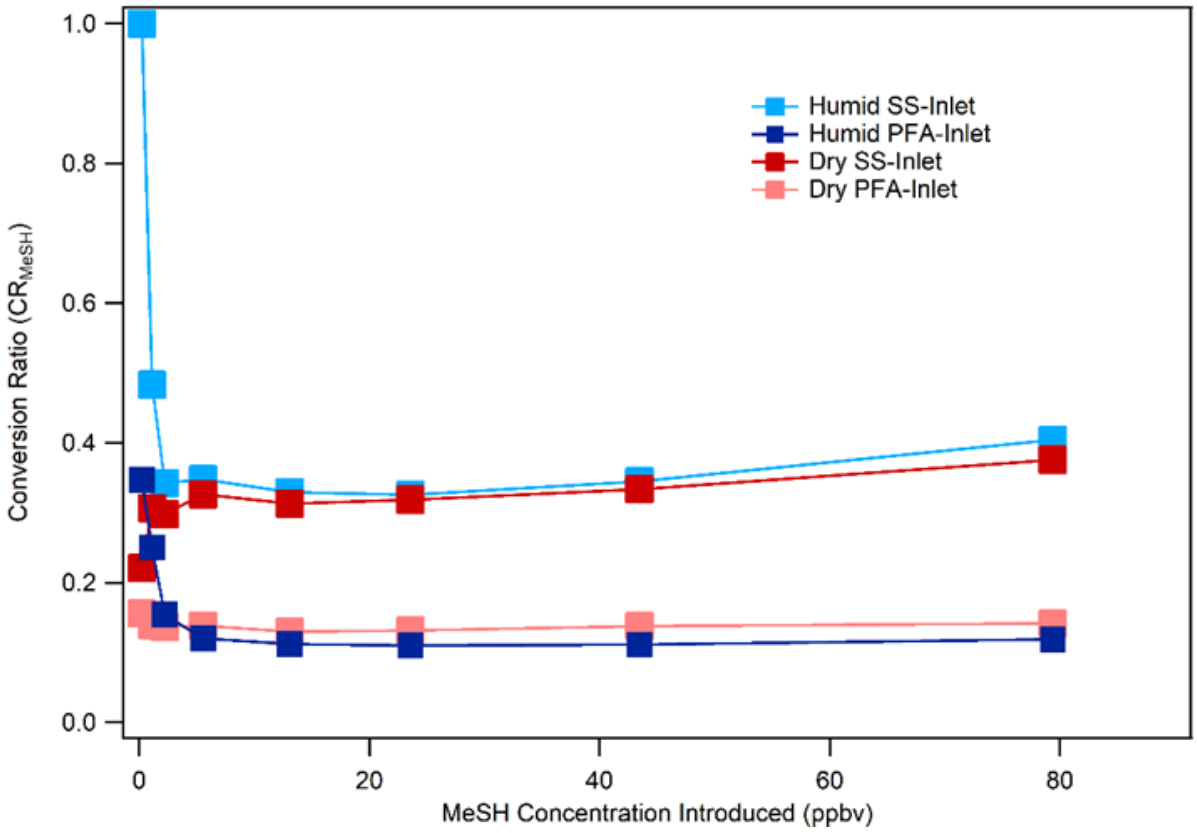


Figure 2.8: Conversion Ratio for DMDS formed on the CI-TOF-MS stainless steel (SS) and perfluoroalkoxy alkane (PFA) inlets from introduced MeSH

Shown in Figure 2.8, the conversion ratios for 4 separate inlet and humidity conditions were obtained across a range of introduced MeSH concentrations. It was found that the presence of the 20 cm stainless steel inlet significantly enhanced conversion of MeSH to DMDS before analysis by the CI-TOF-MS. Despite a fairly high flow rate through the SS inlet (1.8 SLPM), conversion ratios of 0.3-0.4 were observed throughout the concentration range of MeSH measured during the bloom experiments. In both the PFA and SS inlets, the influence of humidity did not seem to affect the conversion ratio significantly. Notably, at lower introduced MeSH

concentrations (<1ppb) for the wet SS condition, the MeSH conversion rate was 1, which could be an artifact of the low MeSH flow rate from the gas cylinder. Nevertheless, the MeSH concentrations encountered in bloom experiments for this work remained above 1ppbv.

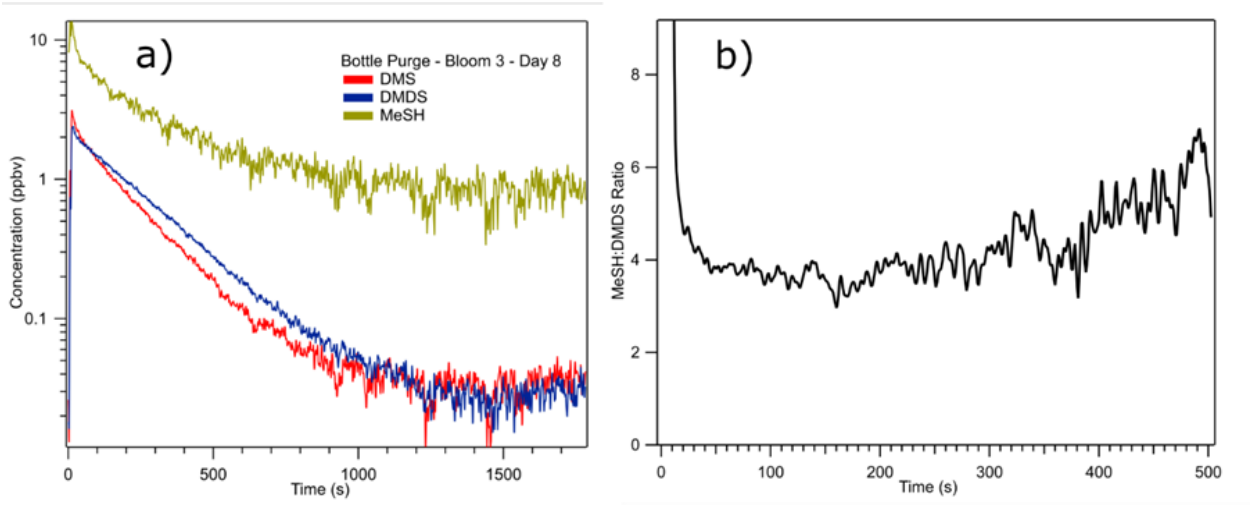


Figure 2.9: a) Purging of organosulfur gases from seawater directly sampled from the outdoor tank, b) MeSH:DMDS concentration ratio obtained from seawater purged with zero air

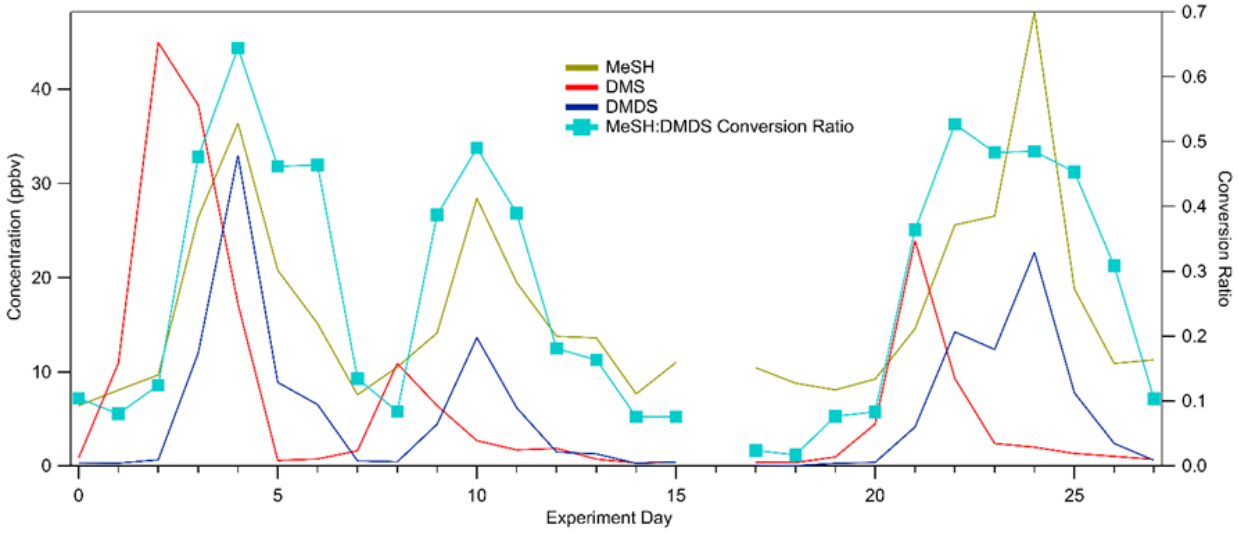


Figure 2.10: Time series gas concentrations of DMS, MeSH, and DMDS for mesocosms 1, 2, and 3 with the calculated conversion ratio assuming all DMDS was formed from MeSH observed

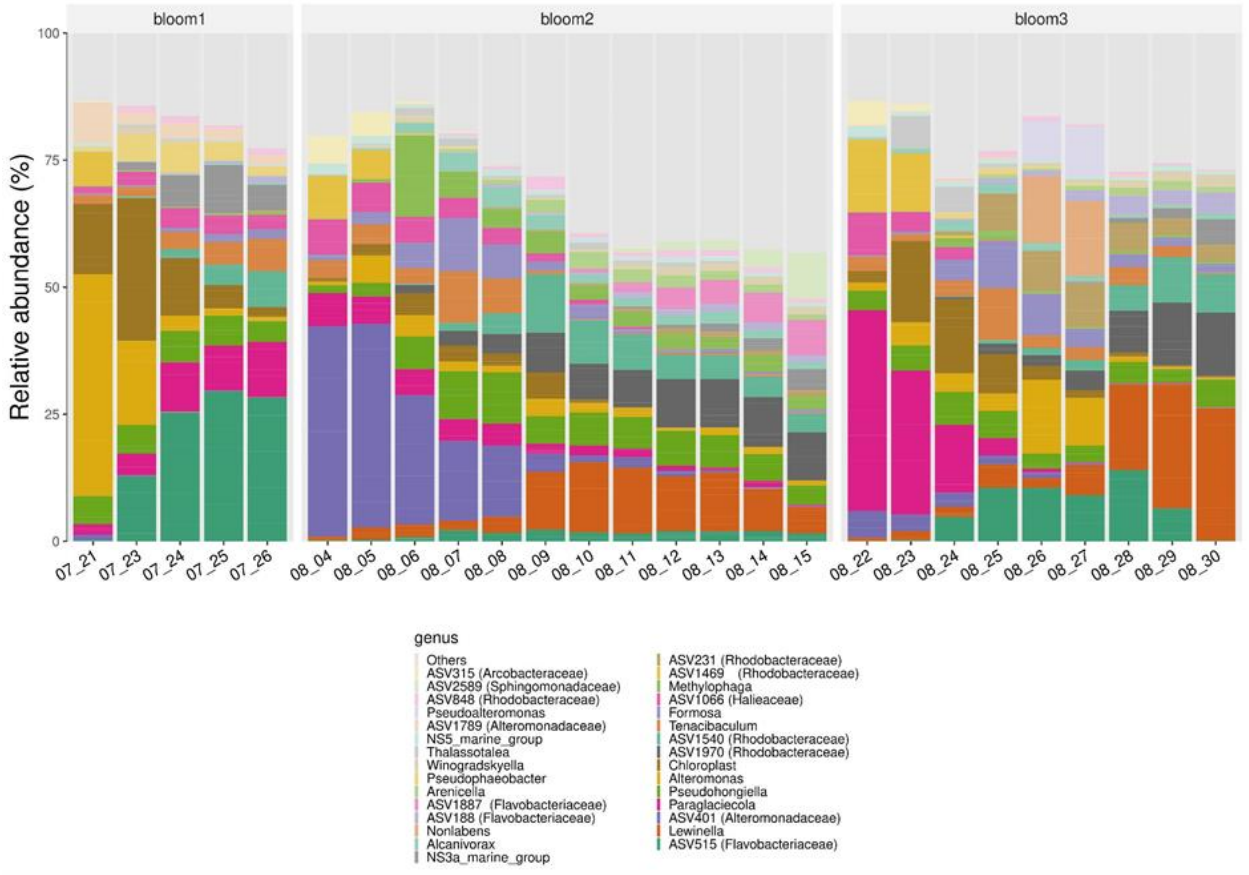


Figure 2.11: Barplots which highlight the temporal dynamic of the microbial communities during the Bloom experiments. The top thirty genera (or ASV, where taxonomic assignment did not reach the genus level) by abundance are shown, all other genera are grouped in “Others”. Replicate MARTs are shown aggregated in the same bar, identified by the date (mm_dd).

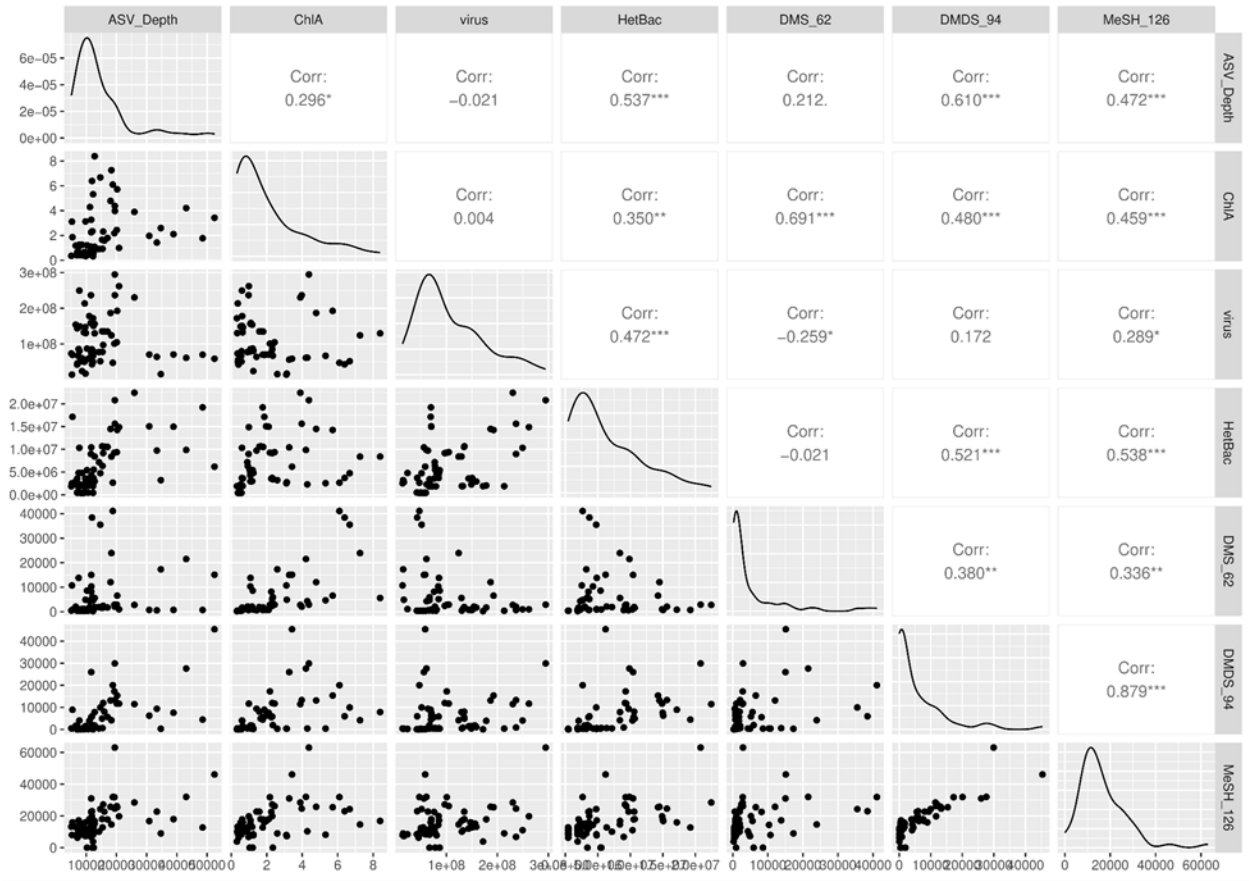


Figure 2.12. Metadata auto-correlation (Pearson correlation coefficient; * $p < 0.05$; ** $p < 0.01$; *** $p < 0.001$)

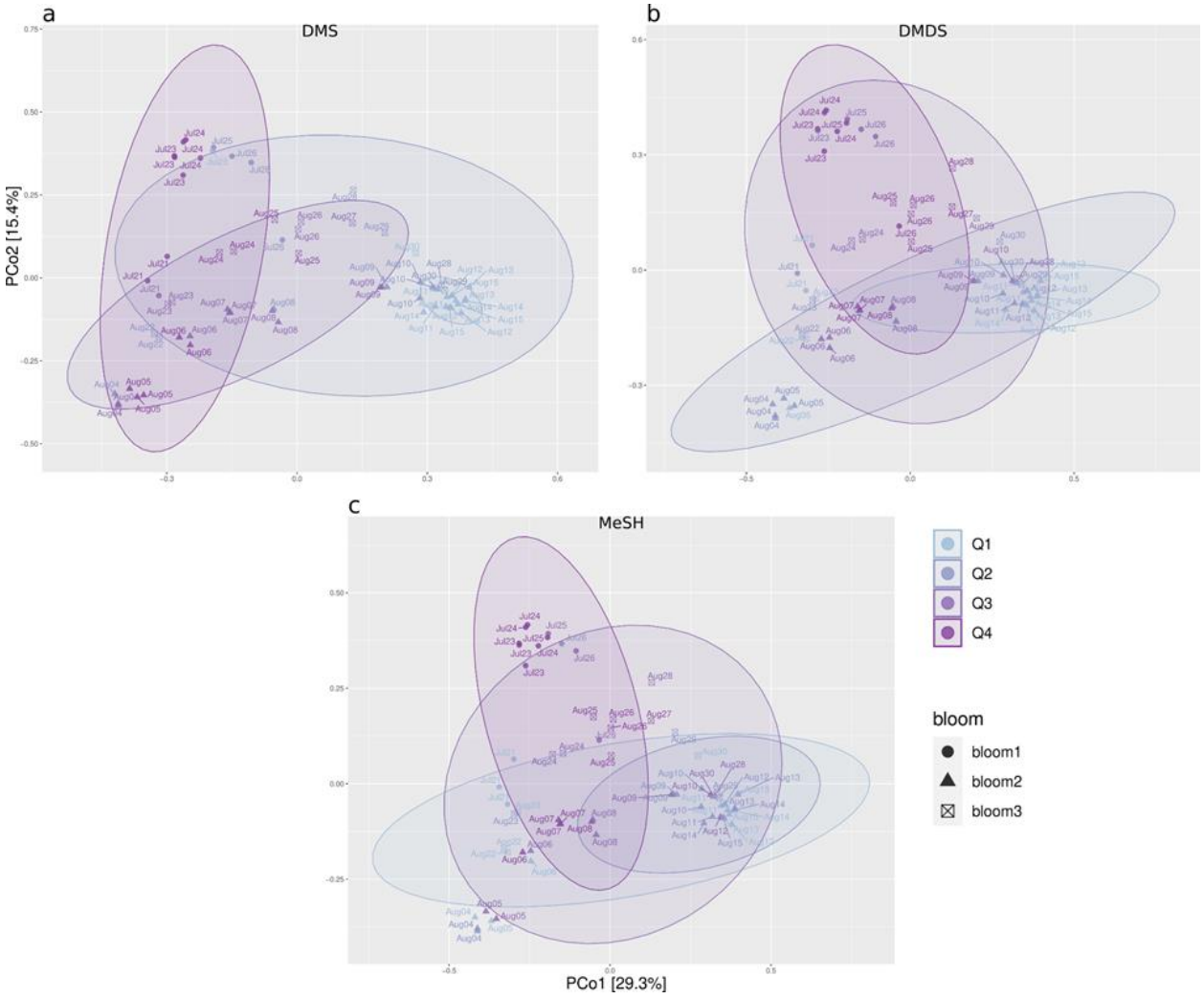


Figure 2.13: PCoA ordination based on Bray-Curtis matrix from the ASV table. Samples are colored according to the concentration of (a) DMS (b) DMDS and (c) MeSH divided into quartiles. Bloom experiments are identified by different shapes.

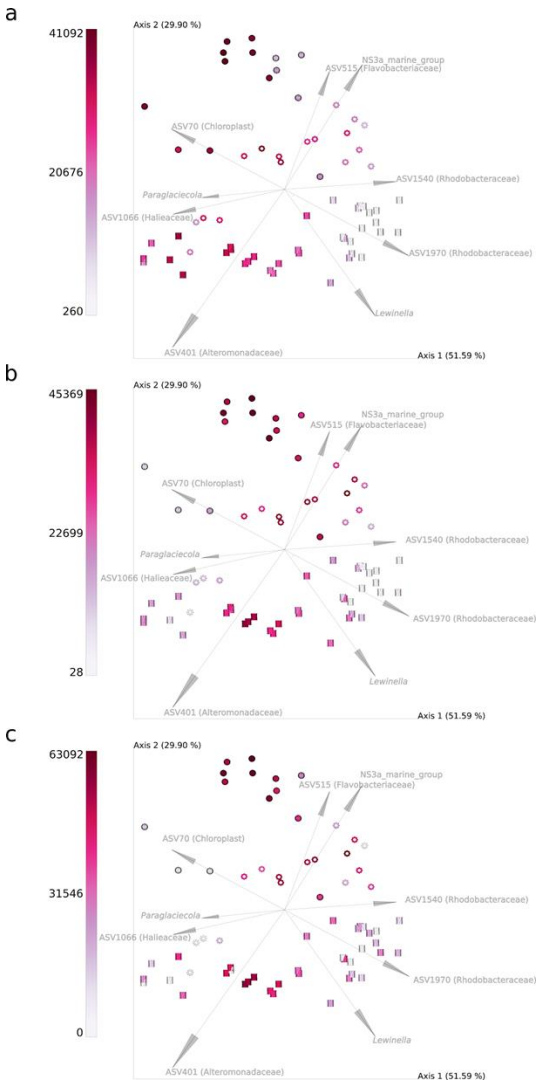


Figure 2.14. Robust Aitchison PCA. Samples are colored according to the concentration of (a) DMS, (b) DMDS and (c) MeSH. Circles, rectangles and rings identify Bloom1, Bloom2 and Bloom3, respectively

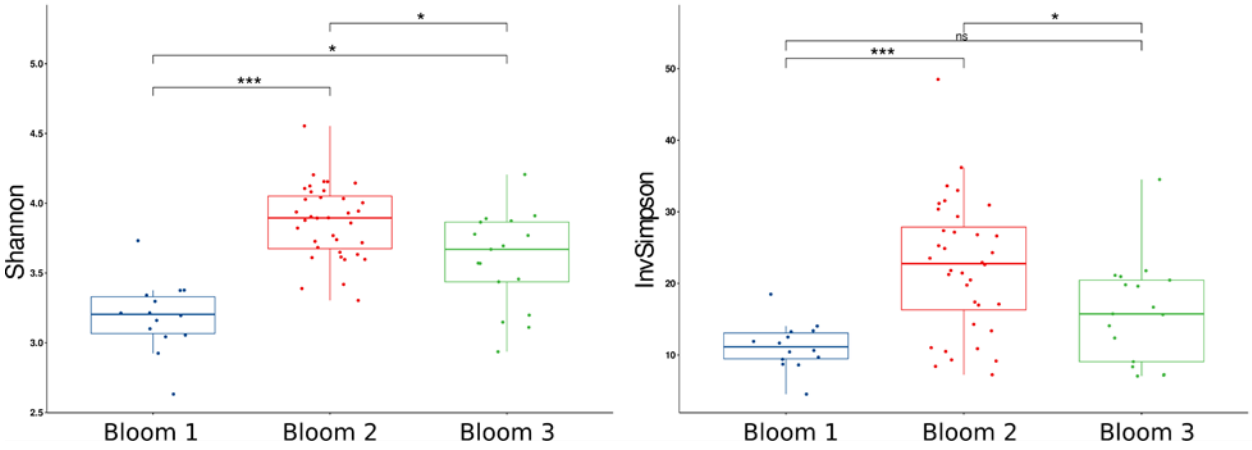


Figure 2.15: Boxplots which show alpha diversity of each Bloom experiment by Shannon and Inverse Simpson indices (* $p < 0.05$; ** $p < 0.01$; *** $p < 0.001$, Kruskall-Wallis test)

Bioinformatic methods

Reads quality and adapter content were assessed by fastQC (Andrews, 2010) and multiQC (Ewels et al., 2016) Raw paired reads were loaded into the QIIME2 (Bolyen et al., 2019; Gonzalez et al., 2018) environment, they were demultiplexed, residual adapters were removed with cutadapt (Martin, 2011), they were denoised, merged and quality trimmed with DADA2 (-p-trunc-q 20, --p-min-overlap 8, --p-n-reads-learn 3000000; Callahan et al., 2016). Once the Amplicon Sequence Variants (ASV) table was produced, accumulation curves of diversity were built by rarefaction. Samples with a sequencing depth lower than 5000 were discarded. Taxonomy was assigned with sklearn using a Naive Bayes classifier trained with SILVA database (release 138; 99% similarity, 16S 515F–806R; Quast et al., 2012). ASV table was used for subsequent diversity analyses and hypotheses testing using R (4.2.1) with packages microeco (Liu et al., 2021; bar plots, Principal Coordinate Analysis (PCoA) ordination, alpha diversity), indicspecies (De Caceres et al., 2016; Indicator Species Analysis) , phyloseq (McMurdie & Holmes, 2013), vegan (PERMANOVA;

Dixon, 2003) and mecodev. Alpha diversity distributions were compared by the non-parametric Kruskal-Wallis test with Dunn's post-hoc. Autocorrelation among metadata was assessed by Pearson correlation. Additionally, Mantel test between the distance matrices from metadata (OSCs concentration, chlorophyll a, total bacterial abundance, virus abundance) and distance matrix from AVS table was performed using the Spearman's rank correlation. In order to compare the widely applied Bray-Curtis based PCoA ordination method with the recently established robust Aitchison PCA (Martino et al., 2019), which for sparse highly diverse compositional data, showed less artifactual sample grouping. This method was also applied to the ASV table using the QIIME2 Deicode plugin. When categorical metadata were required, the distribution of the measured OSCs was partitioned into quartiles (Q1-Q4).

2.10.3 Supplementary Information References

Bolyen, E., Rideout, J.R., Dillon, M.R., Bokulich, N.A., Abnet, C.C., Al-Ghalith, G.A., Alexander, H., Alm, E.J., Arumugam, M., Asnicar, F., Bai, Y., Bisanz, J.E., Bittinger, K., Brejnrod, A., Brislawn, C.J., Brown, C.T., Callahan, B.J., Caraballo-Rodríguez, A.M., Chase, J., Cope, E.K., Da Silva, R., Diener, C., Dorrestein, P.C., Douglas, G.M., Durall, D.M., Duvallet, C., Edwardson, C.F., Ernst, M., Estaki, M., Fouquier, J., Gauglitz, J.M., Gibbons, S.M., Gibson, D.L., Gonzalez, A., Gorlick, K., Guo, J., Hillmann, B., Holmes, S., Holste, H., Huttenhower, C., Huttley, G.A., Janssen, S., Jarmusch, A.K., Jiang, L., Kaehler, B.D., Kang, K.B., Keefe, C.R., Keim, P., Kelley, S.T., Knights, D., Koester, I., Kosciolek, T., Kreps, J., Langille, M.G.I., Lee, J., Ley, R., Liu, Y.-X., Loftfield, E., Lozupone, C., Maher, M., Marotz, C., Martin, B.D., McDonald, D., McIver, L.J., Melnik, A.V., Metcalf, J.L., Morgan, S.C., Morton, J.T., Naimey, A.T., Navas-Molina, J.A., Nothias, L.F., Orchanian, S.B., Pearson, T., Peoples, S.L., Petras, D., Preuss, M.L., Pruesse, E., Rasmussen, L.B., Rivers, A., Robeson, M.S., Rosenthal, P., Segata, N., Shaffer, M., Shiffer, A., Sinha, R., Song, S.J., Spear, J.R., Swafford, A.D., Thompson, L.R., Torres, P.J., Trinh, P., Tripathi, A., Turnbaugh, P.J., Ul-Hasan, S., van der Hooft, J.J.J., Vargas, F., Vázquez-Baeza, Y., Vogtmann, E., von Hippel, M., Walters, W., Wan, Y., Wang, M., Warren, J., Weber, K.C., Williamson, C.H.D., Willis, A.D., Xu, Z.Z., Zaneveld, J.R., Zhang, Y., Zhu, Q., Knight, R., Caporaso, J.G., 2019. Reproducible, interactive, scalable and extensible microbiome data science using QIIME 2. Nat Biotechnol 37, 852–857. https://doi.org/10.1038/s41587-019-0209-9

Callahan, B.J., McMurdie, P.J., Rosen, M.J., Han, A.W., Johnson, A.J.A., Holmes, S.P., 2016. DADA2: High-resolution sample inference from Illumina amplicon data. Nat Methods 13, 581–583. https://doi.org/10.1038/nmeth.3869

De Cáceres, M., Legendre, P., Wiser, S.K., Brotons, L., 2012. Using species combinations in indicator value analyses. Methods in Ecology and Evolution 3, 973–982. https://doi.org/10.1111/j.2041-210X.2012.00246.x

Ewels, P., Magnusson, M., Lundin, S., Käller, M., 2016. MultiQC: summarize analysis results for multiple tools and samples in a single report. Bioinformatics 32, 3047–3048. https://doi.org/10.1093/bioinformatics/btw354

Gonzalez, A., Navas-Molina, J.A., Kosciolek, T., McDonald, D., Vázquez-Baeza, Y., Ackermann, G., DeReus, J., Janssen, S., Swafford, A.D., Orchanian, S.B., Sanders, J.G., Shorenstein, J., Holste, H., Petrus, S., Robbins-Pianka, A., Brislawn, C.J., Wang, M., Rideout, J.R., Bolyen, E., Dillon, M., Caporaso, J.G., Dorrestein, P.C., Knight, R., 2018. Qiita: rapid, web-enabled microbiome meta-analysis. Nat Methods 15, 796–798. https://doi.org/10.1038/s41592-018-0141-9

Liu, C., Cui, Y., Li, X., Yao, M., 2021. microeco: an R package for data mining in microbial community ecology. FEMS Microbiol Ecol 97, fiaa255. https://doi.org/10.1093/femsec/fiaa255

Martin, M., 2011. Cutadapt removes adapter sequences from high-throughput sequencing reads. EMBnet j. 17, 10. https://doi.org/10.14806/ej.17.1.200

Martino, C., Morton, J.T., Marotz, C.A., Thompson, L.R., Tripathi, A., Knight, R., Zengler, K., n.d. A Novel Sparse Compositional Technique Reveals Microbial Perturbations.

McMurdie, P.J., Holmes, S., 2013. phyloseq: an R package for reproducible interactive analysis and graphics of microbiome census data. PLoS One 8, e61217. https://doi.org/10.1371/journal.pone.0061217

Quast, C., Pruesse, E., Yilmaz, P., Gerken, J., Schweer, T., Yarza, P., Peplies, J., Glöckner, F., 2012. The SILVA ribosomal RNA gene database project: Improved data processing and web-based tools. Nucleic acids research 41. https://doi.org/10.1093/nar/gks1219

Simon, Andrews, n.d. Babraham Bioinformatics - FastQC A Quality Control tool for High Throughput Sequence Data [WWW Document]. URL https://www.bioinformatics.babraham.ac.uk/projects/fastqc/ (accessed 8.27.24).

Dixon, P. VEGAN, a package of R functions for community ecology - 2003 - Journal of Vegetation Science - Wiley Online Library [WWW Document], n.d. URL https://onlinelibrary.wiley.com/doi/abs/10.1111/j.1654-1103.2003.tb02228.x (accessed 8.27.24).

Chapter 3. Secondary Aerosols Formation from Mixtures of Marine Volatile Organic Compounds in a Potential Aerosol Mass Oxidative Flow Reactor

3.1 Abstract:

Increasing recognition of the significant contributions secondary organic aerosols can make in marine environments has led to an increase in research focused on understanding the reactions controlling their formation. Most marine laboratory studies to date have focused on the oxidation of individual volatile organic compounds (VOCs), particularly dimethyl sulfide (DMS). Thus, a lack of understanding exists in how complex marine VOC mixtures affect secondary marine aerosol formation and composition. To address this gap, we conducted controlled lab experiments that compare the effects of oxidizing single common marine VOCs versus VOC mixtures on secondary marine aerosol production. We used a potential aerosol mass oxidative flow reactor to investigate marine-relevant VOCs, including DMS, dimethyl disulfide (DMDS), and isoprene. Ion chromatography, chemical ionization mass spectrometry, aerosol time-of-flight mass spectrometry, and particle sizing instruments were employed to study how these mixtures influence the overall composition of marine aerosols. Our findings reveal that mixtures significantly alter the production and composition of secondary marine aerosols. Specifically, we found that isoprene, when oxidized in the presence of DMS and DMDS, affects methanesulfonic acid (MSA) and sulfate ratios, as well as overall aerosol yields. These insights suggest further studies on realistic marine VOC mixtures will help understand and predict the dynamics of secondary marine aerosol formation, therefore improving air quality and climate models and enabling more accurate predictions of marine aerosol impacts on cloud formation and properties.

3.2 Environmental Significance

Secondary marine aerosols (SMA) have been shown to significantly contribute to the marine atmosphere by affecting the formation and lifespan of clouds. Prior research has focused on single VOC studies, leading to a gap in understanding SMA. In this work we look at how mixtures of marine relevant gases impact SMA formation by analyzing the aerosol yields and composition. We found that mixtures of VOCs impacted the production of sulfate and methanesulfonic acid, two species that play a key role in aerosol formation and growth. These results can be used to improve the parametrization of SMA in climate models and their predictive power of future Earth scenarios.

3.3 Introduction

Dimethyl sulfide (DMS) has been estimated to account for more than half of the natural gas-phase sulfur emissions (Dani and Loreto, 2017). Oxidation of DMS has been shown to produce secondary aerosols comprised primarily of sulfate and methanesulfonic acid (MSA) formed through H abstraction and OH addition reaction pathways (Bates et al., 1992; Ye et al., 2022). These oxidation products have atmospheric significance with MSA playing a major role in particle growth, and sulfuric acid enhancing new particle formation (Berresheim et al., 2002; Kulmala et al., 2014; Saltzman et al., 1983; Zhang et al., 2012). Sulfate aerosols can offset the warming effect of greenhouse gases by scattering solar radiation and influencing cloud albedo and lifetime (Lohmann and Feichter, 2005; Twomey, 1974). In the marine environment, secondary aerosols have significantly different cloud forming potential from primary marine aerosols (Mayer et al., 2020). Knowing the factors controlling the production of secondary marine aerosols and their physicochemical properties is required to predict the formation, lifetime, and properties of marine

clouds. For instance, it has been shown that the aerosol mass needed to achieve a similar cloud albedo is 5 times larger for sulfate than for MSA-formed clouds (Hodshire et al., 2019). In the Arctic Sea region, the highest daily concentration of MSA was found to be associated with new particle formation event days over summer (Dall'Osto et al., 2017). Meanwhile, studies along the Antarctic coast have not only estimated the branching ratio between MSA and non-sea salt sulfate from DMS oxidation to be 0.84, but also showed an enrichment of non-sea salt sulfate with respect to MSA for aged air masses with low DMS content (Becagli et al., 2022). However, in areas with higher anthropogenic activity, DMS conversion to MSA was found to be inhibited, thus highlighting that a more complex picture of gaseous emissions will likely lead to differences in secondary marine aerosol particle composition and concentrations (Jiang et al., 2021).

Laboratory studies have examined the oxidation of reduced sulfur compounds over a range of conditions. Van Rooy et al. oxidized DMS and dimethyl disulfide (DMDS) in a smog chamber with relative humidity ranging from 35 to 40%, using hydroxyl radical, nitrate radical, and $O(^3P)$ to examine the yields and formation mechanisms of sulfuric acid and MSA (Van Rooy et al., 2021a). Using these conditions, they determined a higher humidity was necessary for the enhancement of MSA formation. Sulfate and MSA yields from DMS oxidation varied among experiments depending on the environmental conditions and overall ratio and type of gas phase species present. In the past, MSA yields have ranged from 0.5% to 45% with the highest concentrations occurring under high NO_x conditions. Van Rooy et al. estimated 25% of the aerosol mass from DMS oxidation by $O(^3P)$ and NO_x were explained by MSA formation, but this number was much lower only in the presence of the hydroxyl radical. Other authors have also examined DMS oxidation reactions by OH radicals over a range of NO_x concentrations, as well as changes in RH (Ye et al., 2022). However, few studies have considered the impact of other non-sulfur

volatile organic compounds (VOCs) on the products and aerosol yield of DMS oxidation. For example, isoprene, another relatively less studied contributor to marine gas emissions, has been reported as a secondary organic aerosol (SOA) precursor in both terrestrial and marine environments (Ahlberg et al., 2017; Claeys et al., 2004; Lambe et al., 2015). Isoprene SOA potential increases in the presence of acidic particles (Claeys et al., 2004; Lambe et al., 2015). Chen and Jang conducted a study examining the photooxidation of DMS and isoprene in a chamber under various NO_x and humidity conditions and reported a substantial increase in the isoprene yield in the presence of DMS at atmospherically relevant RH. This discovery has significant implications for the marine environment as the oxidation of DMS can provide acidic seed particles that promote isoprene aerosol formation. However, they found that isoprene decreased the MSA yield from 48% to 25.8% (Chen and Jang, 2012). Controlled laboratory experiments are needed to further understand the mechanisms and processes that control the formation of secondary aerosols in marine environments. Herein, we use simplified mixtures comprised of several marine-relevant VOCs to help elucidate secondary marine aerosol properties and yields.

In this study, a flow reactor was used to oxidize mixtures of DMS, DMDS, and isoprene with hydroxyl radical simulating periods ranging from 0.7 to 19.1 days of equivalent oxidation to determine the impact on aerosol yields and sulfate to MSA ratios. To our knowledge, this is the first reported study of reduced sulfur oxidation reactions in a Potential Aerosol Mass Oxidative Flow Reactor (PAM-OFR) (E Kang et al., 2007; Peng and Jimenez, 2020). Aerosol yield and composition were probed as a function of precursor gases (DMS, DMDS, isoprene, and mixtures of DMS/isoprene, DMDS/isoprene, DMS/DMS, and DMS/DMDS/isoprene) and extent of OH exposure.

3.4 Methods

3.4.1 Experimental setup

The experimental setup used in this study is shown in Figure 3.1. Dry zero air was generated using the Model 1001 Zero Air Source (Sabio Environmental). DMS and isoprene concentrations were adjusted using a G-Cal permeation device at room temperature (VICI Metronics) to give a permeation rate of 300 ng min^{-1} (± 5% at 25°C) and 247 ng min^{-1} (± 5% at 25°C), respectively. DMDS concentrations were adjusted by flowing air through a Dynacal permeation tube (VICI Metronics) housed inside a custom-built permeation oven. Permeation rate was 150 ng min^{-1} (± 25% at 50°C). Mass flow controllers (Alicat Scientific) were used to adjust the flows and calibrated against a Defender 520 volumetric primary flow standard (Mesa Labs). Humidified zero air was introduced to make up a total flow of 5 L min^{-1}. The final concentrations are shown in Table 3.1. The gas phase mixture was sent through a potential aerosol mass oxidation flow reactor (PAM-OFR, Aerodyne Inc.) at relative humidity ranging between 50-70%.

The PAM-OFR uses UV lamps with wavelengths of λ = 185 and 254 nm (OFR185 mode) to produce a high concentration of OH radicals (E Kang et al., 2007). Calibration of OH exposure in the OFR was determined by introducing carbon monoxide (initial concentration ≈ 1 ppm) to the OFR at the same airflow rate and relative humidity used during the experiments and measuring the CO decay as a function of lamp voltage using a CO analyzer (APMA-370, Horiba Ltd.). The change in CO concentration yielded the OH exposure versus lamp voltage relationship using the known CO + OH rate coefficient $k_{OH+CO,\ 298K} = 1.5\times10^{-13}$ cm^3 $molec^{-1}$ s^{-1} (Chen and Marcus, 2006). Calibration results are shown in Figure 3.6. The residence time of gases in the OFR was 2.7 min. A diffusion ozone denuder (Carulite-200, Ozone Solutions) was located after the OFR to remove ozone and avoid further oxidation of reaction products. A custom-built silica drier (length:

28 in, diameter: 4 in) was used to dry the aerosols under 25% RH before they were introduced into the particle sizing instrument.

Aerosol yield and characterization were conducted using two experimental approaches. In aerosol yield experiments, lamp voltage was changed every 40 minutes to produce more OH radical and increase the equivalent days of aging. Seven OH exposures were used, ranging from 9.6×10^{10} to 2.5×10^{12} molecules s cm^{-3}, equivalent to 0.7 to 19.1 days of aging assuming typical tropospheric conditions ([OH] = 1.5×10^{6} molecules cm^{-3}). For aerosol characterization experiments, a single OH exposure of 3.8×10^{11} molecules s cm^{-3} was used, equivalent to 2.9 days of aging. Each filter was collected for 22 hours to ensure enough aerosol mass was collected for detection of MSA and sulfate with ion chromatography (see below). More details about yield and aerosol characterization experiments are included in Tables 3.1 and 3.2.

3.4.2 Quantification of VOCs

During the aerosol yield experiments, VOCs (DMS, DMDS, and isoprene) were quantified after the PAM-OFR in real time using a chemical ionization time-of-flight mass spectrometer (CI-TOF-MS), with benzene as the reagent ion (Kim et al., 2016; Lavi et al., 2018). A concentration of 300 ppm benzene vapor was generated by passing 10 standard cubic centimeters per minute (sccm) of ultrahigh-purity N_2 gas over a cylinder of liquid benzene further diluted to concentration with added N_2. Benzene vapor was passed through a 20 mCi Po-210 α-source to generate benzene cluster cation reagent ions, and further drawn through an inline critical orifice at 1.8 standard liters per minute (slpm) into the ion-molecule region (IMR) of the CI-TOF-MS. Sample analyte was similarly drawn into the IMR at the same flow rate as analyte. The IMR pressure was maintained at 60 Torr and voltage at 60 V for all analyses. Analyte ions generated through charge transfer and

ligand switching reactions with benzene cluster cations were focused by a radio frequency ion funnel, and subsequently transferred by an RF-only quadrupole into an orthogonal extraction time-of-flight analyzer (Tofwerk). Co-summed mass spectra from 5–500 m/z were obtained at 1 Hz and analyzed using the Tofware plugin for Igor Pro 8 software. External calibrations were run for DMS, DMDS, and isoprene using the G-cal permeation tubes (DMS and isoprene) and Dynacal permeation tube (DMDS). In addition to the external calibration, the experimental setup was constructed to minimize stainless steel by using a Teflon-coated OFR and reducing the number of stainless-steel fittings to limit reactions on metal surfaces. The supplier for both the Dynacal and G-cal devices (VICI Metronics) assures these standards consist of pure compounds. To ensure this purity, we verified the absence of contaminating species using the CI-TOF-MS spectra.

3.4.3 Quantification of sulfate and methane sulfonic acid

To quantify sulfate and MSA produced by VOC oxidation, filters were collected after the PAM-OFR at 3.5 L min^{-1} for 22 hours (Figure 3.1). Pallflex Tissuquartz filters (Pall) were combusted for 6 hours at 500°C to reduce background contamination signal. After collection, filters were stored at -20°C until the time they were processed. 5 mL of Milli-Q water (Millipore, resistivity of 18.2 MΩ cm at 25°C and total organic carbon below 5 ppb) and 30 minutes of sonication were used to extract the filters. The extracts were analyzed using a Dionex ICS-2000 ion chromatography (IC) system. The ICS-2000 was equipped with an eluent generator (23 mM KOH isocratic run), a Dionex IonPac AS18 2×250 mm column, an AG18 2×50 mm guard column, and an AERS 500 2 mm electric suppressor. The DS6 conductivity detector was held at 35°C. The sample injection volume was 25 µL and the flow rate was 0.25 mL min^{-1}. Under these conditions, MSA was eluted at 3.97 min and sulfate at 6.27 min. MSA (Alfa Aesar, purity > 98%) and sulfate

(Inorganic Ventures, $[SO_4^{2-}]$ = 1001±4 μg mL^{-1}) standard solutions were prepared in Milli-Q water, and calibration solutions were run in the IC along with the filter extracts.

3.4.4 Particle size distribution measurements

During all experiments, particle size distributions of the aerosol produced in the PAM-OFR were measured using a scanning mobility particle sizer (SMPS) at a RH below 25%. The SMPS consists of a differential mobility analyzer (DMA) Model 3081, an electrostatic classifier Model 3082, and a water-based condensation particle counter Model 3787 (TSI, Inc.) and was operated at a sample flow rate of 0.6 L min^{-1} and a sheath flow rate of 3.0 L min^{-1}. Each SMPS scan was 5 minutes over electrical mobility diameters ranging between 14-750 nm. Electrical mobility diameters are assumed to be equal to physical diameters, and thus size and volume distributions presented in Figure 3.2 are shown with physical diameters.

3.4.5 Real-time composition of secondary aerosols

The compositions of 20 and 60 nm secondary aerosols were measured using an aerosol time-of-flight mass spectrometer (ATOFMS) (Gard et al., 1997; Pratt and Prather, 2010). Particles were size selected at 20 nm using a DMA and then passed through a sublimation-deposition growth tube at a flow of 200 sccm, where they were grown with 1,8-bis(tetramethylguanidino)-naphthalene (TMGN) at 100℃ (Li et al., 2023). Particles were then size-selected post growth at 400 nm using a second DMA. This newly developed MALDI method was used because the standard ATOFMS cannot detect particles below 100 nm. After the second size selection, particles were sent into the ATOFMS for size-resolved chemical analysis. In the ATOFMS, the particle beam is first collimated using an aerodynamic lens before measuring the speed of each particle between two continuous wave lasers to determine their size. The signal from the continuous

scattering lasers triggers a Nd:YAG desorption ionization laser at 266 nm which produces positive and negative ions from each individual particle. Since the oxidized products preferentially form negative ions, only the negative ion mass spectra are displayed here.

3.5 Results and Discussion

3.5.1 Particle size distributions for the oxidation of single VOCs

Figure 3.2 presents aerosol size distributions resulting from the oxidation of DMS and DMDS at varying OH exposures. Panels A to C show particle number distributions while D to F show particle volume distributions. The total number and volume concentrations and the median number-weighed and volume-weighed diameters for these distributions are presented in Figure S3.7. At low OH exposures, equivalent of 1.66×10^{11} molecules s cm^{-3} (as shown in Figure 3.2A and 3.7), oxidation of DMDS generates more aerosols than DMS, consistent with DMDS having a faster initial OH rate constant (20×10^{-11} cm^3 $molecules^{-1}$ s^{-1}) compared to DMS (0.44×10^{-11} cm^3 $molecules^{-1}$ s^{-1}) (Atkinson et al., 2009, 1992). At this low OH exposure, DMDS also produced more aerosols by volume than DMS. However, at medium and high exposures, despite DMDS producing more particles than DMS, the total volume concentration is higher for DMS than for DMDS (Figure 3.2D and 3.7). In their DMDS oxidation chamber experiments, Van Rooy et al. observed that aerosol mass continued to increase even after complete consumption of DMDS (Van Rooy et al., 2021a). This led them to hypothesize that slower secondary reactions also contribute to aerosol mass. In our study, this hypothesis provides an explanation for the differences between DMS and DMDS. At the lowest OH exposure, where the fastest DMDS initial oxidation rate is dominant, DMS produced fewer aerosols by number and volume than DMDS. As the OH exposure increased, DMDS was quickly consumed and the products of this initial oxidation led to slower

secondary reactions compared to those of DMS, therefore yielding a lower total aerosol volume. Consistent with this, the median number-weighted diameters from Figure 3.7 show that DMDS produced smaller particles and higher number concentrations than DMS, which again is expected based on the faster DMDS initial oxidation rate. Typically, particles below 100 nm are dominated by nucleation processes, whereas particles above 100 nm are dominated by condensation processes. In this study, we found that reactions in the PAM-OFR were primarily dominated by nucleation (Figure 3.7). Despite the short residence times in the PAM-OFR, we found that about 5% of DMS total aerosol production occurred above 100 nm. In contrast, the DMDS experiments showed less than 1% of particles above 100 nm, suggesting that secondary oxidation reactions with DMS occur faster than those with DMDS, allowing both nucleation and condensation processes to take place. The median volume-weighed diameter for the DMS experiment is around 69 nm at the lowest OH exposure and shifts to 95 nm at the highest OH exposure, further highlighting the particle growth observed in the number size distributions. The volume size distributions for the DMDS experiment peak around 63 nm on average at all OH exposure times. Increasing the OH exposure does not result in a shift in the volume size distribution, indicating that DMDS oxidation is dominated by new particle formation.

3.5.2 Particle size distributions for the oxidation of mixtures

The particle number size distributions for the mixture of DMS and isoprene, DMDS and isoprene, and DMS and DMDS are shown in Figure 3.2, A to C. An additional experiment using a mixture of all three VOCs is also shown. In Figure 3.2 and 3.7, the median number-weighed diameter for the DMS and isoprene mixture, particle size distribution shifts to larger sizes compared to DMS alone, showing that larger particles are being formed in the presence of isoprene. The addition of isoprene not only shifts the distribution but also impacts the production

of aerosols by decreasing the number of secondary aerosols in the DMS experiment. Isoprene also seems to decrease the number of aerosols produced when mixed with DMDS at high OH exposure (Figure 3.7). In contrast to DMS, the presence of isoprene with DMDS enhances the median number-weighed diameter of the distribution in the smaller size range.

The aerosol volume size distributions for the mixtures are shown in Figure 3.2, D to F. Larger total volumes were obtained for the DMS and isoprene mixture compared to DMS alone while the opposite occurs for the combination of DMDS and isoprene (Figure 3.7). Ahlberg et al. found in organic mixture experiments that isoprene shifted the size distribution to larger particles while also reducing the number of particles, a similar behavior to that is observed for DMS (Ahlberg et al., 2017). Since isoprene has a faster reaction rate with OH than DMS and a slower reaction rate than DMDS (Table 3.1), we hypothesize isoprene had a greater impact on the initial DMS aerosol production. Because of the slower initial DMS oxidation and the lower partition coefficient of isoprene PAM-OFR oxidation products to the aerosol phase, fewer particles undergo condensation and growth, yielding larger total volume concentrations for the DMS and isoprene experiment (Figure 3.7) (Lambe et al., 2015). As shown in Figure 3.2A-C, the mixture between DMS, DMDS, and isoprene resulted in a slight decrease in aerosol number production compared to the mixture between DMS and DMDS. This behavior reflects the trends that DMS and DMDS have shown in their individual experiments. Number concentrations decrease both for DMS and DMDS upon the addition of isoprene, therefore explaining the decrease in number concentrations for the DMS, DMDS and isoprene mixture. On the other hand, volume concentrations increase upon the addition of isoprene for DMS and decrease for DMDS. Aerosol volume showed a slight increase upon the addition of isoprene to DMS and DMDS together, which resembles DMS

behavior and suggests again that condensation and growth might become the dominant process when DMS is present.

3.5.3 Aerosol yields for the oxidation of single VOCs versus mixtures

Figure 3.3A presents the aerosol yields for DMS, DMDS, and isoprene, each measured independently. Aerosol yield, calculated from the amount of reacted gas and aerosol mass formed, was highest for DMS, followed by DMDS, and then isoprene. The aerosol yield from DMS oxidation increased consistently with OH exposure, reaching a peak yield of 90%. This is higher than the 50% yield found by Chen and Jang in a chamber study at 45% RH (Chen and Jang, 2012). Other chamber studies reported lower estimates for DMS and DMDS aerosol yield due to the absence of a steady state of aerosol mass with yields of 12% and 25% (Van Rooy et al., 2021a).

In this study, DMS and DMDS had similar aerosol yields at low equivalent days of aging. However, DMS aerosol yield surpassed that of DMDS for 2.9 days and longer aging times. Interestingly, the non-reacted gases produced noteworthy results (Figure 3.8). At 1.3 days of aging, less than 4% of the initial DMDS gas phase concentrations remained, and by 19.1 days of aging, less than 1% was left. Despite DMDS being almost completely reacted at the highest OH exposure, the aerosol yield was only 61%, suggesting the formation of smaller more volatile gas phase products that did not condense on the secondary aerosols.

For DMS, the non-reacted gas phase concentrations were 52% and 9% at 1.3 and 19.1 days of aging. However, at the highest OH exposure, DMS aerosol yield was 85%. As anticipated, isoprene had the lowest aerosol yield, reaching a maximum yield of 10% at the highest OH exposure. At 1.3 days of aging, 11% of isoprene remained unreacted and 8% at 19 days of aging. Despite most of isoprene being reacted, isoprene oxidation in the PAM-OFR resulted in low yields

due to the absence of isoprene epoxy diols (IEPOX) aerosol formation and no enhancement of acidic seed particles (Hu et al., 2016). These results suggest that the majority of isoprene degraded to form volatile gas phase compounds (Kroll et al., 2009; Lambe et al., 2015).

Figure 3.3B shows aerosol yields from mixtures of DMS and isoprene, DMDS and isoprene, DMS and DMDS, and DMS, DMDS, and isoprene. The overall yield from the oxidation of DMS and isoprene together was lower than that of DMS oxidation only. While the formation of isoprene SOA has been shown to be enhanced in the presence of acidic particles, such as DMS oxidation products (sulfate and MSA), the mixture with isoprene decreased sulfate formation from DMS, as shown in Figure 3.4 and discussed in the next section (Lambe et al., 2015). We hypothesize that isoprene and DMS oxidation products are competing for atmospheric oxidants. These results are consistent with previous chamber studies that have shown lower DMS yields in the presence of isoprene (Chen and Jang, 2012). A similar behavior was observed in the case of the DMDS and isoprene mixture in our study; aerosol yield substantially decreased compared to DMDS alone. In this case, at the highest OH exposure, the aerosol yield experienced a 3-fold decrease, leading to a value close to the yield of isoprene alone. For DMS, this decrease was not as dramatic (1.3-fold).

Oxidation of DMS and DMDS mixtures resulted in the highest aerosol yield of any combination, yielding 94%. This result was surprising although we hypothesize that rapid oxidation of DMS to sulfate helped provide the aerosol seeds for the DMDS oxidation products to condense upon leading to a higher yield. Isoprene added to the mixture of DMS and DMDS resulted in a small decrease in the aerosol yield of 89%. The impact of the addition of isoprene on the overall yield of the oxidation of the DMS and DMDS mixture is minimal compared to the impact on DMS or DMDS oxidation alone. We hypothesize the inhibitory effect of isoprene on

aerosol yield is minimized due to the fast oxidation mechanism mentioned above. This behavior also corresponds with the small shift to larger particle sizes in the volume size distribution.

Figure 3.10 shows aerosol yields for VOCs and mixtures plotted against the increase in aerosol mass (ΔM, $\mu g\ m^{-3}$). To gain more knowledge on the properties of the particle phase species, these data were fitted to an absorptive partitioning model (Odum et al., 1996; Slade et al., 2017). At first glance, no dramatic differences were observed between the experiments. This is not surprising given that for all of them except isoprene alone, MSA and sulfate were the main products, and therefore, the most abundant particle phase species. As seen in the top panel of Figure 3.10, DMS yields increased at a faster rate than DMDS, at least for ΔM lower than 20 $\mu g\ m^{-3}$. Again, this agrees with what was suggested above; DMS oxidation products may partition to the aerosol phase at a higher rate than DMDS. Interestingly, the mixture with isoprene seemed to affect the absorption properties only if DMDS was present (Figure 3.10, bottom panel). This could also support the idea that some of the products from DMDS oxidation partition to the particle phase at a lower ratio than for DMS. No differences were observed between the DMS alone and DMS and isoprene curves.

3.5.4 MSA and sulfate ratios in bulk secondary aerosol

The major DMS oxidation products found in the secondary aerosols were MSA and sulfate, which has been shown previously (Bates et al., 1992). Figure 3.4 shows a comparison of the concentrations of these products measured using ion chromatography. Product molar fractions were calculated as the ratio between moles of sulfate or MSA extracted and the initial amount of DMS and/or DMDS over the duration of the filter sampling experiments. For comparison, Figure 3.12 shows aerosol concentrations of sulfate and MSA in $\mu g\ m^{-3}$ for each experiment.

Although dominant, the concentration of sulfate showed a significant decrease for DMS oxidation in the presence of isoprene (Figure 3.12, $p < 0.05$ for a paired t-test). The concentration of MSA remained unchanged with and without isoprene (Figure 3.13). This leads to the conclusion that isoprene might interfere with the DMS oxidation pathway that forms sulfate. In the DMDS experiment, we also found sulfate to be the dominant oxidation product. When isoprene was added, both sulfate and MSA increased, but the change was significant for the latter (Figure 3.13, $p < 0.01$ for a paired t-test). As opposed to what occurred during the DMS experiment, isoprene does not appear to inhibit either oxidation pathway for DMDS.

Formation of MSA in these experiments is consistent with previous experiments. The reactions were run between 50-70% RH and without addition of NO_x. Barnes et al. found little MSA formed under similar low NO_x and high RH conditions (Barnes et al., 2006). Van Rooy et al. suggested that NO_x and high RH were required to produce a significant amount of MSA (Van Rooy et al., 2021a). We found low concentrations of MSA due to the low NO_x concentration. However, adding a non-sulfur compound increased the MSA product concentrations. In contrast to previous chamber work that suggested high concentrations of NO_x (in the order of hundreds of ppb) were required for the oxidation pathway of DMS to MSA, our results suggest that in a PAM-OFR this is not the case.

The MSA and sulfate results obtained for mixtures of DMS and DMDS and DMS, DMDS, and isoprene did not show significant changes between each experiment or when compared to DMS alone. This could possibly be attributed, again, to the faster aerosol production exhibited by DMS that outcompeted slower reactions in the DMDS oxidation pathway.

3.5.5 MSA and sulfate ratios in individual secondary aerosols

Online single particle analysis via ATOFMS produced consistent chemical composition results to those found using ion chromatography. Figure 3.14 shows the average mass spectra of 60 nm particles produced by the various VOCs and mixtures after they have been coated with matrix 1,8-bis(tetramethylguanidino)naphthalene (TMGN) for real-time analysis using ATOFMS (Li et al., 2023). Similar to offline results, the most abundant peaks present in the 60 nm single particle spectra are sulfate and MSA. The ability of the ATOFMS to detect MSA and sulfate ions has been previously demonstrated by Gaston et al., which validates the peak assignments provided here (Gaston et al., 2010). In addition, sulfuric acid ($^{195}H_2SO_4HSO_4^-$) is present as well (Pratt and Prather, 2010). Figure 3.5 shows the fraction of particles containing sulfate, MSA, and sulfuric acid along with their respective peak areas after subtracting the background from the matrix. Since ATOFMS cannot determine mass concentrations, the peak area of the ions provides insight on the particle composition. While DMS alone produced the greatest number of particles containing MSA (92%), the VOC mixture of DMS, DMDS, and isoprene combined produced particles with the highest peak area of MSA present. DMDS, both individually and in the presence of isoprene, produced the lowest amount of MSA out of all the mixtures, though there is a slight increase in the number of particles with MSA present once isoprene is added (4.9% to 5.6% with the addition of isoprene). DMS, on the other hand, shows a decrease in the number of particles containing MSA when DMDS or isoprene are added. When comparing the single-particle and bulk data for MSA, while both the DMS and DMDS experiments produced similar amounts of MSA in the bulk, there is significantly less MSA present at 60 nm for DMDS. It appears either MSA produced from DMDS is concentrated in a smaller number of particles than in the DMS experiment or the MSA

fraction is lower for this size of particles. We hypothesize particle growth rates and different oxidation mechanisms impact the MSA fraction.

All single particle experiments showed that over 75% of the particles contained sulfate, with DMS producing the greatest number of particles containing sulfate. This number decreases with the addition of DMDS and/or isoprene. The highest sulfate peak area was present in the DMDS experiment, while a larger fraction of sulfate-containing particles was produced by the oxidation of DMDS and isoprene together. While the sulfuric acid peak areas were relatively low for all experiments, the highest values were found in particles produced from the oxidation of DMDS; notably these peak areas increased with the addition of isoprene. To determine if there were any differences in the composition of smaller particles, 20 nm particles were also measured (Figure 3.15). Compared to 60 nm particles, the 20 nm particles show no presence of sulfuric acid but similar trends for sulfate and MSA (Figure 3.16). Increased content of sulfuric acid in single particles has been attributed to longer particle lifetime and cloud processing (Pratt and Prather, 2010). The higher fraction of sulfuric acid in the DMDS particles is likely due to its faster OH reaction rate compared to DMS; sulfuric acid formation has been shown experimentally in a recent flow reactor study (Berndt et al., 2023). In addition, the particles with the smallest fraction of MSA, those produced from DMDS oxidation, have the largest fraction of sulfuric acid.

3.6 Conclusion

The oxidation processes of reduced marine sulfur gas phase compounds have been previously studied in both field and laboratory experiments. In marine environments, sulfur species have been shown to produce secondary marine aerosols that play a critical role in cloud formation. This represents the first laboratory experiment looking at the oxidation of DMDS in a PAM-OFR,

as well as the oxidation of mixtures of DMS, DMDS, and isoprene, three major marine VOCs with a crucial role in the atmosphere. We report aerosol yields of reduced sulfur compounds in a PAM-OFR that have not been measured before. We found that DMDS forms more aerosols than DMS at equivalent aging times. DMS particle phase products grow faster than those produced by DMDS oxidation. In the case of DMS, there was enough time in the OFR for condensation to occur without preexisting aerosols added. This shows that, although particle formation processes in PAM-OFR are dominated by nucleation, fast reactions can allow for condensation processes to also occur.

In this study, we determined that oxidation of DMS results in a higher aerosol yield than DMDS and isoprene. At the highest exposure time, almost 90% of DMS is oxidized to the aerosol phase and only 60% and 10% for DMDS and isoprene, respectively. Although DMS had the highest yields, DMS loss was slower than DMDS loss resulting in 52% and 4%, respectively, of unreacted gas at the lowest OH exposure. The remaining 39% of DMDS oxidation products in the gas phase (versus only 6% from DMS) adds a substantial amount of gas phase products that have the potential to alter the composition of the atmosphere impacting further oxidation reactions and enhancing condensation on existing aerosols. This impact has been shown in our DMS and DMDS mixture experiment, which led to a higher yield likely because of gas phase DMDS oxidation products condensation on recently produced aerosols. With DMDS having a lower yield but still producing more particles in number, the mixing ratios of DMDS in marine environments could have a significant impact on the cloudiness over the oceans by increasing the number of cloud condensation nuclei present, potentially influencing marine cloud cover. Interestingly, when mixing DMDS and DMS, the fraction of particles containing MSA, sulfate, and sulfuric acid concentrations decreased compared to DMS alone, for 60 nm particles. These results suggest a potential enhancement of other oxidation products when these two sulfur species are mixed. The

presence of DMDS considerably alters the composition, number, and size of secondary aerosols, supporting the need to study other marine-relevant sulfur species, including methanethiol. In addition to marine-derived sulfur compounds, anthropogenic sulfur species, such as benzothiazole, should also be studied as they have been shown to be present in marine environments (Franklin et al., 2021).

DMS and DMDS are known to produce similar OH oxidation products as shown in previous chamber experiments (Van Rooy et al., 2021a, 2021b). We found that for both VOCs the main oxidation product was sulfate followed by MSA and, when mixed, the product ratio between the two was altered. Although the comprehensive characterization of all oxidation products, e.g. by untargeted methods, is outside the scope of this work, on-going experiments using electrospray ionization coupled to high-resolution Orbitrap mass spectrometry have confirmed MSA and sulfate as main oxidation products, followed by a plethora of sulfur-containing organic compounds in low concentrations. Figure 3.17 shows positive and negative mode Orbitrap spectra from the mixture of DMS, DMDS, and isoprene. Our results also suggest that the production of MSA in a humid environment did not require the addition of NO_x into the system. The introduction of isoprene to the mix exhibited a contrasting effect on these sulfur compounds: while it reduced sulfate concentration in DMS oxidation, it enhanced both sulfate and MSA levels in DMDS. Furthermore, the different composition of the single particle aerosols from mixtures of these VOCs will likely impact the composition of the atmosphere. The combination of the three intensified the amount of MSA and sulfate present compared to each individual gas, leading to a potential increase of acidity in the atmosphere. This emphasizes the complex interactions between trace gases in atmospheric systems. Even a single compound like isoprene can markedly alter DMS and DMDS oxidation pathways. This study underscores the importance of examining mixtures to comprehend alterations

in oxidation products and relative concentrations. Future work will expand the complexity of these mixtures by sampling marine air in coastal environments through the PAM-OFR to explore the impact on aerosol production, thus complementing recent studies carried out by our group and collaborators on marine VOC emissions from laboratory mesocosms (Kilgour et al., 2022). Moreover, while experiments were always performed at a humidity close to 70%, the present work did not explore the influence of relative humidity and is certainly a point to be addressed in future studies. Going forward, further research is required to unravel the mechanisms that govern the impact of marine organic compounds on the oxidation of reduced sulfur compounds, as well as the presence of oxidants other than OH (e.g. NO_x, Cl), thus shedding light on the behavior of secondary marine aerosols and their influence in cloud formation and lifetime.

3.7 Author contributions

ANM, LC, and KAP conceptualized the study. ANM, LC, and KAK conducted the experiments. ANM, LC, and KAK analyzed the data and composed the figures. ANM and LC led the manuscript writing. ANM, LC, KAK, and KAP contributed to the editing and reviewing of the article.

3.8 Conflicts of interest

There are no conflicts to declare.

3.9 Acknowledgments

This material is based upon work supported by the National Science Foundation through the Center for Aerosol Impacts on Chemistry of the Environment, an NSF Center for Chemical Innovation (CHE-1801971). Any opinions, findings, and conclusions, or recommendations expressed in this material are those of the author(s) and do not necessarily reflect the views of the

National Science Foundation. We thank Kathryn J. Mayer, Neal Arakawa, Jonathan H. Slade and Robert S. Pomeroy for their assistance and helpful feedback.

Chapter 3, in full, is a reprint of material with permission from *Environmental Science: Atmospheres*, 2024. Moore, A. N., Cancelada, L., Kimble, K. A., & Prather, K. A. "Secondary Marine Aerosol Formation from Mixtures of Volatile Organic Compounds in a Potential Aerosol Mass Oxidative Flow Reactor" *Environmental. Sciences.: Atmospheres, 2024*,***4***, *351-361*. Copyright 2024 Royal Society of Chemistry. The dissertation author and Lucia Cancelada are the primary investigators and co-first authors of this manuscript.

3.10 Figures

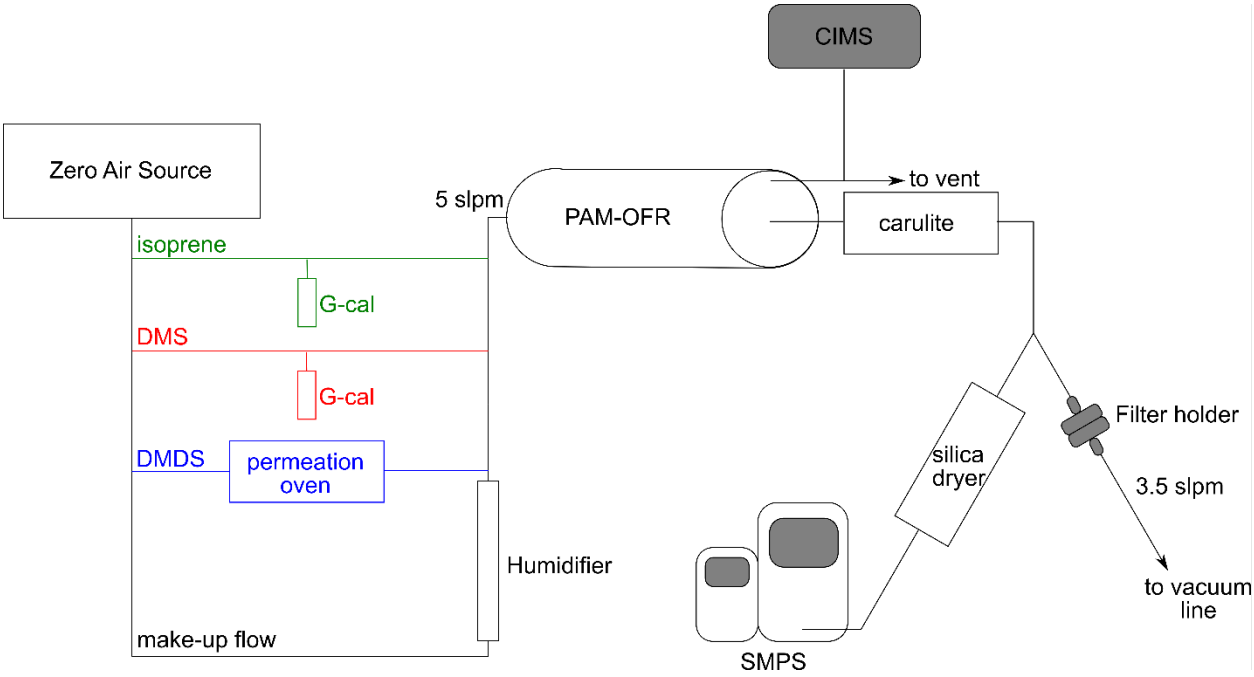


Figure 3.1: Schematic diagram of experimental setup used for secondary marine aerosol reaction studies.

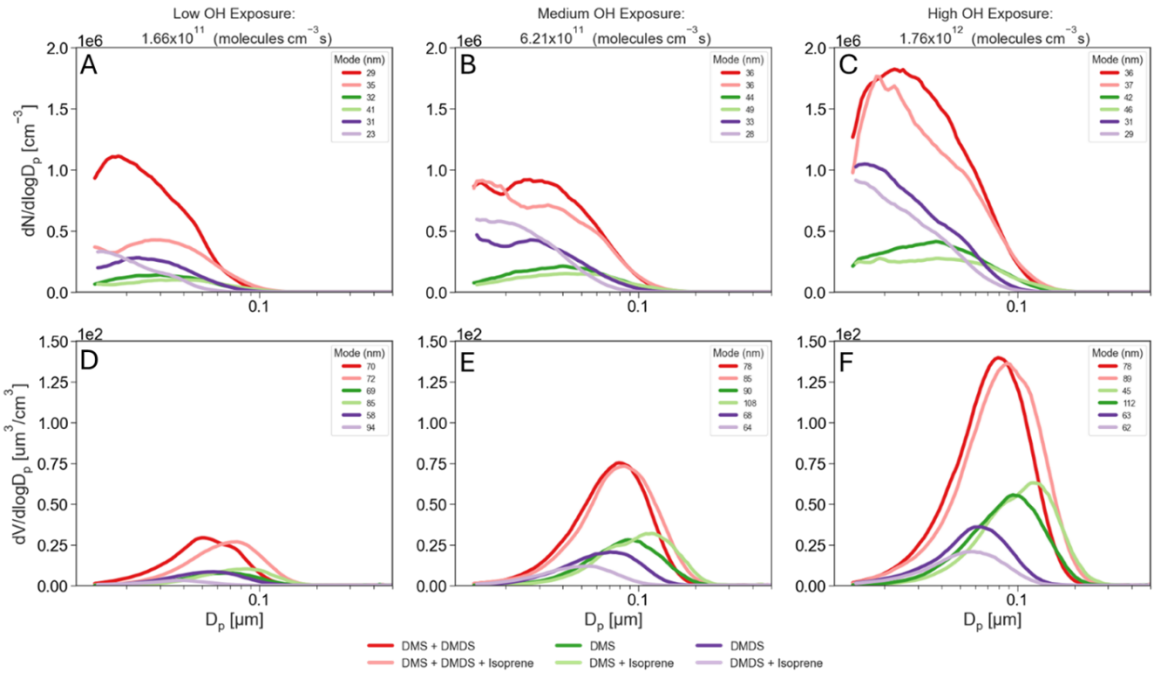


Figure 3.2: Particle number (top) and volume (bottom) distributions for low, medium and high OH exposure (VOCs and mixtures combined on each panel).

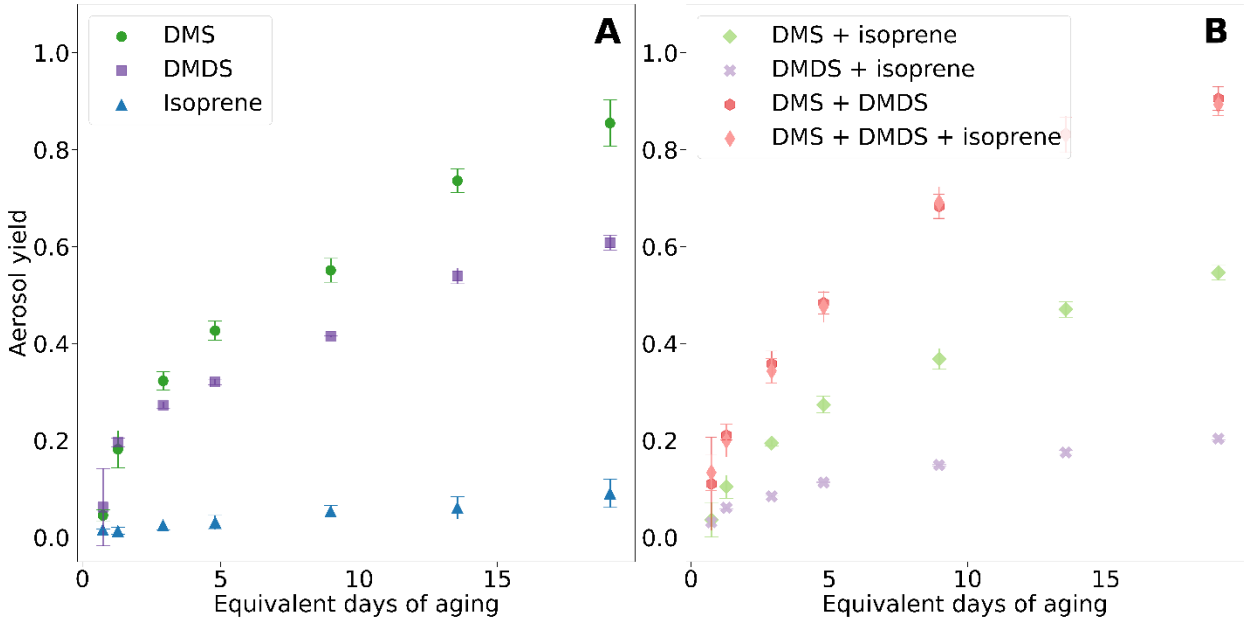


Figure 3.3: Aerosol yields for VOCs and mixtures. (A) Pure compounds. (B) Mixtures. Error bars represent the standard deviation of three trials.

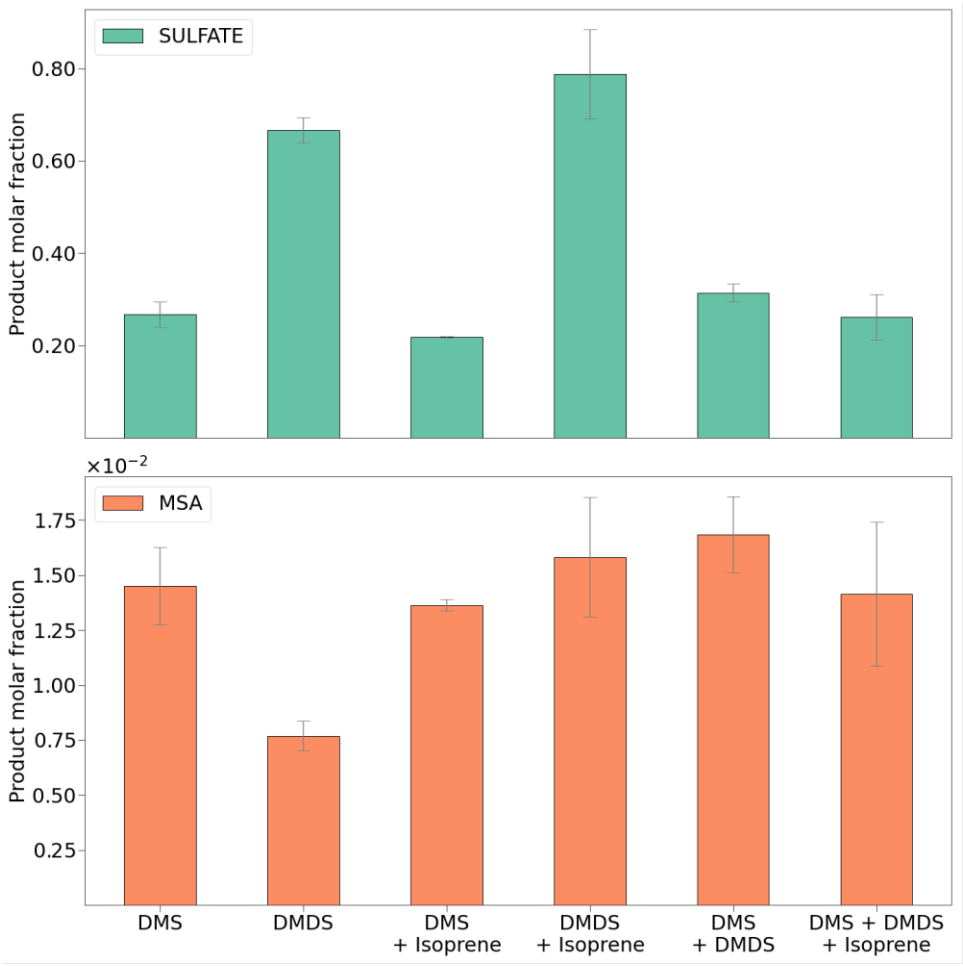


Figure 3.4: MSA and sulfate molar fractions for DMS, DMDS, and mixtures with isoprene. Error bars represent the standard deviation of four trials.

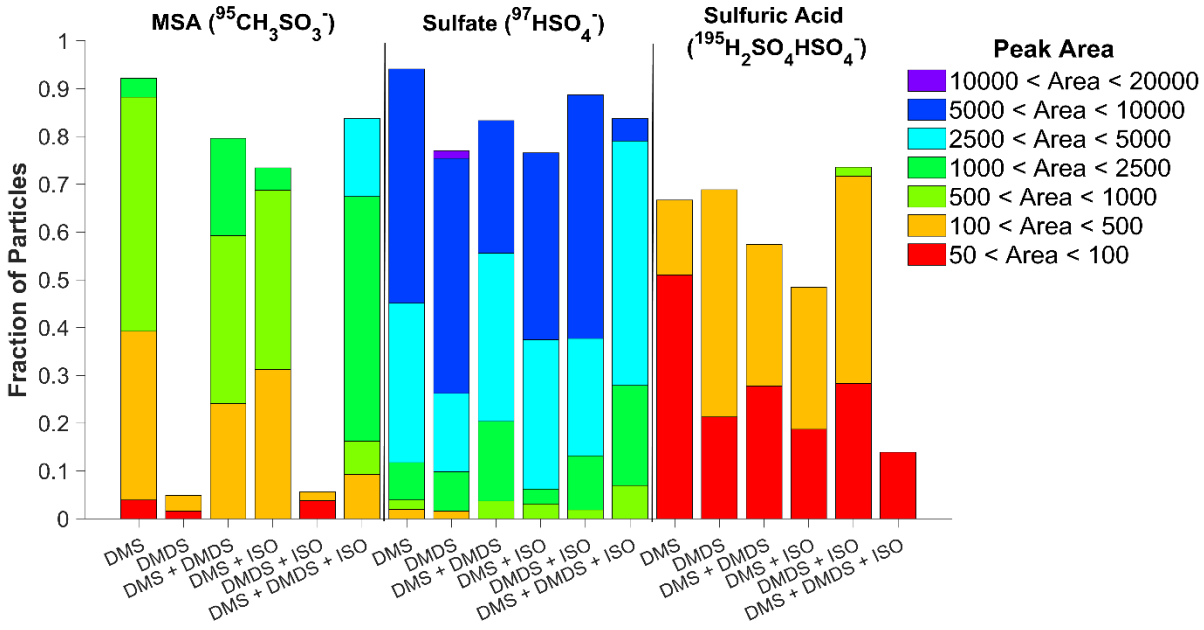


Figure 3.5: Fraction of 60 nm particles produced by the different VOCs and mixtures that contain MSA, sulfate, and sulfuric acid. Colors represent the fraction of particles that present peak areas falling in specific ranges.

3.11 Tables

Table 3.1: Experimental conditions for aerosol yield experiments. (1): (Atkinson et al., 1992), (2): (Atkinson et al., 1989), (3): (Burkholder et al., 2020).

Experiment	VOC source	VOC concentration (ppb)	OH exposure (molecules s cm^{-3})	OH reaction rate constant (cm^3 $molecules^{-1}$ s^{-1})
DMS	G-cal	16	9.6×10^{10} – 2.5×10^{12}	0.44×10^{-11} (1)
DMDS	Permeation tube	9		20×10^{-11} (2)
Isoprene	G-cal	15		10×10^{-11} (3)
DMS + isoprene	G-cal	15 (DMS) 11 (isoprene)		
DMDS + isoprene	Permeation tube (DMDS) G-cal (isoprene)	6 (DMDS) 15 (isoprene)		
DMS + DMDS	G-cal (DMS) Permeation tube (DMDS)	18 (DMS) 9 (DMDS)		
DMS + DMDS + isoprene	G-cal (DMS) Permeation tube (DMDS) G-cal (isoprene)	15 (DMS) 9 (DMDS) 12 (isoprene)		

3. 12 References

Ahlberg, E., Falk, J., Eriksson, A., Holst, T., Brune, W.H., Kristensson, A., Roldin, P., Svenningsson, B., 2017. Secondary organic aerosol from VOC mixtures in an oxidation flow reactor. Atmospheric Environment 161, 210–220. https://doi.org/10.1016/J.ATMOSENV.2017.05.005

Atkinson, R., Baulch, D.L., Cox, R.A., Hampson, R.F., Kerr Chairman, J.A., Troe, J., 2009. Evaluated Kinetic and Photochemical Data for Atmospheric Chemistry: Supplement III. IUPAC Subcommittee on Gas Kinetic Data Evaluation for Atmospheric Chemistry. Journal of Physical and Chemical Reference Data 18, 881. https://doi.org/10.1063/1.555832

Atkinson, R., Baulch, D.L., Cox, R.A., Hampson, R.F., Kerr Chairman, J.A., Troe, J., 1989. Evaluated Kinetic and Photochemical Data for Atmospheric Chemistry: Supplement III. IUPAC Subcommittee on Gas Kinetic Data Evaluation for Atmospheric Chemistry. Journal of Physical and Chemical Reference Data 18, 881–1097. https://doi.org/10.1063/1.555832

Atkinson, R., Baulch, D.L., Cox, R.A., Hampson, R.F., Kerr, J.A., Troe, J., 1992. Evaluated kinetic and photochemical data for atmospheric chemistry: Supplement IV. IUPAC subcommittee on gas kinetic data evaluation for atmospheric chemistry. Atmospheric Environment Part A, General Topics 26, 1187–1230. https://doi.org/10.1016/0960-1686(92)90383-V

Barnes, I., Hjorth, J., Mihalapoulos, N., 2006. Dimethyl sulfide and dimethyl sulfoxide and their oxidation in the atmosphere. Chemical Reviews 106, 940–975. https://doi.org/10.1021/cr020529+

Bates, T.S., Calhoun, J.A., Quinn, P.K., 1992. Variations in the methanesulfonate to sulfate molar ratio in submicrometer marine aerosol particles over the South Pacific Ocean. Journal of Geophysical Research 97, 9859–9865. https://doi.org/10.1029/92JD00411

Becagli, S., Barbaro, E., Bonamano, S., Caiazzo, L., Di Sarra, A., Feltracco, M., Grigioni, P., Heintzenberg, J., Lazzara, L., Legrand, M., Madonia, A., Marcelli, M., Melillo, C., Meloni, D., Nuccio, C., Pace, G., Park, K.T., Preunkert, S., Severi, M., Vecchiato, M., Zangrando, R., Traversi, R., 2022. Factors controlling atmospheric DMS and its oxidation products (MSA and nssSO42-) in the aerosol at Terra Nova Bay, Antarctica. Atmospheric Chemistry and Physics 22, 9245–9263. https://doi.org/10.5194/ACP-22-9245-2022

Berndt, T., Hoffmann, E.H., Tilgner, A., Stratmann, F., Herrmann, H., 2023. Direct sulfuric acid formation from the gas-phase oxidation of reduced-sulfur compounds. Nat Commun 14, 4849. https://doi.org/10.1038/s41467-023-40586-2

Berresheim, H., Elste, T., Tremmel, H.G., Allen, A.G., Hansson, H.C., Rosman, K., Dal Maso, M., Mäkelä, J.M., Kulmala, M., O'Dowd, C.D., 2002. Gas-aerosol relationships of H2SO4, MSA, and OH: Observations in the coastal marine boundary layer at Mace Head, Ireland.

Journal of Geophysical Research: Atmospheres 107, PAR 5-1. https://doi.org/10.1029/2000JD000229

Burkholder, J.B., Sander, S.P., Abbatt, J.P.D., Barker, J.R., Cappa, C., Crounse, J.D., Dibble, T.S., Huie, R.E., Kolb, C.E., Kurylo, M.J., Orkin, V.L., Percival, C.J., Wilmouth, D.M., Wine, P.H., 2020. Chemical Kinetics and Photochemical Data for Use in Atmospheric Studies Evaluation Number 19 NASA Panel for Data Evaluation.

Chen, T., Jang, M., 2012. Secondary organic aerosol formation from photooxidation of a mixture of dimethyl sulfide and isoprene. Atmospheric Environment 46, 271–278. https://doi.org/10.1016/J.ATMOSENV.2011.09.082

Chen, W.C., Marcus, R.A., 2006. On the theory of the reaction rate of vibrationally excited CO molecules with OH radicals. The Journal of Chemical Physics 124, 024306. https://doi.org/10.1063/1.2148408

Claeys, M., Graham, B., Vas, G., Wang, W., Vermeylen, R., Pashynska, V., Cafmeyer, J., Guyon, P., Andreae, M.O., Artaxo, P., Maenhaut, W., 2004. Formation of Secondary Organic Aerosols Through Photooxidation of Isoprene 303, 1173–1177.

Dall'Osto, M., Beddows, D.C.S., Tunved, P., Krejci, R., Ström, J., Hansson, H.C., Yoon, Y.J., Park, K.T., Becagli, S., Udisti, R., Onasch, T., O'Dowd, C.D., Simó, R., Harrison, R.M., 2017. Arctic sea ice melt leads to atmospheric new particle formation. Scientific Reports 2017 7:1 7, 1–10. https://doi.org/10.1038/s41598-017-03328-1

Dani, K.G.S., Loreto, F., 2017. Trade-Off Between Dimethyl Sul fi de and Isoprene Emissions from Marine Phytoplankton. Trends in Plant Science 22, 361–372. https://doi.org/10.1016/j.tplants.2017.01.006

Franklin, E.B., Alves, M.R., Moore, A.N., Kilgour, D.B., Novak, G.A., Mayer, K., Sauer, J.S., Weber, R.J., Dang, D., Winter, M., Lee, C., Cappa, C.D., Bertram, T.H., Prather, K.A., Grassian, V.H., Goldstein, A.H., 2021. Atmospheric Benzothiazoles in a Coastal Marine Environment. Cite This: Environ. Sci. Technol 55, 15705–15714. https://doi.org/10.1021/acs.est.1c04422

Gard, E., Mayer, J.E., Morrical, B.D., Dienes, T., Fergenson, D.P., Prather, K.A., 1997. Real-Time Analysis of Individual Atmospheric Aerosol Particles: Design and Performance of a Portable ATOFMS. Analytical Chemistry 69, 4083–4091. https://doi.org/10.1021/ac970540n

Gaston, C.J., Pratt, K.A., Qin, X., Prather, K.A., 2010. Real-Time Detection and Mixing State of Methanesulfonate in Single Particles at an Inland Urban Location during a Phytoplankton Bloom. Environmental Science and Technology 44, 1566–1572. https://doi.org/10.1021/ES902069D

Hodshire, A.L., Campuzano-Jost, P., Kodros, J.K., Croft, B., Nault, B.A., Schroder, J.C., Jimenez, J.L., Pierce, J.R., 2019. The potential role of methanesulfonic acid (MSA) in aerosol formation and growth and the associated radiative forcings. Atmospheric Chemistry and Physics 19, 3137–3160. https://doi.org/10.5194/ACP-19-3137-2019

Hu, W., Palm, B.B., Day, D.A., Campuzano-Jost, P., Krechmer, J.E., Peng, Z., De Sá, S.S., Martin, S.T., Alexander, M.L., Baumann, K., Hacker, L., Kiendler-Scharr, A., Koss, A.R., De Gouw, J.A., Goldstein, A.H., Seco, R., Sjostedt, S.J., Park, J.-H., Guenther, A.B., Kim, S., Canonaco, F., Prévôt, A.S.H., Brune, W.H., Jimenez, J.L., 2016. Volatility and lifetime against OH heterogeneous reaction of ambient isoprene-epoxydiols-derived secondary organic aerosol (IEPOX-SOA). Atmos. Chem. Phys 16, 11563–11580. https://doi.org/10.5194/acp-16-11563-2016

Jiang, B., Xie, Z., Qiu, Y., Wang, L., Yue, F., Kang, H., Yu, X., Wu, X., 2021. Modification of the Conversion of Dimethylsulfide to Methanesulfonic Acid by Anthropogenic Pollution as Revealed by Long-Term Observations. ACS Earth and Space Chemistry 5, 2839–2845. https://doi.org/10.1021/ACSEARTHSPACECHEM.1C00222/SUPPL_FILE/SP1C00222_SI_001.XLSX

Kang, E., Root, M.J., Toohey, D.W., Brune, W.H., 2007. and Physics Introducing the concept of Potential Aerosol Mass (PAM) 5727–5744.

Kilgour, D.B., Novak, G.A., Sauer, J.S., Moore, A.N., Dinasquet, J., Amiri, S., Franklin, E.B., Mayer, K., Winter, M., Morris, C.K., Price, T., Malfatti, F., Crocker, D.R., Lee, C., Cappa, C.D., Goldstein, A.H., Prather, K.A., Bertram, T.H., 2022. Marine gas-phase sulfur emissions during an induced phytoplankton bloom. Atmospheric Chemistry and Physics 22, 1601–1613. https://doi.org/10.5194/acp-22-1601-2022

Kim, M.J., Zoerb, M.C., Campbell, N.R., Zimmermann, K.J., Blomquist, B.W., Huebert, B.J., Bertram, T.H., 2016. Revisiting benzene cluster cations for the chemical ionization of dimethyl sulfide and select volatile organic compounds. Atmospheric Measurement Techniques 9, 1473–1484. https://doi.org/10.5194/amt-9-1473-2016

Kroll, J.H., Smith, J.D., Che, D.L., Kessler, S.H., Worsnop, D.R., Wilson, K.R., 2009. Measurement of fragmentation and functionalization pathways in the heterogeneous oxidation of oxidized organic aerosol. Phys. Chem. Chem. Phys. 11, 8005–8014. https://doi.org/10.1039/B905289E

Kulmala, M., Petäjä, T., Ehn, M., Thornton, J., Sipilä, M., Worsnop, D.R., Kerminen, V.M., 2014. Chemistry of Atmospheric Nucleation: On the Recent Advances on Precursor Characterization and Atmospheric Cluster Composition in Connection with Atmospheric New Particle Formation. https://doi.org/10.1146/annurev-physchem-040412-110014 65, 21–37. https://doi.org/10.1146/ANNUREV-PHYSCHEM-040412-110014

Lambe, A.T., Chhabra, P.S., Onasch, T.B., Brune, W.H., Hunter, J.F., Kroll, J.H., Cummings, M.J., Brogan, J.F., Parmar, Y., Worsnop, D.R., Kolb, C.E., Davidovits, P., 2015. Effect of

oxidant concentration, exposure time, and seed particles on secondary organic aerosol chemical composition and yield. Atmospheric Chemistry and Physics 15, 3063–3075. https://doi.org/10.5194/ACP-15-3063-2015

Lavi, A., Vermeuel, M.P., Novak, G.A., Bertram, T.H., 2018. The sensitivity of benzene cluster cation chemical ionization mass spectrometry to select biogenic terpenes. Atmospheric Measurement Techniques 11, 3251–3262. https://doi.org/10.5194/amt-11-3251-2018

Li, L., Kimble, K.A., Mitts, B.A., Heilig, M., Qiao, Y., Lee, J., Prather, K.A., Hogan, C.J., 2023. Nanoparticle growth in thermally diffusive sublimation-condensation systems with low vapor pressure solids. Journal of Aerosol Science 173. https://doi.org/10.1016/j.jaerosci.2023.106225

Lohmann, U., Feichter, J., 2005. Global indirect aerosol effects: A review. Atmospheric Chemistry and Physics 5, 715–737. https://doi.org/10.5194/ACP-5-715-2005

Mayer, K.J., Wang, X., Santander, M.V., Mitts, B.A., Sauer, J.S., Sultana, C.M., Cappa, C.D., Prather, K.A., 2020. Secondary Marine Aerosol Plays a Dominant Role over Primary Sea Spray Aerosol in Cloud Formation. https://doi.org/10.1021/acscentsci.0c00793

Odum, J.R., Hoffmann, T., Bowman, F., Collins, D., Flagan, R.C., Seinfeld, J.H., 1996. Gas/Particle Partitioning and Secondary Organic Aerosol Yields. Environ. Sci. Technol. 30, 2580–2585. https://doi.org/10.1021/es950943+

Peng, Z., Jimenez, J.L., 2020. Radical chemistry in oxidation flow reactors for atmospheric chemistry research. Chemical Society Reviews 49, 2570–2616. https://doi.org/10.1039/C9CS00766K

Pratt, K.A., Prather, K.A., 2010. Aircraft measurements of vertical profiles of aerosol mixing states. Journal of Geophysical Research Atmospheres 115, 1–10. https://doi.org/10.1029/2009JD013150

Saltzman, E.S., Savoie, D.L., Zika, R.G., Prospero, J.M., 1983. Methane sulfonic acid in the marine atmosphere. Journal of Geophysical Research: Oceans 88, 10897–10902. https://doi.org/10.1029/JC088IC15P10897

Slade, J.H., de Perre, C., Lee, L., Shepson, P.B., 2017. Nitrate radical oxidation of γ-terpinene: hydroxy nitrate, total organic nitrate, and secondary organic aerosol yields. Atmospheric Chemistry and Physics 17, 8635–8650. https://doi.org/10.5194/acp-17-8635-2017

Twomey, S., 1974. Pollution and the planetary albedo. Atmospheric Environment (1967) 8, 1251–1256. https://doi.org/10.1016/0004-6981(74)90004-3

Van Rooy, P., Drover, R., Cress, T., Michael, C., Purvis-Roberts, K.L., Silva, P.J., Nee, M.J., Cocker, D., 2021a. Methanesulfonic acid and sulfuric acid Aerosol Formed through

oxidation of reduced sulfur compounds in a humid environment. Atmospheric Environment 261, 118504. https://doi.org/10.1016/J.ATMOSENV.2021.118504

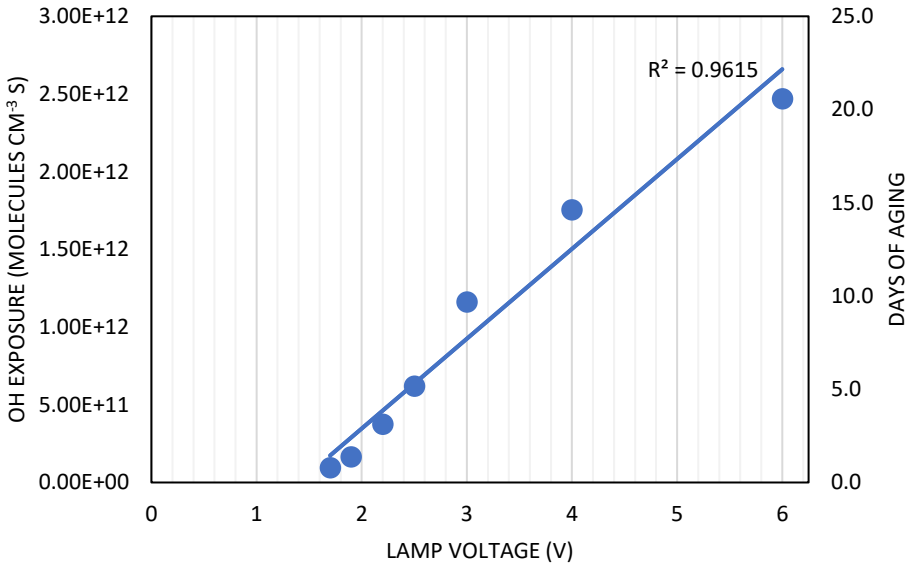
Van Rooy, P., Purvis-Roberts, K.L., Silva, P.J., Nee, M.J., Cocker, D., 2021b. Characterization of secondary products formed through oxidation of reduced sulfur compounds. Atmospheric Environment 256, 118148. https://doi.org/10.1016/j.atmosenv.2020.118148

Ye, Q., Goss, M.B., Krechmer, J.E., Majluf, F., Zaytsev, A., Li, Y., Roscioli, J.R., Canagaratna, M., Keutsch, F.N., Heald, C.L., Kroll, J.H., 2022. Product distribution, kinetics, and aerosol formation from the OH oxidation of dimethyl sulfide under different RO_2 regimes. Atmospheric Chemistry and Physics 22, 16003–16015. https://doi.org/10.5194/ACP-22-16003-2022

Zhang, R., Khalizov, A., Wang, L., Hu, M., Xu, W., 2012. Nucleation and growth of nanoparticles in the atmosphere. Chemical Reviews 112, 1957–2011. https://doi.org/10.1021/CR2001756/ASSET/CR2001756.FP.PNG_V03

3.13 Supplementary Information

3.13.1 Supplementary Information Figures



[CO] (ppm)	Lamp voltage (V)	OH exposure (molecules cm^{-3} s)	Days of aging
0.9967	0	0	0
0.9825	1.7	9.57E+10	0.7
0.9722	1.9	1.66E+11	1.3
0.9418	2.2	3.78E+11	2.9
0.9080	2.5	6.21E+11	4.8
0.8372	3.0	1.16E+12	9.0
0.7659	4.0	1.76E+12	13.5
0.6880	6.0	2.47E+12	19.1

Figure 3.6: Calibration curve for PAM-OFR lamps

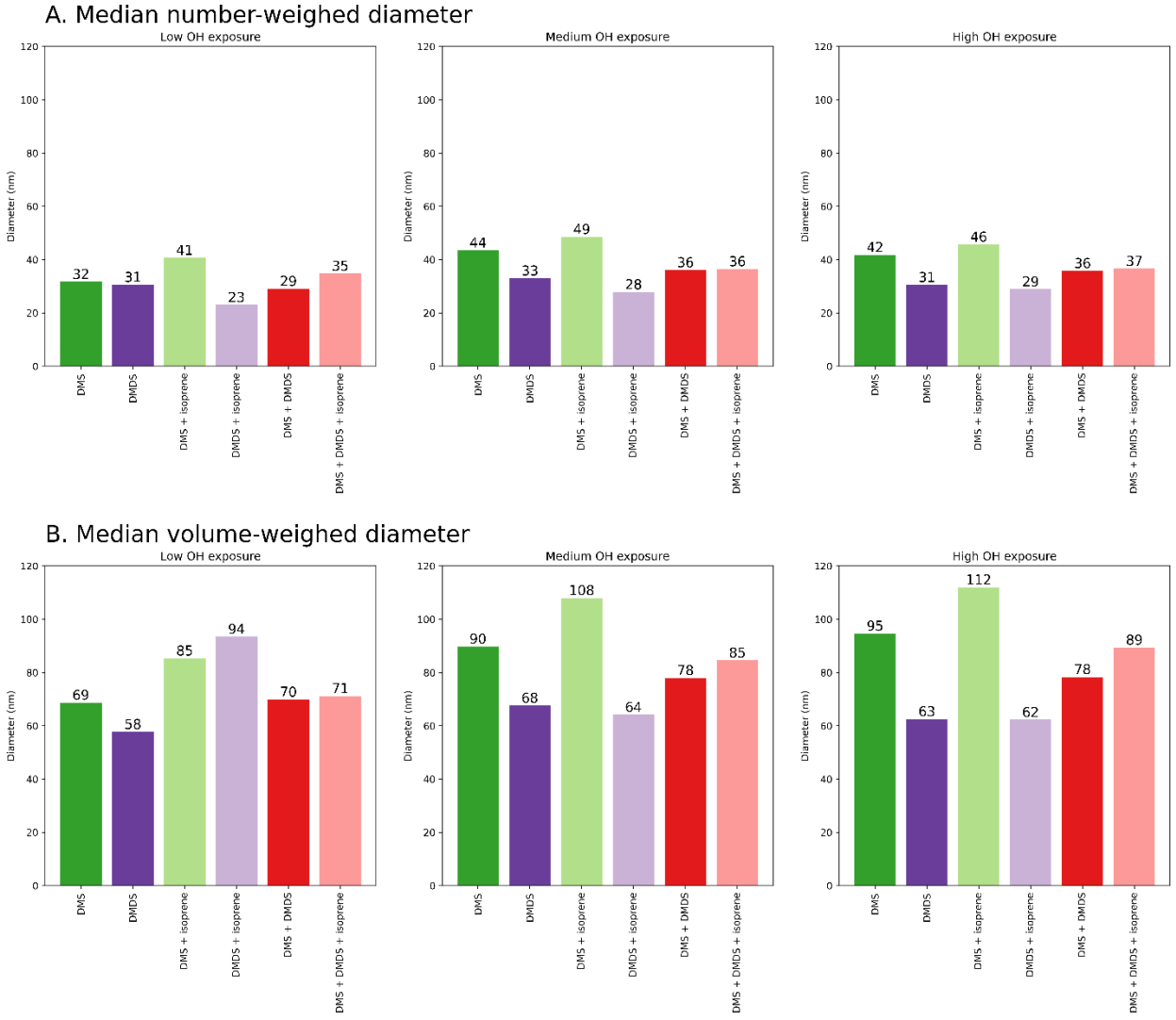


Figure 3.7: Particle number and volume distribution parameters for low, medium and high OH exposure (VOCs and mixtures).

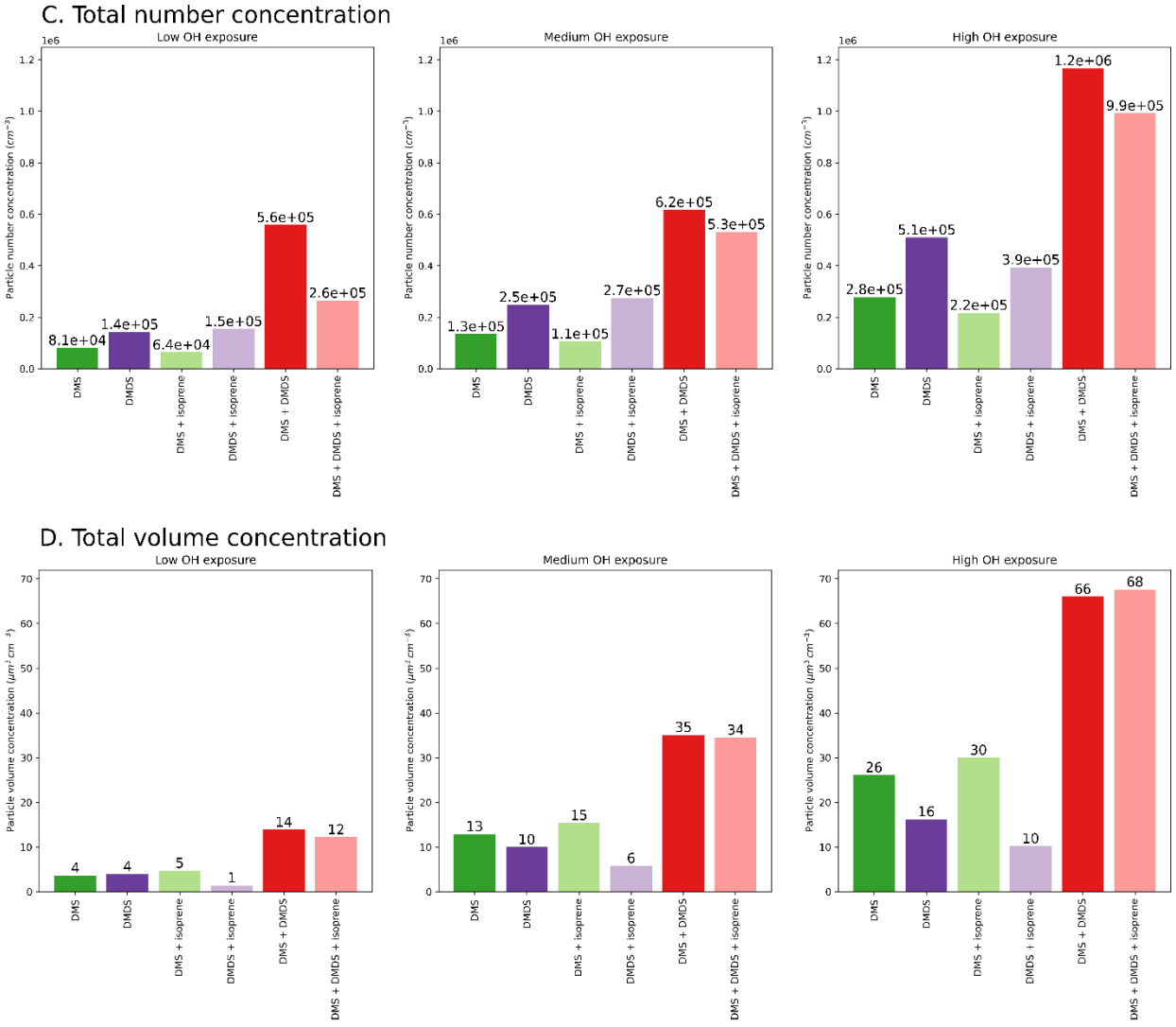


Figure 3.7: Particle number and volume distribution parameters for low, medium and high OH exposure (VOCs and mixtures).

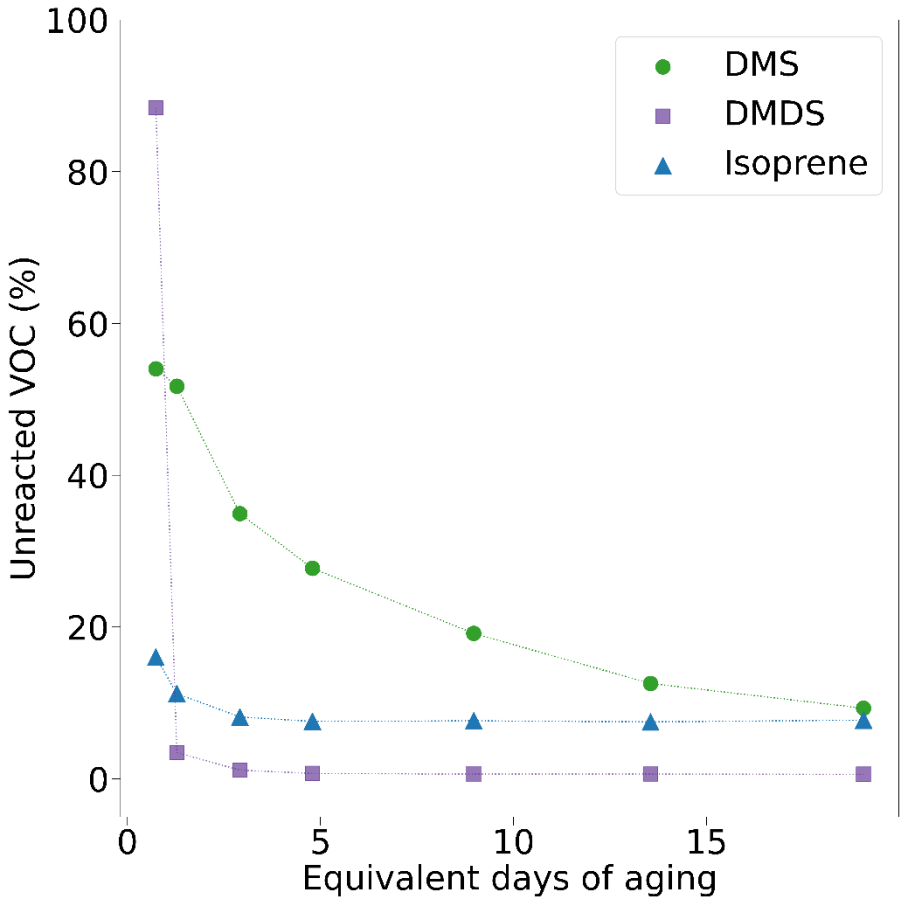


Figure 3.8: Percent non-reacted gas for DMS, DMDS and isoprene yield experiments.

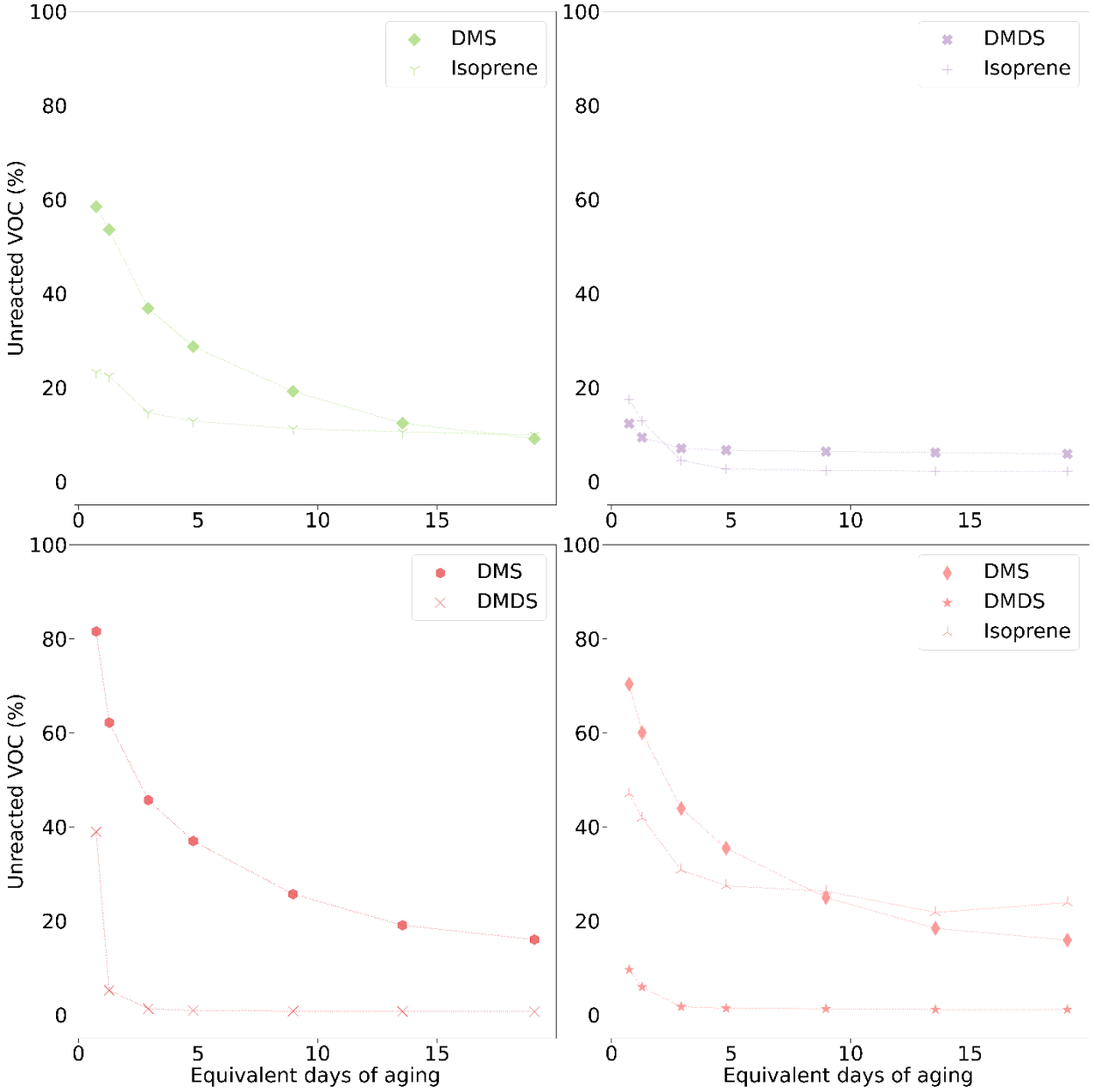


Figure 3.9: Non-reacted gas (in %) for mixture yield experiments (left: DMS and isoprene, right: DMDS and isoprene).

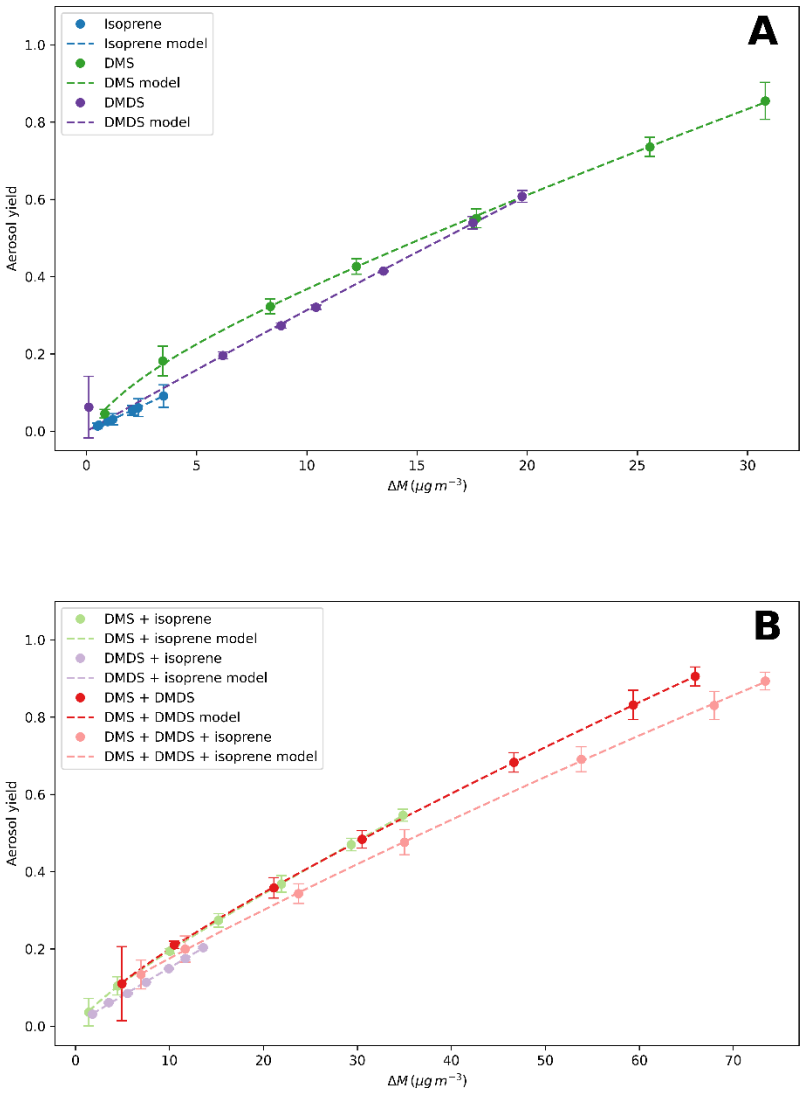


Figure 3.10: Aerosol yields vs. aerosol mass increase for individual VOCs and mixtures. A. Pure compounds. B. Mixtures. Dashed lines correspond to the fitting of the absorptive partitioning model from Odum et al. (1996). Error bars represent the standard deviation of three trials.

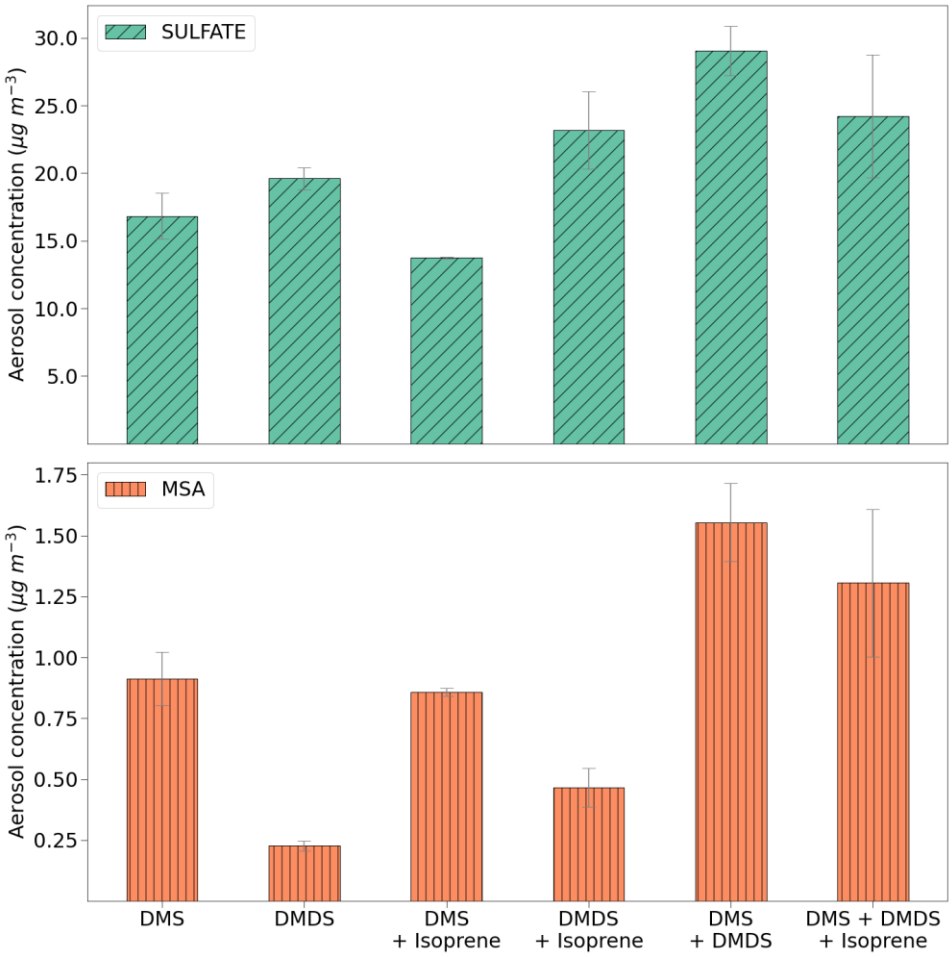


Figure 3.11: MSA and sulfate aerosol concentrations molar fractions for DMS, DMDS, and mixtures with isoprene. Error bars represent the standard deviation of four trials.

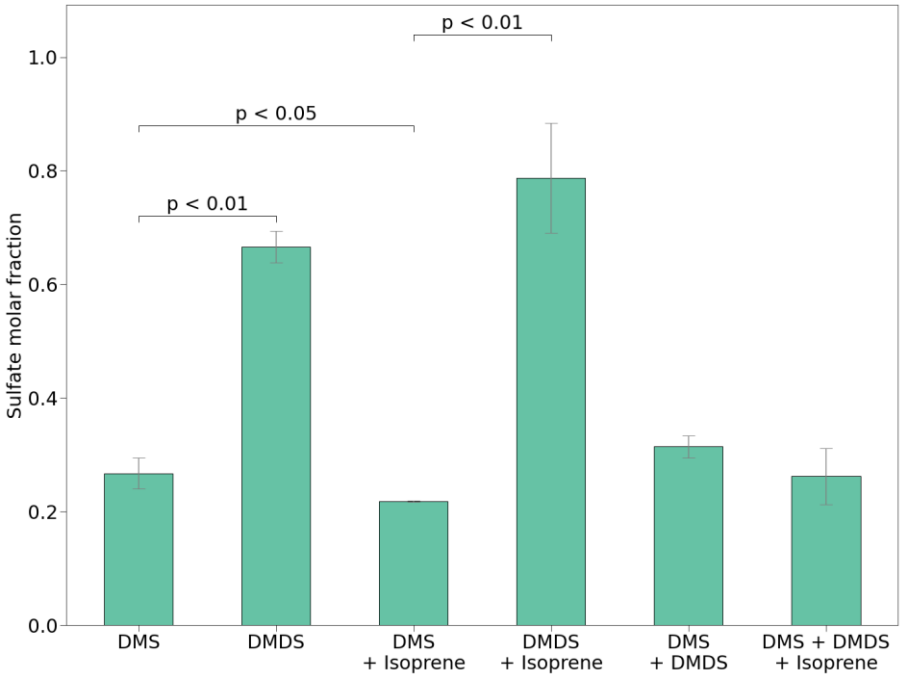


Figure 3.12: Sulfate molar fraction for DMS, DMDS, DMS/isoprene and DMDS/isoprene experiments. P-values under 0.01 and 0.05 are shown for a paired t-test (two tails). Error bars represent the standard deviation of four trials.

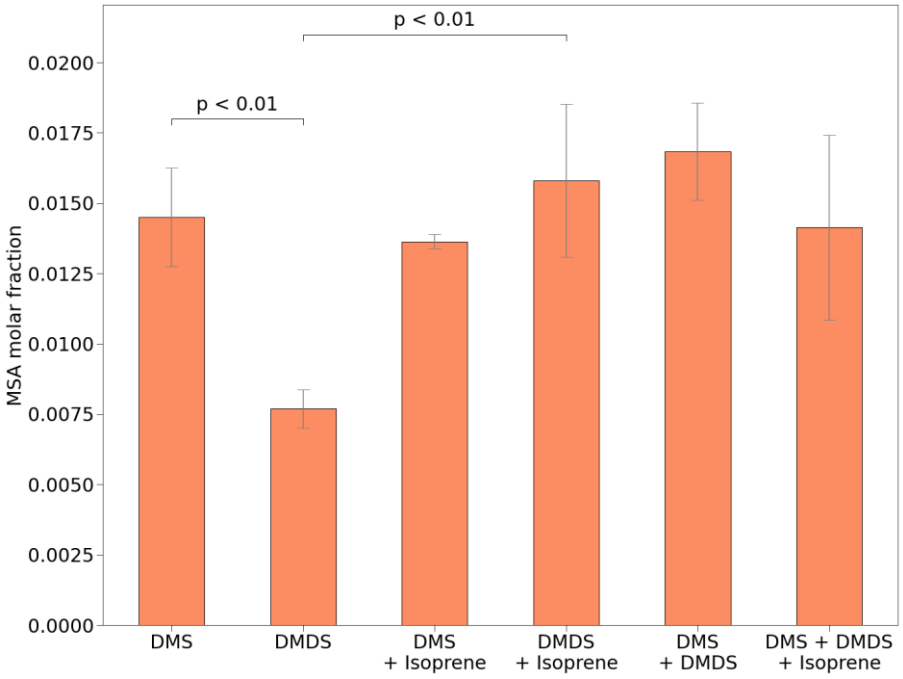


Figure 3.13: MSA molar fraction for DMS, DMDS, DMS/isoprene and DMDS/isoprene experiments. P-values under 0.01 are shown for a paired t-test (two tails). Error bars represent the standard deviation of four trials.

.

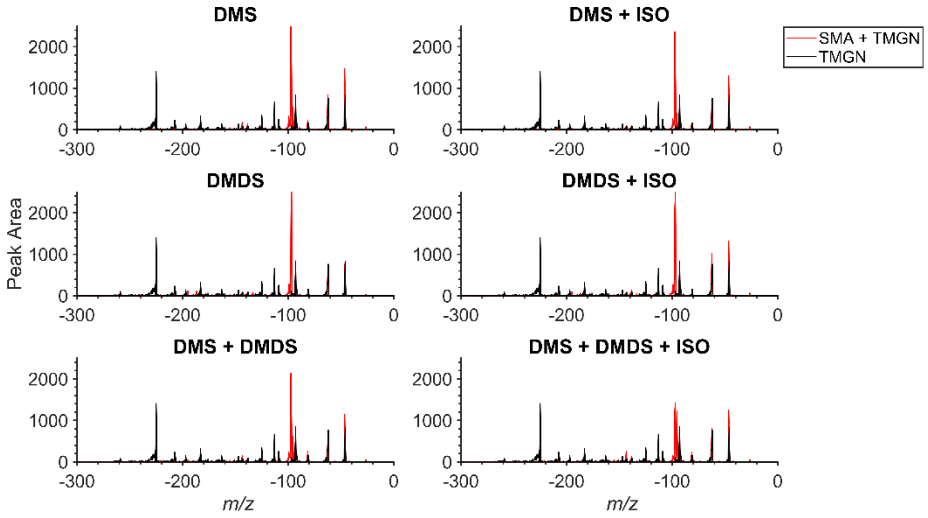


Figure 3.14: Average mass spectra of 60 nm particles produced by various VOCs and mixtures after they have been coated with matrix TMGN (red lines). Black lines represent the average spectra of homogeneously nucleated TMGN particles

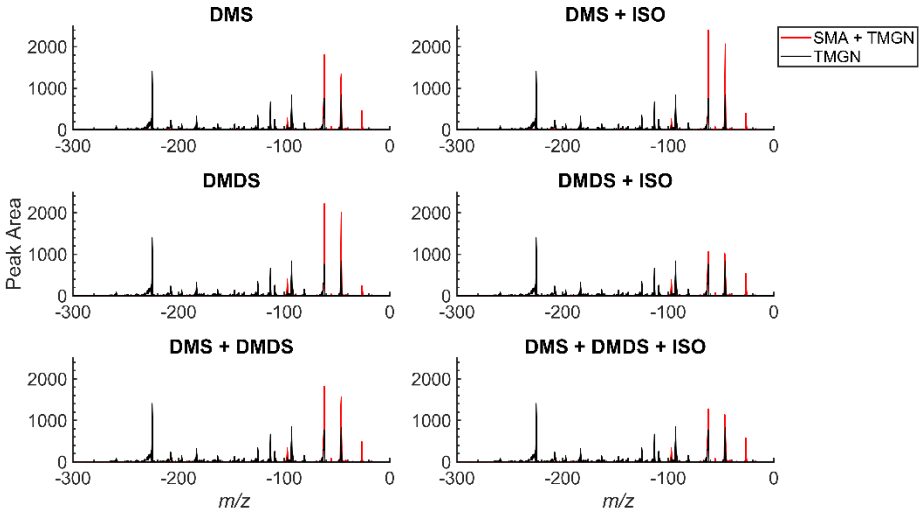


Figure 3.15: Average mass spectra of 20 nm particles produced by various VOCs and mixtures after they have been coated with matrix TMGN (red lines). Black lines represent the average spectra of homogeneously nucleated TMGN particles.

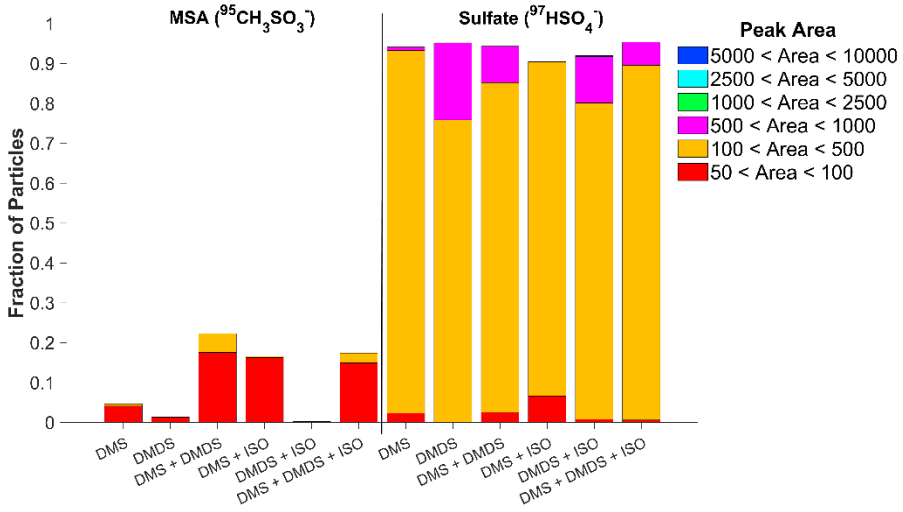


Figure 3.16: Fraction of 20 nm particles produced by the different VOCs and mixtures that contain MSA and sulfate. Colors represent the fraction of particles that present peak areas falling in specific ranges.

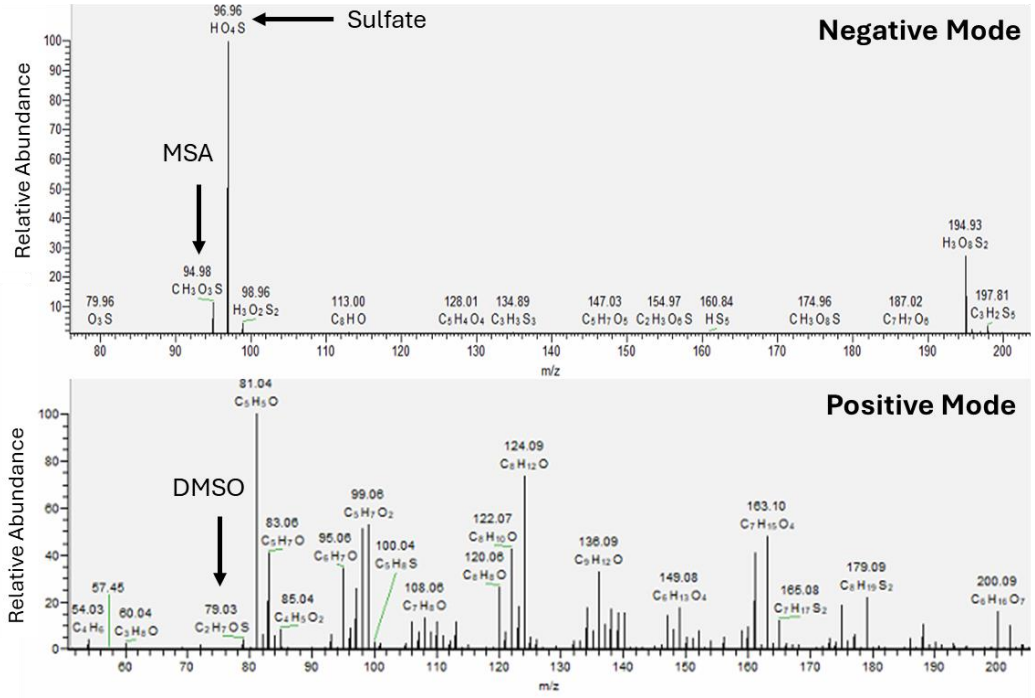


Figure 3.17: Positive and negative mode Orbitrap spectra from the mixture of DMS, DMDS, and Isoprene. Sulfate, MSA, and dimethyl sulfoxide (DMSO) have been identified.

3.13.2 Supplementary Information Table

Table 3.2: Experimental conditions for aerosol filter experiments

Experiment	VOC source	VOC concentration (ppb)	OH exposure (molecules s cm^{-3})
DMS	G-cal	16	3.8×10^{11}
DMDS	Permeation tube	9	
Isoprene	G-cal	15	
DMS + isoprene	G-cal	15 (DMS) 11 (isoprene)	
DMDS + isoprene	Permeation tube (DMDS) G-cal (isoprene)	6 (DMDS) 15 (isoprene)	
DMS + DMDS	G-cal (DMS) Permeation tube (DMDS)	18 (DMS) 9 (DMDS)	
DMS + DMDS + isoprene	G-cal (DMS) Permeation tube (DMDS) G-cal (isoprene)	15 (DMS) 9 (DMDS) 12 (isoprene)	

Chapter 4. Secondary Marine Aerosol Formation from Volatile Organic Compounds Emitted from Phytoplankton Blooms

4.1 Abstract

Emissions of volatile organic compounds (VOCs) from oceans can contribute significantly to the marine atmospheric composition. VOCs can be produced biologically from marine phytoplankton and transferred to the atmosphere, where they can interact with other atmospheric oxidants, such as OH radicals, to undergo chemical reactions that result in the formation of secondary marine aerosols (SMA). Coastal and remote ocean field studies have examined the formation and composition of secondary marine aerosols, however the complexity have proved challenging to separate primary and secondary aerosols. Few laboratory experiments have looked at the formation of SMA but there still remains many uncertainties. To address this gap, three phytoplankton blooms were conducted to analyze changes in VOC concentrations and SMA formation as a function of biological activity. VOC measurements identified distinct changes of dimethyl sulfide, dimethyl disulfide, and isoprene over the course of the bloom. Dimethyl disulfide concentrations significantly exceeded the other VOC concentrations. Further, dimethyl disulfide was found to have a large contribution to secondary marine aerosol number concentrations and isoprene was found to impact the aerosol size distributions. This study highlights the significant impact of both non-sulfur and sulfur containing compounds on the formation of secondary marine aerosols.

4.2 Introduction

Oceanic emissions of primary aerosols and VOCs contribute significantly to the dynamics of the atmosphere, leading to changes in aerosol properties; directly and indirectly impacting the

global radiative budget. VOCs can be oxidized to form lower volatile compounds that can nucleate to form new particles or condense on existing particles, forming secondary marine aerosols (SMA). Both primary and secondary aerosols can act as cloud condensation nuclei (CCN), though they have different cloud forming potential (Mayer et al., 2020). To date, research has shown that correlations between CCN and marine biological activity are driven by SMA produced from biogenic VOCs. In the Southern Ocean, marine biological VOCs have been attributed to 35-80% of CCN (Vallina et al., 2006). In addition, Mayer et al., conducted a laboratory experiment and found that during realistic phytoplankton bloom conditions SMA controlled cloud properties (Mayer et al., 2020). Although a few studies have found connections between marine biogenic VOCs and SMA, the processes constraining their emissions and formation are still poorly understood. Specifically, the impact biological activity has on the number, size, and concentration of SMA remains unknown.

Marine phytoplankton and bacteria are the main contributors of VOCs emitted from the ocean, especially sulfur compounds and hydrocarbons, such as isoprene (Dani and Loreto, 2017). Dimethyl sulfide (DMS), the most abundant sulfur species emitted from the ocean, is a biological VOC that originates from the bacterial cleavage of the marine osmolyte dimethyl sulfoniopropionate (DMSP) (Charlson et al., 1987). Methanethiol is also produced from DMSP through the demethylation pathway, and subsequently, the abiotic dimerization of methanethiol forms dimethyl disulfide (DMDS) (Kiene, 1996; Perraud et al., 2016). Marine isoprene is thought to be a result of phytoplankton response to environmental conditions, such as temperature and acidification (Dani and Loreto, 2017). Although isoprene is primarily considered a terrestrial VOC, in the marine boundary layer it can have concentrations ranging in the same order of magnitude as DMS (Dani and Loreto, 2017). Once emitted to the atmosphere, sulfur compounds and isoprene

can contribute significantly to SMA. Laboratory studies have shown that changes in simplistic mixtures of VOCs can impact the number, size, and composition of secondary aerosols (Bougiatioti et al., 2020; Moore et al., 2024). Knowing how marine VOCs contribute to SMA is imperative to providing a better understanding of these aerosol's contributions to the global climate system.

Secondary marine aerosol impact on climate is determined by their number, size and composition (Mansour et al., 2020). They are largely comprised of sulfate, nitrate, ammonium, and organics (Mayer et al., 2020). The oxidation of sulfur VOCs leads to the formation of sulfate and methane sulfonic acid (MSA), which impacts new particle formation and aerosol growth, respectively (Bates et al., 1992; Ye et al., 2022). A model of marine secondary organic aerosols suggested that DMS oxidation can account for 78% of secondary aerosols (Li et al., 2020). In addition, in the China Sea, it was determined that sulfate was the most abundant compound of PM 2.5 (Li et al., 2020). While the DMS oxidation product, sulfate, can dominate the composition of secondary marine aerosols, the organic fraction has a strong impact on the water uptake of an aerosol, as organics change the kappa value (Rosati et al., 2022). These changes will impact an aerosols effectiveness to act as a CCN. The interchange between organic and sulfur compound underscores the importance of examining marine VOC emissions and their oxidative processes.

In this study, three phytoplankton blooms were conducted to measure the temporal evolution of the biogenic VOC production and assess the changes in the formation of the secondary marine aerosols. The VOCs emitted from the seawater were oxidized in a potential aerosol mass oxidative flow reaction to measure the size and number of the aerosols as a function of marine biological activity.

4.3 Methods

4.3.1 Experimental Setup

Three 20-L Nalgene bottles were filled with seawater collected from Ellen Browning Pier at Scripps Institute of Oceanography (La Jolla, CA; 32°51´56.8"N: 117° 15´38.48"W). To remove debris and zooplankton, the seawater was filtered with 50 um nitex mesh during collection. A phytoplankton bloom was induced by adding f/2 algal growth medium (Proline, Aquatic Eco-Systems, Apopka, FL) and 245 mg sodium metasilicate to induce a phytoplankton diatom dominated bloom. The progression of the blooms was measured daily with a handheld fluorometer (Aquafluor, Turner Designs, San Jose, CA). Each bottle contained submerged Teflon tubing with holes to bubble in zero air from a zero air generator (Sabio Environmental) at various flow rates depending on the sampling condition. The three sampling conditions, shown in Figure 4.1, were using the Potential Aerosol Mass Oxidative Flow Reactor (PAM-OFR, Aerodyne) (Kang et al., 2007) to generate aerosols and gather sizing information with a scanning mobility particle sizer (SMPS), sampling with a chemical ionization time-of-flight- mass spectrometer (CI-ToF-MS) to measure VOCs, and no sampling. The bubbling flow rates with zero air were 5.5 standard liters per minute (slpm), 2.2 slpm, and 1 slpm, respectively. The headspace of each bottle was sampled for VOCs every day for 30 minutes. This ensured enough time for a steady concentration to be reached.

A flow rate of 5 LPM was sent to the PAM-OFR to oxidize the VOCs. Each bottle was sampled for 20 hours through the PAM-OFR to measure the secondary aerosol size distribution and collect the aerosols on filters. The PAM-OFR was operated in 185 nm mode, which uses UV lamps with wavelengths of = 185 and 254 nm to generate OH radicals. To calibrate the OH

exposure in the OFR, 1 ppm of carbon monoxide was introduced into the PAM, at the same flow rate and relative humidities as the experiment, to measure the CO decay as a function of lamp voltage using a CO analyzer. The CO + OH rate coefficient KOH+CO, 298k = 1.5x10^-12 cm3 molec-1 s-1 was used to determine the OH concentration and equivalent days of aging at each voltage. The PAM-OFR was operated at 2.2 V, equivalent to 2.9 days. The calibration is shown in Figure 4.5. To remove ozone and prevent further oxidation reactions, a diffusion ozone denuder was placed after the OFR prior to the sizing instrument. A custom-built silica drier was used after the denuder to dry the aerosols before they reached the SMPS.

4.3.2 Quantification of VOCs

VOCs from the carboys were analyzed using a real time CI-ToF-MS (Kim et al., 2016). Benzene was used as the reagent and generated by flowing 10 standard cubic centimeters per minute of ultrahigh purity N_2 gas through a cylinder of liquid benzene and diluted to with N_2 to a final concentration of 300 ppm. A 20 mCi Po-210 alpha-source was used to generate benzene cluster cation reagent ions that are then carried to the ion molecule region (IMR) through a 1.8 standard liter per minute (slpm) critical orifice. The analyte was also drawn to the IMR with a critical orifice at 1.8 slpm. In the IMR, the pressure and the voltage were held at 60 Torr and 60V throughout the entire experiment. Analyte ions generated through chemical ionizations reactions with benzene cluster cations were transferred to the ion funnel, which is used to focus the ion beam and decluster the ions. The ion beam is then transferred by an RF-only quadrupole to the orthogonal time of flight mass analyzer. A TOFWARE plugin for Igor 8 was used to perform the data analysis of the co-summed mass spectra collected at 1 Hz. External calibrations were performed for DMS, DMDS, and isoprene using Dynacal Permeation Tubes.

4.3.3 Particle Size Distribution Measurements

The particle size distributions of the aerosols generated in the PAM-OFR were measured using a SMPS. The SMPS combines a differential mobility analyzer (DMA) Model 3081, an electrostatic classifier Model 3082, and a water-based condensation particle counter Model 3787 (TSI, Inc.). It was operated with a sample flow rate of 0.6 L min^{-1} and a sheath flow rate of 3.0 L min^{-1}. The SMPS scanned the electrical mobility diameters between 14-750 nm every 5 minutes. With the electrical mobility diameters assumed to be equal to physical diameters, the size and volume distributions presented are shown with physical diameters.

4.4 Results and Discussion

Marine VOC emissions are largely driven by changes in biological activity. Figure 4.2 presents the VOC concentrations (DMS, DMDS, and isoprene) and Chlorophyll a (Chl. a) concentrations over the course of three phytoplankton blooms. Chl. a is used as a proxy for biological activity in seawater and is used to track the progression of phytoplankton blooms through three phases: growth, exponential, and senescence (Behrenfeld et al., 1997). The Chl-a values, measured by fluorescence, range from 0.4 – 19.8 µg L^{-1} which falls within the detected range found in the same sampling location (McGowan et al., 2017). Blooms 1 and 2 peak at 13.8 and 19.8 µg L^{-1} respectively, while bloom 3 only reaches a maximum of 4.2 µg L^{-1}. The changes in the concentrations of DMS, DMDS, and isoprene over the course of the bloom were measured daily as shown in Figure 4.2. For all three blooms the concentration of DMS remained relatively low ranging from 20-100 ppt and peaking to 172, 323, and 15 for blooms 1, 2, and 3 respectively. DMS reaches its peach during the death phase of bloom 1 and 2 and peaks at the same time as Chl. a for bloom 3. This trend is similar to what has been shown in another laboratory phytoplankton

bloom experiment (Kilgour et al., 2022). The concentration of DMDS significantly exceed that of DMS with concentrations surpassing 1000 pptv during the death phase. In this experiment, the formation of DMDS is primarily attributed to the conversion of MeSH to DMDS on the surfaces of stainless steel (Perraud et al., 2016). The experimental design included stainless steel fittings inside of the carboy to allow for bubbling. A pervious experiment found in a similar experiment that 35% of MeSH can be converted to DMDS on stainless steel surfaces (Sauer et al., in prep). While the concentration of MeSH wasn't measured, the trend as shown in Figure 4.7, follows the same trend as DMDS, leading to the hypothesis that a majority of DMDS produced was from the dimerization of MeSH. In addition, the R^2 values for the correlation between MeSH and DMDS (Figure 4.6) were 91, 88, and 86 for blooms 1, 2, and 3 respectively. Isoprene had concentrations in the low pptv range throughout the bloom and peaked during the death phase for all 3 blooms. The trend of monoterpenes was also measured, as shown in Figure 4.7, and follows a similar trend to that of isoprene.

While DMS, DMDS, isoprene, MeSH, and monoterpenes were the only compounds identified and/or quantified, the complexity of the mass spectra indicates the presence of other VOCs that were not identified. The benzene CI-TOF-MS is a selective ionization instrument that limits the ability to measure the breadth of compounds that can be emitted from seawater. Therefore, other compounds that contribute to SMA formation could have been present, such as amines, oxygenated VOCs, and hydrocarbons. Although this study focuses on the primary compounds known to contribute to SMA, it's important to acknowledge that other compounds may have been present. For example, coastal seawater experiments have shown that anthropogenic compounds, such as benzothiazole, can be emitted and contribute to SMA formation (Franklin et al., 2021).

Figure 4.3A-C shows the particle number distributions over the course of each bloom. For bloom 1 the mode of the number distribution shifts to a lower diameter, from 23 µm to 16 µm, as the bloom progresses. Blooms 2 and 3 do not exhibit a distinctive change in the mode of the size distribution, however, the mode for all three blooms is the highest on the first day size distributions were measured for each bloom. During the exponential growth phase of each bloom, the percent of isoprene to the total concentration of DMS, DMDS, and isoprene was the largest, ranging from 20 to 50 percent, leading to the hypothesis that isoprene and other non-sulfur organics were contributing to the growth of the secondary marine aerosols during that time period. Laboratory oxidation studies have shown that isoprene can shift the size distributions to larger size modes by the oxidation products condensing onto existing particles. Vaattovaara et al., has suggested that isoprene oxidation products do not participate in nucleation but are contributors to particle growth of particles above 5 nm (O'Dowd and de Leeuw, 2007; Vaattovaara et al., 2006). They determined this to be a result of the Kelvin effect impacting the condensation of organics on smaller size particles (Vaattovaara et al., 2006). The PAM-OFR oxidation primarily dominates in nucleation but the fast reaction of DMS with OH can produce particles that act as seed particles to allow the condensation of isoprene oxidation products to occur. Although isoprene was the only non-sulfur compound quantified, monoterpenes were measured and possibly contributed to the SMA formation as well. Zhao et al., conducted an OFR experiment oxidizing α-pinene at various concentrations resulting in a shift of the number size distribution to larger particles as they increased the α-pinene concentration (Zhao et al., 2021). They attributed this to an enhancement of condensation and particle growth (Zhao et al., 2021). Atmospheric models have also shown that periods of high monoterpene production can alter the size distribution (Kim et al., 2017). The impact of these non-DMS organic compounds are relevant to this experiment as the oxidation

experiments were conducted at $1.66x10^{11}$ molecules s cm^{-3}, equivalent to 2.9 days of aging. Previous laboratory experiments have shown that at lower days of aging, isoprene and other similar compounds react to form low-volatility compounds that can nucleate and condense, contributing to the organic mass fraction of secondary aerosols (Mayer et al., 2020). However, at higher OH exposures, these compounds are degraded forming volatile compounds that are not condensing or nucleating (Lambe et al., 2015).

As the fraction drops and the DMDS concentration increases, there is a decrease in the mode. This can be a result of a decrease in isoprene or an increase of the DMDS concentration. Previous VOC mixture studies have shown that size distributions of mixtures between DMS, DMDS, and isoprene favor the DMDS distribution (Moore et al., 2024). DMDS has the fastest rate constant with OH radicals, possibly causing there to be less isoprene oxidation, resulting in a change of the mode as the bloom progresses.

For blooms 2 and 3, the change in number distribution is more drastic for the change in concentration than the change in the mode. The mode only decreases slightly from 20 nm to 16 nm and 19 nm to 17 nm during blooms 2 and 3, respectively. The number concentration corresponds to the intensity of the combined DMS, DMDS, and isoprene concentration for those two blooms. In bloom 2, day 15 had the highest measured number concentration and VOC concentration and day 7 had the lowest VOC and number concentration. Similarly, in bloom 3, day 15 and day 7 had the highest and lowest VOC and number concentrations, respectively. Previous data has shown that DMDS had a greater effect on the change in number concentration than DMS (Moore 2024). Bloom 1, which had minimal change in the number concentration, had the lowest percentage of DMDS, further showing the impact DMDS can have on the number concentration.

Figure 4.4 displays the number concentration and the VOC concentrations for each bloom. For all three blooms, the number concentration decreases during the exponential growth phase of the bloom, and in bloom 2 it increases during the peak and decreases during the death phase and bloom 3 increases for both phases. In addition, the number concentration corresponds to the intensity of DMDS. The strong correlation between DMDS and the number concentration is most likely driven by the oxidation of DMDS producing two sulfate molecules for every DMDS molecule, leading to more aerosol formation than DMS oxidation. Kreidenweis et al., conducted outdoor smog chamber experiments to examine the oxidation of DMS and DMS with a variety of conditions (Kreidenweis et al., 1991). In the high NO_x experiment, they found that DMDS produced more aerosols than in the DMS experiment, $N=10^5$ cm -3, vs with N = 2500 cm- 3, respectively (Kreidenweis et al., 1991).

Although methanethiol has a similar trend as DMDS, we do not expect it to impact the number concentration as much as DMDS because it only contributes one sulfur per MeSH. To our knowledge, no single component studies of methanethiol have been conducted to look at its contribution to the formation of secondary aerosols and how it changes the size distributions. Future simple mixture studies are needed to better understand the impact MeSH has on the formation of SMA.

The peak number concentration differs significantly, $5e^{-6}$, $12e^{-6}$, and $18e^{-6}$ for blooms 1, 2, and 3, respectively. When comparing the number concentration and chl-a, no correlations were found. Bloom 3 had the highest number concentration and lowest Chl. a concentration. The number concentration appears to be highly dependent on the VOC composition and concentration.

Along with the number concentration and size distribution changing across the bloom, the aerosol mass also changed. Figure 4.8 shows the aerosol mass as a function of Chl. a for all three blooms. Previous laboratory bloom experiments have seen a connection between Chl. a and aerosol mass where the aerosol mass follows the same trend as Chl. a. Blooms 1 and 2 show that similar trends, however bloom 3 does not change with Chl. a as much as the other blooms. This could be a result of the bloom not being as intense as the others or changes in the bacterial dynamics of the bloom.

4.5 Conclusion

The secondary marine aerosol formation is highly dependent on biological activity and VOC emissions (Mayer et al., 2020). At the beginning of each bloom, isoprene concentrations were higher than DMS and DMDS and the death phase of the bloom resulted in the highest concentrations of all three VOCs. The high DMDS concentrations were determined to be a result of DMDS biological production and MeSH dimerization on stainless steel surfaces in the seawater. The formation of DMDS has been shown to significantly impact secondary marine aerosol. When there was a substantial amount of DMDS, the aerosol size distribution resembled previously reported single DMDS experiments. Furthermore, the aerosol number fraction correlated with the concentration of DMDS in bloom 2 and bloom 3.

In bloom 1, isoprene had the highest fraction of the total measured VOCs at the beginning of the bloom and impacted the size distribution by shifting the mode of the distribution to larger sizes. The distribution mode then decreased when the isoprene fraction decreased as the bloom progressed. During periods of high isoprene, other non-sulfur compounds could have also been emitted, contributing to the size distribution.

Continuation of laboratory studies analyzing VOC composition and SMA formation are needed to further reduce the uncertainties of secondary aerosols. Coupling these blooms with online high resolution gas and particle phase instruments can also reduce losses in offline sample processing. This work has shown that at certain periods, DMDS and isoprene can exceed the concentrations of DMS. Furthermore, DMS has been thought to be the most impactful sulfur VOC but these results suggest that other sulfur compounds like DMDS can be as, if not more, significant than DMS. Further work is needed to explore MeSH contribution to secondary marine aerosols.

4.6 Acknowledgements

This material is based upon work supported by the National Science Foundation through the Center for Aerosol Impacts on Chemistry of the Environment, an NSF Center for Chemical Innovation (CHE-1801971). Any opinions, findings, and conclusions, or recommendations expressed in this material are those of the author(s) and do not necessarily reflect the views of the National Science Foundation.

Chapter 4, in full, is currently being prepared for submission for publication of the material. Moore, A. N. & Prather, K. A. (2024). “Secondary Marine Aerosol Formation from Volatile Organic Compounds Emitted from Phytoplankton Blooms.” The dissertation author is the primary investigator and author of this manuscript.

4.7 Figures

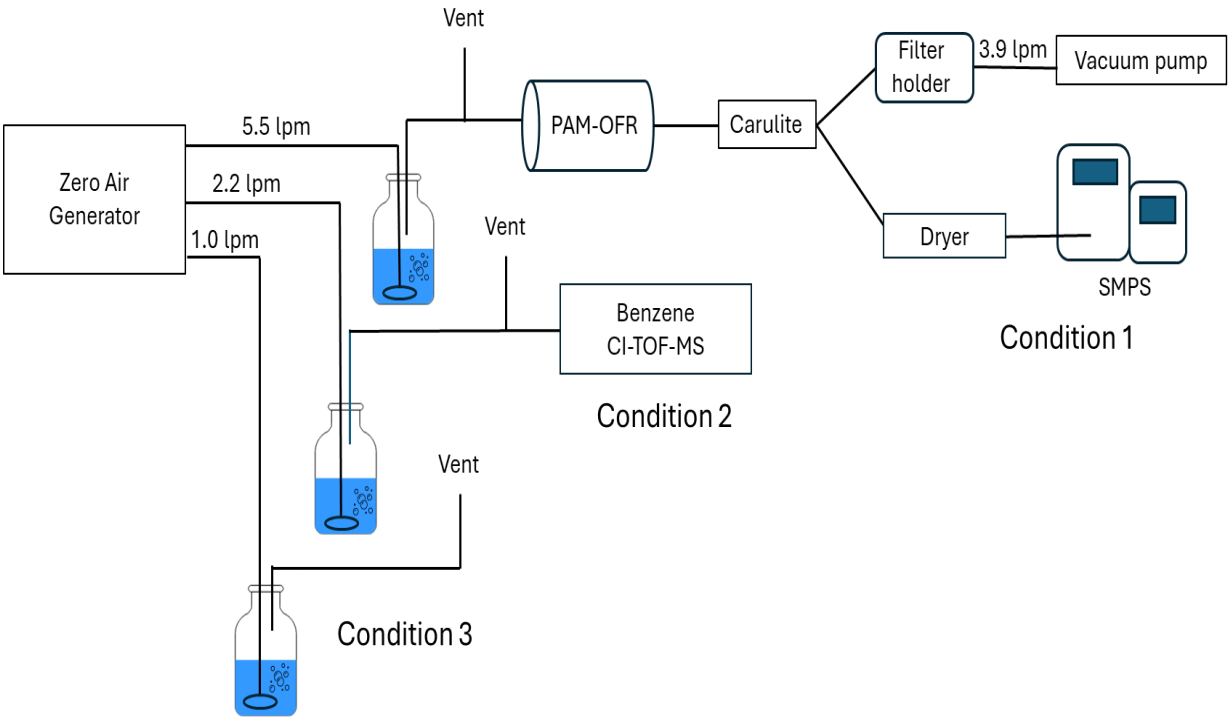


Figure 4.1: Schematic diagram for the three experimental conditions.

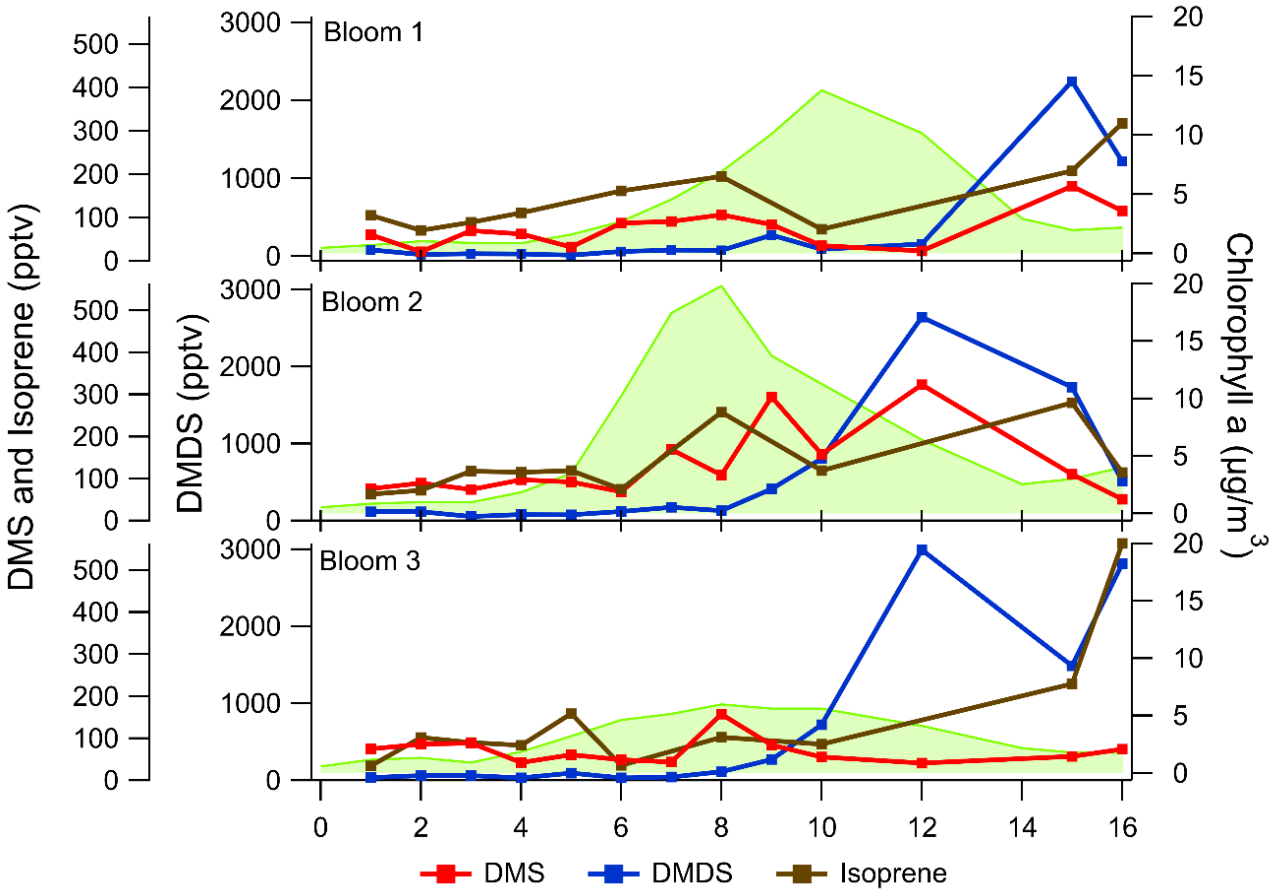


Figure 4.2: Headspace DMS, DMDS, and isoprene concentrations for bloom 1 (top), bloom 2 (middle), and bloom 3 (bottom) co-plotted with the chlorophyll a concentration. The VOC concentrations are an average of a daily 30 min sampling period.

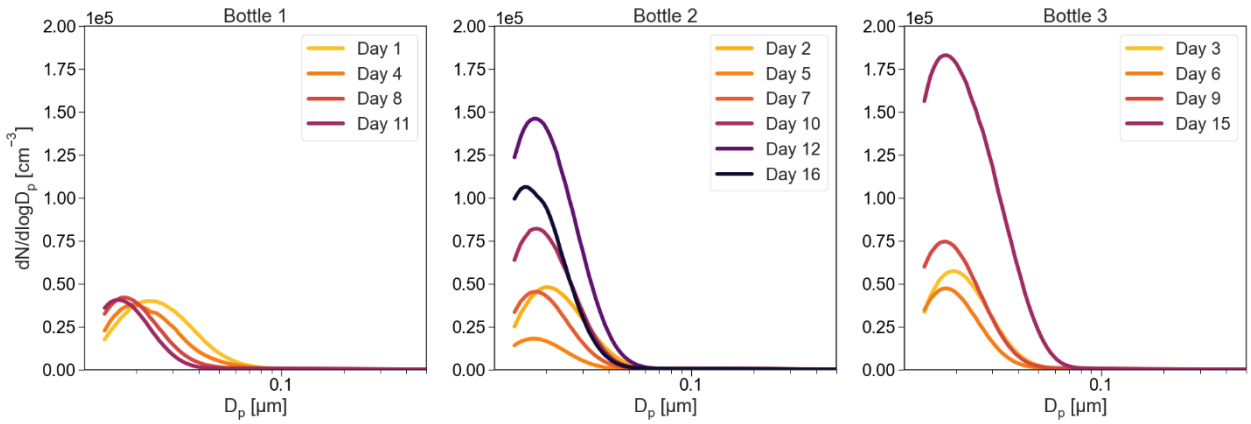


Figure 4.3: Particle number distributions over the course of bloom 1 (A), bloom 2 (B), and bloom 3 (C).

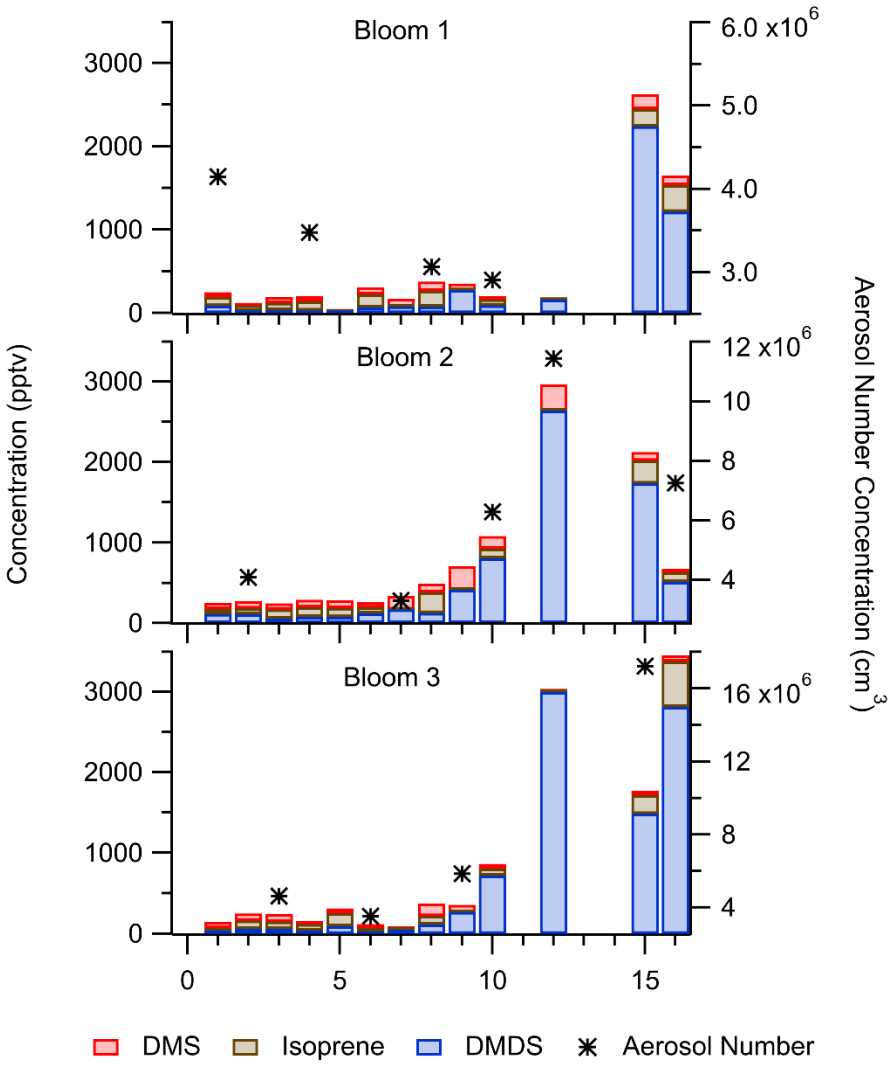


Figure 4.4: Bar plot of DMS, DMDS, and isoprene concentrations co-plotted with the aerosol number concentrations over the course of each bloom.

4.8 References

Bates, T.S., Calhoun, J.A., Quinn, P.K., 1992. Variations in the methanesulfonate to sulfate molar ratio in submicrometer marine aerosol particles over the South Pacific Ocean. Journal of Geophysical Research 97, 9859–9865. https://doi.org/10.1029/92JD00411

Bougiatioti, A., Nenes, A., Lin, J.J., Brock, C.A., de Gouw, J.A., Liao, J., Middlebrook, A.M., Welti, A., 2020. Drivers of cloud droplet number variability in the summertime in the southeastern United States. Atmospheric Chemistry and Physics 20, 12163–12176. https://doi.org/10.5194/acp-20-12163-2020

Charlson, R.J., Lovelock, J.E., Andreae, M.O., Warren, S.G., 1987. Oceanic phytoplankton, atmospheric sulphur, cloud albedo and climate. Nature 1987 326:6114 326, 655–661. https://doi.org/10.1038/326655a0

Dani, K.G.S., Loreto, F., 2017. Trade-Off Between Dimethyl Sul fi de and Isoprene Emissions from Marine Phytoplankton. Trends in Plant Science 22, 361–372. https://doi.org/10.1016/j.tplants.2017.01.006

Franklin, E.B., Alves, M.R., Moore, A.N., Kilgour, D.B., Novak, G.A., Mayer, K., Sauer, J.S., Weber, R.J., Dang, D., Winter, M., Lee, C., Cappa, C.D., Bertram, T.H., Prather, K.A., Grassian, V.H., Goldstein, A.H., 2021. Atmospheric Benzothiazoles in a Coastal Marine Environment. Cite This: Environ. Sci. Technol 55, 15705–15714. https://doi.org/10.1021/acs.est.1c04422

Kang, E., Root, M.J., Toohey, D.W., Brune, W.H., 2007. and Physics Introducing the concept of Potential Aerosol Mass (PAM) 5727–5744.

Kiene, R.P., 1996. Production of methanethiol from dimethylsulfoniopropionate marine surface waters 54, 69–83.

Kilgour, D.B., Novak, G.A., Sauer, J.S., Moore, A.N., Dinasquet, J., Amiri, S., Franklin, E.B., Mayer, K., Winter, M., Morris, C.K., Price, T., Malfatti, F., Crocker, D.R., Lee, C., Cappa, C.D., Goldstein, A.H., Prather, K.A., Bertram, T.H., 2022. Marine gas-phase sulfur emissions during an induced phytoplankton bloom. Atmospheric Chemistry and Physics 22, 1601–1613. https://doi.org/10.5194/acp-22-1601-2022

Kim, M.J., Novak, G.A., Zoerb, M.C., Yang, M., Blomquist, B.W., Huebert, B.J., Cappa, C.D., Bertram, T.H., 2017. Air-Sea exchange of biogenic volatile organic compounds and the impact on aerosol particle size distributions. Geophysical Research Letters 44, 3887–3896. https://doi.org/10.1002/2017GL072975

Kim, M.J., Zoerb, M.C., Campbell, N.R., Zimmermann, K.J., Blomquist, B.W., Huebert, B.J., Bertram, T.H., 2016. Revisiting benzene cluster cations for the chemical ionization of dimethyl sulfide and select volatile organic compounds. Atmospheric Measurement Techniques 9, 1473–1484. https://doi.org/10.5194/amt-9-1473-2016

Kreidenweis, S.M., Yin, F., Wang, S.-C., Grosjean, D., Flagan, R.C., Seinfeld, J.H., 1991. Aerosol formation during photooxidation of organosulfur species. Atmospheric Environment. Part A. General Topics, Symposium on Global Climatic Effects of Aerosols 25, 2491–2500. https://doi.org/10.1016/0960-1686(91)90165-4

Lambe, A.T., Chhabra, P.S., Onasch, T.B., Brune, W.H., Hunter, J.F., Kroll, J.H., Cummings, M.J., Brogan, J.F., Parmar, Y., Worsnop, D.R., Kolb, C.E., Davidovits, P., 2015. Effect of oxidant concentration, exposure time, and seed particles on secondary organic aerosol chemical composition and yield. Atmospheric Chemistry and Physics 15, 3063–3075. https://doi.org/10.5194/ACP-15-3063-2015

Li, S., Sarwar, G., Zhao, J., Zhang, Y., Zhou, S., Chen, Y., Yang, G., Saiz-Lopez, A., 2020. Modeling the Impact of Marine DMS Emissions on Summertime Air Quality Over the Coastal East China Seas. Earth and Space Science 7, e2020EA001220. https://doi.org/10.1029/2020EA001220

Mansour, K., Decesari, S., Facchini, M.C., Belosi, F., Paglione, M., Sandrini, S., Bellacicco, M., Marullo, S., Santoleri, R., Ovadnevaite, J., Ceburnis, D., O'Dowd, C., Roberts, G., Sanchez, K., Rinaldi, M., 2020. Linking Marine Biological Activity to Aerosol Chemical Composition and Cloud-Relevant Properties Over the North Atlantic Ocean. Journal of Geophysical Research: Atmospheres 125, e2019JD032246. https://doi.org/10.1029/2019JD032246

Mayer, K.J., Wang, X., Santander, M.V., Mitts, B.A., Sauer, J.S., Sultana, C.M., Cappa, C.D., Prather, K.A., 2020. Secondary Marine Aerosol Plays a Dominant Role over Primary Sea Spray Aerosol in Cloud Formation. https://doi.org/10.1021/acscentsci.0c00793

McGowan, J.A., Deyle, E.R., Ye, H., Carter, M.L., Perretti, C.T., Seger, K.D., de Verneil, A., Sugihara, G., 2017. Predicting coastal algal blooms in southern California. Ecology 98, 1419–1433. https://doi.org/10.1002/ecy.1804

Moore, A.N., Cancelada, L., Kimble, K.A., Prather, K.A., 2024. Secondary aerosol formation from mixtures of marine volatile organic compounds in a potential aerosol mass oxidative flow reactor. Environ. Sci.: Atmos. 4, 351–361. https://doi.org/10.1039/D3EA00169E

O'Dowd, C.D., de Leeuw, G., 2007. Marine aerosol production: a review of the current knowledge. Philosophical Transactions of the Royal Society A: Mathematical, Physical and Engineering Sciences 365, 1753–1774. https://doi.org/10.1098/rsta.2007.2043

Perraud, V., Meinardi, S., Blake, D.R., Finlayson-Pitts, B.J., 2016. Challenges associated with the sampling and analysis of organosulfur compounds in air using real-time PTR-ToF-MS and offline GC-FID. Atmospheric Measurement Techniques 9, 1325–1340. https://doi.org/10.5194/amt-9-1325-2016

Photosynthetic rates derived from satellite-based chlorophyll concentration - Behrenfeld - 1997 - Limnology and Oceanography - Wiley Online Library [WWW Document], n.d. URL https://aslopubs.onlinelibrary.wiley.com/doi/abs/10.4319/lo.1997.42.1.0001 (accessed 6.11.24).

Rosati, B., Isokääntä, S., Christiansen, S., Jensen, M.M., Moosakutty, S.P., Wollesen De Jonge, R., Massling, A., Glasius, M., Elm, J., Virtanen, A., Bilde, M., 2022. Hygroscopicity and CCN potential of DMS derived aerosol particles. Atmospheric Chemistry and Physics Discussions 20, 1–28.

Sauer, J. S., Moore, A. N., Malfatti, F., Ametrano, C. G., Minich, J. J., Dinasquet, J., Mayer, K. J., Santander, M. D., Pendergraft, M., Mitts, B., Lee, C., Wang, X., Rico, B., Knight, R., Timothy, B. H. and Prather, K. A. (2024). Factors controlling production of dimethyl sulfide, methanethiol, and dimethyl disulfide during controlled mesocosm experiments. (2024). In prep.

Vaattovaara, P., Huttunen, P.E., Yoon, Y.J., Joutsensaari, J., Lehtinen, K.E.J., O'Dowd, C.D., Laaksonen, A., 2006. The composition of nucleation and Aitken modes particles during coastal nucleation events: evidence for marine secondary organic contribution. Atmospheric Chemistry and Physics 6, 4601–4616. https://doi.org/10.5194/acp-6-4601-2006

Vallina, S.M., Simó, R., Gassó, S., 2006. What controls CCN seasonality in the Southern Ocean? A statistical analysis based on satellite-derived chlorophyll and CCN and model-estimated OH radical and rainfall. Global Biogeochemical Cycles 20, 2005GB002597. https://doi.org/10.1029/2005GB002597

Ye, Q., Goss, M.B., Krechmer, J.E., Majluf, F., Zaytsev, A., Li, Y., Roscioli, J.R., Canagaratna, M., Keutsch, F.N., Heald, C.L., Kroll, J.H., 2022. Product distribution, kinetics, and aerosol formation from the OH oxidation of dimethyl sulfide under different RO_2 regimes. Atmospheric Chemistry and Physics 22, 16003–16015. https://doi.org/10.5194/ACP-22-16003-2022

Zhao, R., Zhang, Q., Xu, X., Zhao, W., Yu, H., Wang, W., Zhang, Y., Zhang, W., 2021. Effect of experimental conditions on secondary organic aerosol formation in an oxidation flow reactor. Atmospheric Pollution Research 12, 205–213. https://doi.org/10.1016/j.apr.2021.01.011

4.9 Supplementary Information

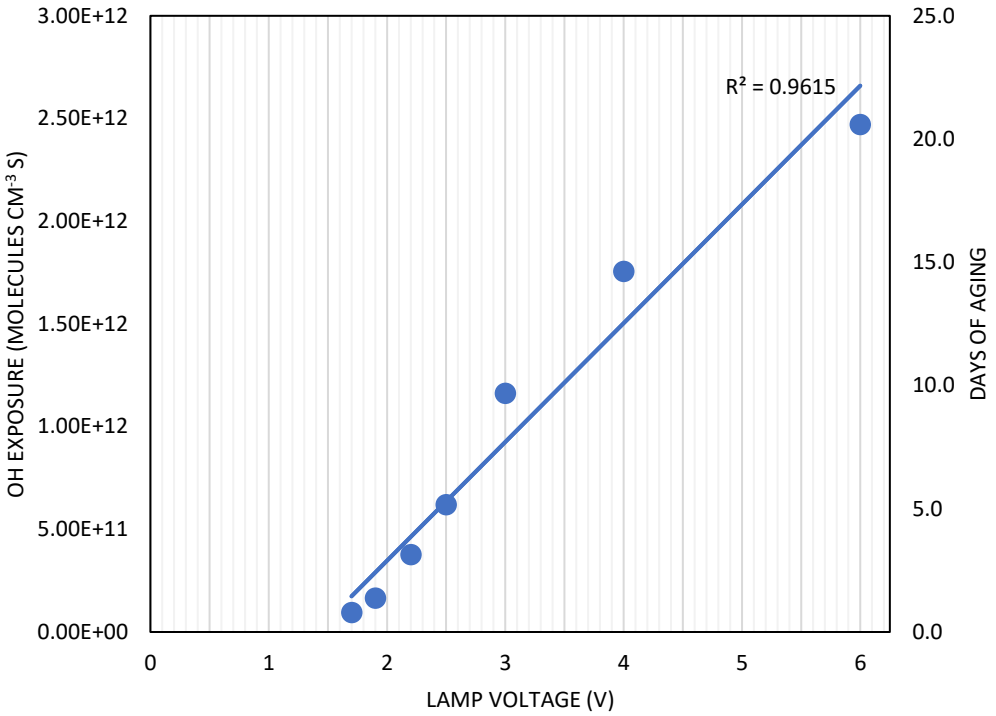


Figure 4.5: Calibration curve for the PAM-OFR

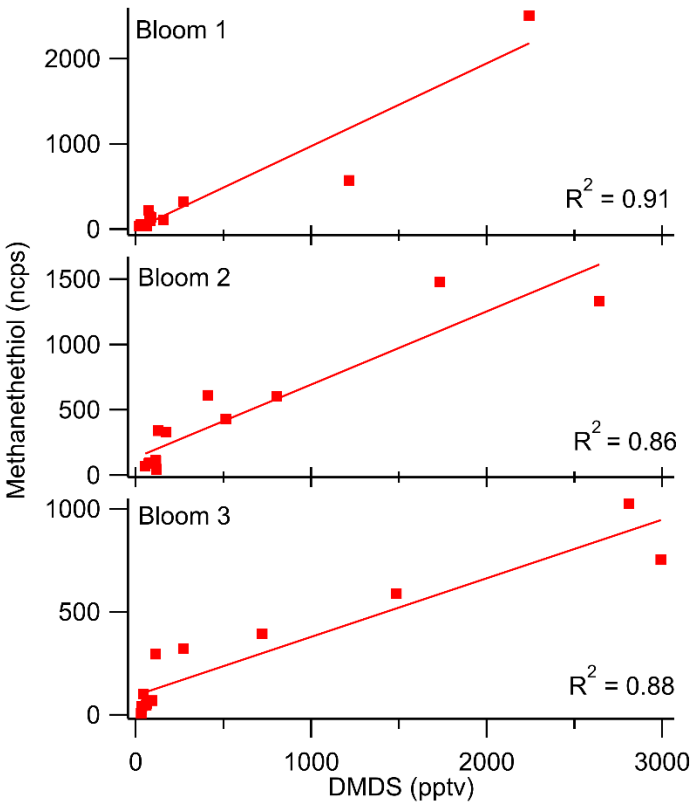


Figure 4.6: Correlation between DMDS concentration and methanethiol (MeSH) normalized counts per seconds.

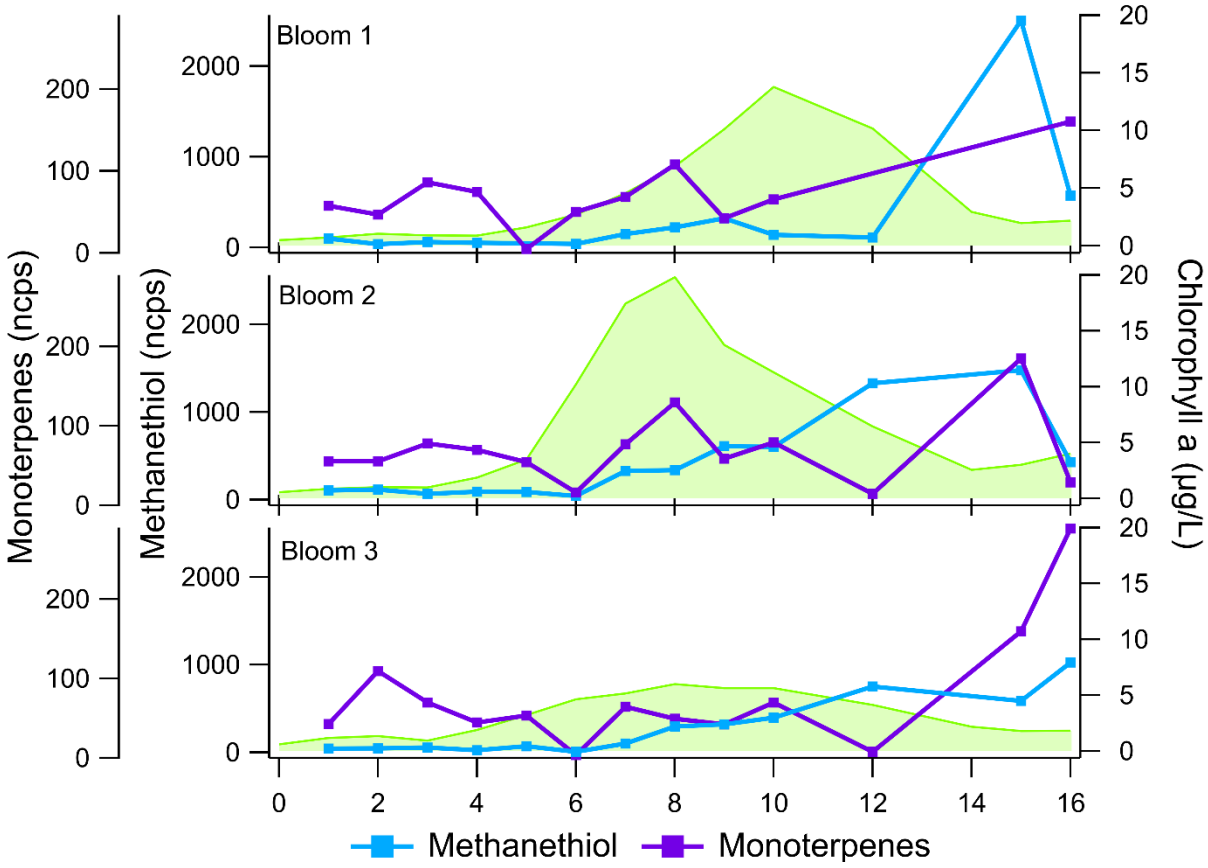


Figure 4.7: Time series of MeSH and monoterpenes normalized counts per second (ncps) co-plotted with chlorophyll a (chl. a) over the course of three blooms.

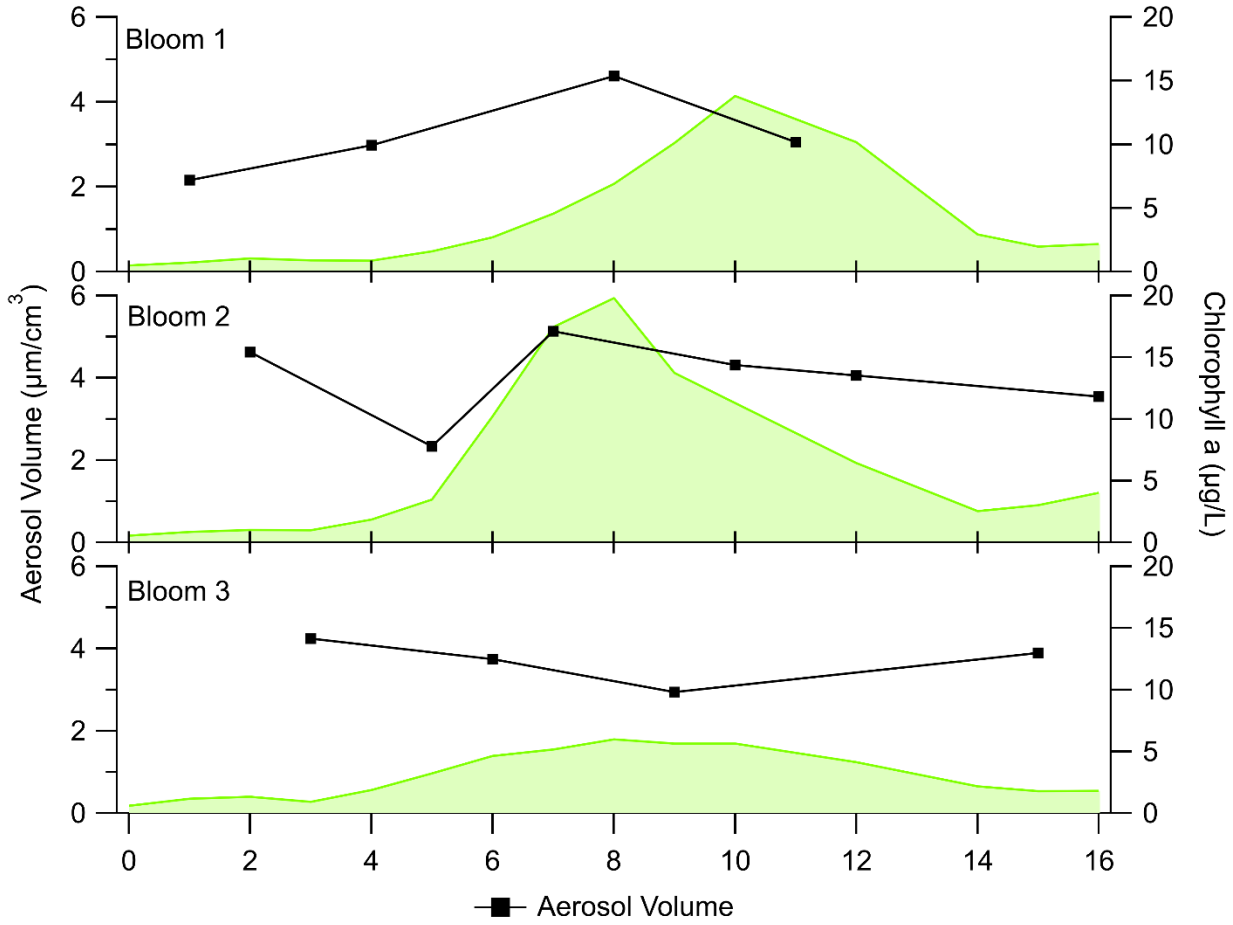


Figure 4.8: Aerosol volume for each bloom co plotted with chl. a

Chapter 5. Conclusions

5.1 Synopsis

This dissertation investigates the production of marine VOCs from biological production and the formation of secondary marine aerosols from the oxidation of marine VOCs. Chapter 2 shows a mesocosm experiment that produced unexpectedly high concentrations of DMDS and MeSH that exceeded DMS during periods of the phytoplankton blooms. Chapter 3 shows that the formation of SMA in a PAM-OFR from mixtures of marine relevant VOCs differs significantly from single VOC experiments and presents the first DMS and DMDS aerosol yield value in a PAM-OFR. Chapter 4 describes the changes in SMA over the course of three phytoplankton blooms and highlights the importance of non-sulfur organic compounds to SMA formation.

5.2 Conclusions

5.2.1 Factors Controlling Production of Dimethyl Sulfide, Methanethiol, and Dimethyl Disulfide During Controlled Phytoplankton-Bacterial Mesocosm Experiments

Marine biological production of dimethyl sulfide has been studied for years, yet there are still many uncertainties. Chapter 2 analyses the production of organosulfur compounds from biological activity. MeSH and DMDS were measured in concentrations higher than that of DMS during periods of the bloom. DMS was found to be highly correlated with Chl. a intensities, which corresponds with field and satellite measurements as well (Galí et al., 2018; Gros et al., 2023). On the other hand, MeSH and DMDS peak after the bloom and track similarly with the trend of heterotrophic bacteria. When comparing the concentrations between bloom 1 vs blooms 2 and 3, the results showed that when the chl. a was higher, resulting in a larger senesce phase, the concentrations of DMS was high but MeSH and DMDS were low. Whereas, during less intense

blooms (blooms 2 and 3) MeSH and DMDS concentrations were higher than DMS. We hypothesize that the nutrient availability is different between the low and high senescent periods, impacting the bacterial gene expression and nutrient needs. Bacteria can also contain both DMSP genes that produce DMS and MeSH, with some being shown to produce them simultaneously, thus highlighting that taxonomic shifts may not occur but changes in the DMSP degradation pathways (Sun et al., 2016). While it is important to get a better understanding of specific compounds, these results found that the interaction between and presence of certain bacteria may drive the production of VOCs.

5.2.2 Secondary Aerosol Formation from Mixtures of Volatile Organic Compounds in a Potential Aerosol Mass Oxidative Flow Reactor

To date, many laboratory studies have only focused on the oxidation of individual VOCs leading to lack of understanding of how complex marine VOC mixtures impact SMA formation and composition (Van Rooy et al., 2021b; Ye et al., 2022). Chapter 3 describes oxidation laboratory experiments comparing induvial vs mixtures of marine relevant VOCs to bridge the gap in understanding SMA. This is the first experiment to report the aerosol yields of DMS and DMDS in the PAM-OFR and these results help understand the oxidation of seawater emitted VOCs in Chapter 4. It was determined that while DMS had a higher yield, DMDS produced more particles in number. This result further highlights the importance of DMDS described in Chapter 2 and the impact DMDS can have on clouds by potentially increasing the number of CCN. When adding isoprene to the mixture, the sulfate concentration from DMDS oxidation reduced but enhanced the sulfate and MSA concentration from DMDS oxidation. The results show that one compound like isoprene can impact DMS and DMDS oxidation pathways, underscoring the importance of studying mixtures. The PAM-OFR has not been used often with marine relevant VOCs. These

results are in line with similar experiments conducted in chambers, highlighting the PAM-OFRs ability to be utilized in marine systems (Chen and Jang, 2012; Van Rooy et al., 2021b, 2021a).

5.2.3 Secondary Marine Aerosol Formation from Volatile Organic Compounds Emitted from Phytoplankton Blooms

Although there have been many laboratory and field measurements assessing the formation of SMA, it is still largely understood (Mayer et al., 2020; O'Dowd and Leeuw, 2007). The complexity of the marine atmosphere has led to the need for laboratory experiments to bridge the gap. Chapter 4 presents the VOC production and SMA formation over the course of three phytoplankton blooms. This work increases the complexity of the mixture experiments conducted in Chapter 3. During periods of high isoprene to DMS and DMDS ratios, the size distributions were shifted to larger particle sizes. This shift helps with particle growth to sizes that can act as CCN. Similar to what was shown in Chapter 2, DMDS was a large contributor to the number concentration, strongly correlating with the change in number concentration throughout the bloom.

5.3 Ongoing and Future Directions

5.3.1 Factors Controlling Marine Biogenic VOCs

Chapter 2 combines marine biological measurements and VOC composition to understand how microbiology impacts VOC emissions during phytoplankton blooms. This work was able to identify general trends across the bloom as well as highlight taxa that correlated with gas production, including phytoplankton community analysis will also be beneficial for enhancing our understanding of both phytoplankton and bacteria contributions. Further work should utilize aqueous gas measurements of VOCs and their precursors to better understand the possible bacterial switch of DMSP as well as any additional precursors. Field studies have primarily utilized aqueous

measurements with a few laboratory studies beginning to incorporate DMSP measurements (Asher et al., 2011; Gros et al., 2023; Kilgour et al., 2022; Masdeu-Navarro et al., 2024). As seen in this study, the complexity of the seawater makes it challenging to identify which compounds specifically contribute to gas production, therefore smaller scale model studies focusing on a few known compounds will continue to our knowledge. Specifically, this study identified Rhodobacteraceae as a compound that is hypothesized to contribute to both MeSH and DMS.

5.3.2 Secondary Aerosol Characterization Studies

Chapter 3 utilized controlled experiments to oxidize DMS, DMDS, and isoprene to assess their oxidation potential indivually and in mixtures. Although these results have helped lay the foundation for more complex seawater experiments, there are other marine relevant VOCs that should be studied in a controlled set up. MeSH, as previously discussed, is another marine biologically produced VOCs but has very few oxidation studies (Douroudgari et al., 2020) and should be assessed in these mixture studies. Additionally, coastal environments have a strong contribution from anthropogenic compounds. A recent study found that benzothiazole, an anthropogenic sulfur species, can contribute to aerosol formation (Franklin et al., 2021). Mixing biogenic and anthropogenic compounds will better represent the coastal environment (Friedman et al., 2016; Kari et al., 2019; Xu et al., 2021).

While hydroxyl radicals are primarily used in oxidation experiments, there are other radicals, such as chlorine, found in the atmosphere. Chlorine radicals are often present at lower levels than OH radicals, but they can still have an impact on oxidation and radical cycling due to it having faster reaction rates (Baker et al., 2016). In the marine boundary layer Cl radical concentrations are higher and have the possibility to compete with OH radicals for the oxidation

of VOCs(Baker et al., 2016; Wingenter et al., 1996). To assess the impact chlorine has on the oxidation of marine relevant VOCs, the PAM-OFR can be modified to generate chlorine radicals. Clorine radicals can be generated in the PAM-OFR through photolysis of chlorine (Cl_2) or photolysis of oxalyl chloride ($Cl_2Cl_2O_2$) using 313 nm lamps. A previous study compared the oxidation of anthropogenic precursors by Cl_2, Br_2, and OH and found that Cl_2 may enhance SOA formation in regions with biogenic and anthropogenic emissions (Lambe et al., 2022). Conducting chlorine oxidation experiments will contribute extensively to our understanding of SMA formation.

5.3.3 Secondary Marine Aerosol Formation from Seawater

Chapter 4 examined the emissions of marine seawater derived VOCs using a chemical ionization time-of-flight mass spectrometer and measured the number concentration and size distribution of SMA. Future work should investigate size—resolved composition by using a particle impactor that will separate the aerosols for off-line analysis. Additionally, the CI-TOF-MS can be modified to allow for on-line aerosol compositional analysis by adding in a heated inlet to volatilize the organic compounds in the aerosols. Combining the heated inlet with a negative mode ionization reagent ion, such as iodine or acetate, will provide real time and minimal fragmentation of organics. Similar instruments have been used to study secondary aerosols but not in marine systems (Aljawhary et al., 2013).

Future work will also involve analyzing the emissions and aerosol formation from polluted coastal waters. This study examined coastal seawater from Scripps Pier, which has been used as a control or “clean” comparison for polluted water. Imperial beach has been impacted by the run-

off from the Tijuana Estuary. Previous work has analyzed the transfer of viruses and bacteria in the aerosols (Pendergraft et al., 2023).

5.4 References

Aljawhary, D., Lee, A.K.Y., Abbatt, J.P.D., 2013. High-resolution chemical ionization mass spectrometry (ToF-CIMS): Application to study SOA composition and processing. Atmospheric Measurement Techniques 6, 3211–3224. https://doi.org/10.5194/amt-6-3211-2013

Asher, E.C., Dacey, J.W.H., Mills, M.M., Arrigo, K.R., Tortell, P.D., 2011. High concentrations and turnover rates of DMS, DMSP and DMSO in Antarctic sea ice. Geophysical Research Letters 38, 1–5. https://doi.org/10.1029/2011GL049712

Baker, A.K., Sauvage, C., Thorenz, U.R., van Velthoven, P., Oram, D.E., Zahn, A., Brenninkmeijer, C.A.M., Williams, J., 2016. Evidence for strong, widespread chlorine radical chemistry associated with pollution outflow from continental Asia. Sci Rep 6, 36821. https://doi.org/10.1038/srep36821

Chen, T., Jang, M., 2012. Secondary organic aerosol formation from photooxidation of a mixture of dimethyl sulfide and isoprene. Atmospheric Environment 46, 271–278. https://doi.org/10.1016/J.ATMOSENV.2011.09.082

Douroudgari, H., Vahedpour, M., Mohammadi, S., 2020. Atmospheric reaction of methyl mercaptan with hydroxyl radical as an acid rain primary agent. Sci Rep 10, 18081. https://doi.org/10.1038/s41598-020-74767-6

Franklin, E.B., Alves, M.R., Moore, A.N., Kilgour, D.B., Novak, G.A., Mayer, K., Sauer, J.S., Weber, R.J., Dang, D., Winter, M., Lee, C., Cappa, C.D., Bertram, T.H., Prather, K.A., Grassian, V.H., Goldstein, A.H., 2021. Atmospheric Benzothiazoles in a Coastal Marine Environment. Cite This: Environ. Sci. Technol 55, 15705–15714. https://doi.org/10.1021/acs.est.1c04422

Friedman, B., Brophy, P., Brune, W.H., Farmer, D.K., 2016. Anthropogenic Sulfur Perturbations on Biogenic Oxidation: SO 2 Additions Impact Gas-Phase OH Oxidation Products of α - and β - Pinene. https://doi.org/10.1021/acs.est.5b05010

Galí, M., Levasseur, M., Devred, E., Simó, R., Babin, M., 2018. Sea-surface dimethylsulfide (DMS) concentration from satellite data at global and regional scales. Biogeosciences 15, 3497–3519. https://doi.org/10.5194/bg-15-3497-2018

Gros, V., Bonsang, B., Sarda-Estève, R., Nikolopoulos, A., Metfies, K., Wietz, M., Peeken, I., 2023. Concentrations of dissolved dimethyl sulfide (DMS), methanethiol and other trace gases in context of microbial communities from the temperate Atlantic to the Arctic Ocean. Biogeosciences 20, 851–867. https://doi.org/10.5194/bg-20-851-2023

Kari, E., Hao, L., Ylisirniö, A., Buchholz, A., Leskinen, A., Yli-Pirilä, P., Nuutinen, I., Kuuspalo, K., Jokiniemi, J., Faiola, C., Schobesberger, S., Virtanen, A., 2019. Dual effect of anthropogenic emissions on the formation of biogenic SOA. Atmospheric Chemistry and Physics Discussions 1, 1–35.

Kilgour, D.B., Novak, G.A., Sauer, J.S., Moore, A.N., Dinasquet, J., Amiri, S., Franklin, E.B., Mayer, K., Winter, M., Morris, C.K., Price, T., Malfatti, F., Crocker, D.R., Lee, C., Cappa, C.D., Goldstein, A.H., Prather, K.A., Bertram, T.H., 2022. Marine gas-phase sulfur emissions during an induced phytoplankton bloom. Atmospheric Chemistry and Physics 22, 1601–1613. https://doi.org/10.5194/acp-22-1601-2022

Lambe, A.T., Avery, A.M., Bhattacharyya, N., Wang, D.S., Modi, M., Masoud, C.G., Ruiz, L.H., Brune, W.H., 2022. Comparison of secondary organic aerosol generated from the oxidation of laboratory precursors by hydroxyl radicals, chlorine atoms, and bromine atoms in an oxidation flow reactor. Environ. Sci.: Atmos. 2, 687–701. https://doi.org/10.1039/D2EA00018K

Masdeu-Navarro, M., Mangot, J.-F., Xue, L., Cabrera-Brufau, M., Kieber, D.J., Rodríguez-Ros, P., Gardner, S.G., Bergauer, K., Herndl, G.J., Marrasé, C., Simó, R., 2024. Diel variation of seawater volatile organic compounds, DMSP-related compounds, and microbial plankton inside and outside a tropical coral reef ecosystem. Front. Mar. Sci. 11. https://doi.org/10.3389/fmars.2024.1341619

Mayer, K.J., Wang, X., Santander, M.V., Mitts, B.A., Sauer, J.S., Sultana, C.M., Cappa, C.D., Prather, K.A., 2020. Secondary Marine Aerosol Plays a Dominant Role over Primary Sea Spray Aerosol in Cloud Formation. https://doi.org/10.1021/acscentsci.0c00793

O'Dowd, C.D., Leeuw, G. de, 2007. Marine aerosol production: a review of the current knowledge. Philosophical Transactions of the Royal Society A: Mathematical, Physical and Engineering Sciences 365, 1753–1774. https://doi.org/10.1098/RSTA.2007.2043

Pendergraft, M.A., Belda-Ferre, P., Petras, D., Morris, C.K., Mitts, B.A., Aron, A.T., Bryant, M., Schwartz, T., Ackermann, G., Humphrey, G., Kaandorp, E., Dorrestein, P.C., Knight, R., Prather, K.A., 2023. Bacterial and Chemical Evidence of Coastal Water Pollution from the Tijuana River in Sea Spray Aerosol. Environ. Sci. Technol. 57, 4071–4081. https://doi.org/10.1021/acs.est.2c02312

Sun, J., Todd, J.D., Thrash, J.C., Qian, Y., Qian, M.C., Temperton, B., Guo, J., Fowler, E.K., Aldrich, J.T., Nicora, C.D., Lipton, M.S., Smith, R.D., De Leenheer, P., Payne, S.H., Johnston, A.W.B., Davie-Martin, C.L., Halsey, K.H., Giovannoni, S.J., 2016. The abundant marine bacterium Pelagibacter simultaneously catabolizes dimethylsulfoniopropionate to the gases dimethyl sulfide and methanethiol. Nature Microbiology 1, 16065. https://doi.org/10.1038/nmicrobiol.2016.65

Van Rooy, P., Drover, R., Cress, T., Michael, C., Purvis-Roberts, K.L., Silva, P.J., Nee, M.J., Cocker, D., 2021a. Methanesulfonic acid and sulfuric acid Aerosol Formed through

oxidation of reduced sulfur compounds in a humid environment. Atmospheric Environment 261, 118504. https://doi.org/10.1016/J.ATMOSENV.2021.118504

Van Rooy, P., Purvis-Roberts, K.L., Silva, P.J., Nee, M.J., Cocker, D., 2021b. Characterization of secondary products formed through oxidation of reduced sulfur compounds. Atmospheric Environment 256, 118148. https://doi.org/10.1016/j.atmosenv.2020.118148

Wingenter, O.W., Kubo, M.K., Blake, N.J., Smith Jr., T.W., Blake, D.R., Rowland, F.S., 1996. Hydrocarbon and halocarbon measurements as photochemical and dynamical indicators of atmospheric hydroxyl, atomic chlorine, and vertical mixing obtained during Lagrangian flights. Journal of Geophysical Research: Atmospheres 101, 4331–4340. https://doi.org/10.1029/95JD02457

Xu, L., Du, L., Tsona, N.T., Ge, M., 2021. Anthropogenic Effects on Biogenic Secondary Organic Aerosol Formation. Advances in Atmospheric Sciences 38, 1053–1084. https://doi.org/10.1007/S00376-020-0284-3

Ye, Q., Goss, M.B., Krechmer, J.E., Majluf, F., Zaytsev, A., Li, Y., Roscioli, J.R., Canagaratna, M., Keutsch, F.N., Heald, C.L., Kroll, J.H., 2022. Product distribution, kinetics, and aerosol formation from the OH oxidation of dimethyl sulfide under different RO_2 regimes. Atmospheric Chemistry and Physics 22, 16003–16015. https://doi.org/10.5194/ACP-22-16003-2022